

Slip Modelling, Estimation and Control of Omnidirectional Wheeled Mobile Robots with Powered Caster Wheels

Li Yuan Ping
(*B.Eng. (Hons.), XJTU, Xi'an*)

A THESIS SUBMITTED
FOR THE DEGREE OF DOCTOR OF PHILOSOPHY
DEPARTMENT OF MECHANICAL ENGINEERING
NATIONAL UNIVERSITY OF SINGAPORE

2009

ACKNOWLEDGMENTS

First of all, I would like to thank my supervisors Professor Marcelo Ang and Dr. Lin Wei for their guidance, advice, inspiration and encouragements. The broad knowledge and serious academic attitude of my supervisors would benefit my life and always motivate me to never stopping thinking, learning and contributing to scientific work.

I couldn't have decided to become a roboticist without the experience of participating in a robotic game during the final year of my undergraduate studies. I will always remember the excitement I had with the team to build the robots. Special thanks to Mr. Zhang Yu Quan, my partner of building the first robot in my life. It was that first experience that inspired my interest and excitement for robotics.

The support of a collaborative research project grant from National University of Singapore and Singapore Institute of Manufacturing Technology (SIMTech) is gratefully acknowledged. The attachment in SIMTech during my Ph.D candidature made me understand that much fun of robotics is coming from making robots work in practical applications. I would like to thank Dr. Lim Chee Wang, my nice boss in SIMTech, who has provided me great help in troubleshooting the mobile robot during the last four years. Also thanks to Mr. Lim Tao Ming for all the good ideas and his programming support for my work. I would also like to thank Dr. Lim Ser Yong, the mentor of the whole team, for his advice. Special thanks to Dr. Denny Oetomo who

helped me in writing my first technical paper on robotics. Also thanks to Drs. Koh Niak Wu and Mana Seadan for their help along the way.

Other sources of inspiration and knowledge have come from Mr. T. Bandyopadhyay, Professor David Hsu from National University of Singapore, Professors Teresa Zielinska and Cezary Zinlinski from Warsaw University of Technology. The collaborations and discussions with them greatly broadened my knowledge in robotics.

I would most especially like to thank my parents, my whole family and all my good friends in both China and Singapore for their support and love. I want to tell them that they are the most important ones to me in the world.

TABLE OF CONTENTS

	Page
Acknowledgments	i
Abstract	viii
List of Tables	xi
List of Figures	xii
Chapters:	
1. Introduction	1
1.1 Background and Motivations	1
1.1.1 Traversability of Wheeled Mobile Robots (WMRs)	1
1.1.2 Vehicle Dynamics	3
1.1.3 Multi-Fingered Grasping	4
1.1.4 Mobile Manipulation	6
1.2 Research Gaps	8
1.3 Aims and Scope	9

1.4	Contributions	10
1.5	Outline	10
2.	Literature Review	12
2.1	Modelling and Analysis of WMRs	12
2.1.1	Nonholonomic and Holonomic WMRs	12
2.1.2	Dynamic Modelling of WMRs	13
2.1.3	Slip Modelling of WMRs	14
2.2	Slip in Other Areas	15
2.2.1	Vehicle Dynamics	15
2.2.2	Rough Terrain Mobility	16
2.2.3	Multiple Frictional Contact Tasks	17
2.2.4	Mobile Manipulation	18
2.3	Slip and Friction Estimation	19
2.4	Slip Reduction and Slip-based Traction Control	20
2.5	Slip-based Terrain Identification	24
3.	Slip Modelling of WMRs with Powered Caster Wheels (PCWs)	26
3.1	Mobility Analysis	27
3.2	Kinematic Modelling	31
3.2.1	Displacement Kinematic Model	31
3.2.2	Differential Kinematic Model	35
3.2.3	Odometry	42

3.2.4	Singularity Analysis	43
3.3	Dynamic Modelling	46
3.3.1	Augmented Object Model	47
3.3.2	Slip-based Wheel-Ground Interaction Model	50
4.	Real Time Slip Detection and Estimation	55
4.1	Slip Detection with Cost Effective Sensors	55
4.1.1	Slip Detection with Encoder	56
4.1.2	Slip Detection with Inertia Measurement Unit	60
4.2	Slip Estimation with Sliding Mode Observer	63
4.2.1	Velocity Observer with Joint Velocity Measurement	63
4.2.2	Velocity Observer with Joint Angle Measurement	65
5.	Slip Controllers: Design and Implementation	69
5.1	Sliding Mode Slip Compensation	70
5.1.1	Sliding Mode Kinematic Control	71
5.1.2	Chattering Reduction	74
5.2	Internal Force Control	77
5.2.1	Internal Force Minimization	80
5.2.2	Traction Limit Avoidance	84
5.2.3	Slip Constraint Force Control	88
5.3	Slip Control for Rough Terrain Navigation	96
5.3.1	Sliding Mode Slip Ratio Control	97

5.3.2	Adaptive Terrain Identification	101
5.4	Summary: Multi-Objective Controller Design	109
6.	Conclusions	113
6.1	Research Review	113
6.2	Contributions	114
6.3	Limitations	115
6.4	Future Work	116
	Bibliography	118
Appendices		
A.	Publications	129
A.1	Publications Arising from the PhD Work	129
A.2	Publications on Other Research Areas	130
B.	Augmented Object Model for the Tested Robot	131
B.1	Kinetic Energy Matrix Λ	131
B.2	Coriolis/Centrifugal Force Vector ϑ	132
C.	Basics of Sliding Mode	134

D. Virtual Prototyping	137
----------------------------------	-----

ABSTRACT

Wheel slip problem has been mainly studied in the fields of vehicle dynamics and outdoor mobile robot navigation. Different from these areas that usually consider non-holonomic Wheeled Mobile Robots (WMRs), this research focuses on the wheel slip problem in the case of omnidirectional WMRs with Powered Caster Wheels (PCWs). PCW-based WMRs are chosen because they are omnidirectional, singularity free and redundantly actuated.

Most existing modelling methodologies of WMRs are based on the “pure rolling without slipping” assumption, thus most existing motion control schemes of WMRs assume that there is no slip and traction between the wheel and the ground is always maintained. However, it is observed that slip often occurs in WMRs with PCWs. Moreover, in mission critical tasks such as planetary exploration, traction between the wheel and the ground must always be maintained and the wheel slip critically determines the traction performance of the robot. These are the main motivations for this research.

This research distributes the efforts on three main aspects of the wheel slip problem for WMRs with PCWs: slip modelling, slip detection and slip control.

By removing the assumption of “pure rolling without slipping”, we model WMRs with slip for both the kinematic and dynamic models. Borrowing ideas from vehicle

dynamics, a new wheel-ground interaction model is developed that describes the explicit relation between slip ratio and traction force. For the convenience of describing wheel slip and internal force analysis for WMRs with PCWs, longitudinal and lateral velocities of wheel center are chosen as the generalized velocities of the robot, rather than the rolling and steering velocities of the wheel.

Several slip detection and estimation schemes are proposed in this research. For the purpose of explicit slip estimation, sliding mode observer based on the vehicle dynamic model is proposed to estimate the actual vehicle velocity using only joint angle measurements. All the proposed slip detection and estimation schemes are easily realized and demonstrated to be suitable for real time implementation. The performance of the proposed slip detection schemes is validated by both simulations and real time experiments.

The main contribution of this research is the proposition of several slip control schemes for effectively controlling the wheel slip effects. Sliding mode slip compensation scheme is proposed to achieve much better wheel motion synchronization. Slip constraint force control scheme is proposed based on the internal force analysis for WMRs with PCWs. Actuation redundancy of the mobile robot is used in the slip constraint force control scheme to minimize wheel slip. In the slip constraint force control scheme, the operational space space is decoupled with the internal force space so that multi-objective control is achieved. Extensive simulation and experimental results are presented to validate the performance of the proposed slip constraint force control.

To extend the applications of the proposed slip detection and control schemes, those schemes have been incorporated into the unified force/motion control framework

for a mobile manipulator. Testing for a force controlled wheeled mobile robot is presented with the slip constraint force control implemented. Slip control techniques that are suitable for rough terrain navigation are also studied. Sliding mode slip ratio control and adaptive terrain identification are proposed to achieve reliable rough terrain navigation.

LIST OF TABLES

Table	Page
3.1 Definition of parameters and variables in Fig. 3.5	37
5.1 Control algorithm of the <i>Sliding Mode Enhanced Resolved Motion Rate Control (SME-RMRC)</i> scheme.	73
5.2 Control algorithm of the <i>Internal Force Minimization (IFM)</i> scheme.	83
5.3 Control algorithm of the <i>Traction Limit Avoidance (TLA)</i> scheme.	85
5.4 Control algorithm of the <i>Slip Constraint Force Control (SCFC)</i> scheme.	90
5.5 Control algorithm of the <i>Unified Force/Motion with Slip Constraint Force Control (UFM-SCFC)</i> scheme.	94

LIST OF FIGURES

Figure	Page
1.1 Indoor planar smooth surface, one of the typical environments for wheeled mobile robots. Image of the Pioneer P3-DX mobile robot. Source: http://www.mobilerobots.com .	3
1.2 Outdoor unstructured rough terrain, another typical environment for wheeled mobile robots. Image of the Phoenix Mars rover. Source: http://nssdc.gsfc.nasa.gov .	4
1.3 The field of vehicle dynamics studies the dynamic behavior of ground vehicles. How the wheel slip affects the dynamic behavior of the vehicle is well studied in vehicle dynamics. Image source: http://www.zf.com .	5
1.4 Slip problem also occurs in multi-fingered grasping tasks. Image of the DLR hand grasping a glass bottle. Source: http://www.dlr.de .	6

3.3 A Powered Caster Wheel can be considered as a serial manipulator with 3 joints in each instance. The 3 joints are: the instantaneous revolute joint (σ) whose rotation axis is the vertical axis at the contact point between wheel and ground; the virtual prismatic joint ($\rho\mathbf{r}$) whose translational axis is the forward direction of the wheel caused by the wheel rolling motion; the revolute joint (ϕ) that represents the steering motion of the wheel.	29
3.4 Velocity of wheel center and slip velocity of the contact between wheel and ground.	36
3.5 Frame assignments, parameter and variable definitions of a mobile robot with n Powered Caster Wheels. See Table 3.1 for the detailed explanations of the notations.	38
3.6 Examples of a singular configuration in the mobile robot with Powered Caster Wheels for different selective actuation situations. In (a), only one rolling actuator from one of the wheels is active. In (b), only one steering actuator from one of the wheels is active. In (c), only one wheel is fully actuated and the rest of wheels are selectively actuated.	46

3.7 By considering each Powered Caster Wheel (PCW) as a serial manipulator with 3 joints as shown in Fig. 3.3, a mobile robot with PCWs can be considered as cooperative serial manipulators grasping a common object at the end-effectors of each manipulator. By this consideration, the Augmented Object Model can be used to model the dynamics of WMRs with PCWs.	48
3.8 Relationship between the longitudinal friction coefficient and the slip ratio. In the stable region of this curve, the friction coefficient increases with the slip ratio. In the unstable region of this curve, the wheel slips significantly and the wheel loses traction.	54
4.1 Wheel slip can be detected using the redundant wheel encoders. For those wheels that are slipping, the calculated slip velocities of them are not consistent with those of the rest of wheels. This detection scheme becomes invalid if all wheels are slipping simultaneously.	58
4.2 With the assist of external sensors such as Inertia Measurement Unit (IMU), wheel slip can be detected by comparing the velocities sensed by the wheel encoders and the IMU.	62

4.3 In the simulation of one wheel motion, wheel velocity estimated using the sliding mode observer with joint velocity measurement is plotted verses the actual velocity of the wheel. The settling time for convergence is about 0.12 second.	66
4.4 In the simulation of one wheel motion, wheel velocity estimated using the sliding mode observer with only joint angle measurement is plotted verses the actual velocity of the wheel. The settling time for convergence is about 0.15 second.	68
5.1 Control diagram of the Sliding Mode Enhanced Resolved Motion Rate Control (SME-RMRC) scheme. TP: trajectory planner, SD: slip detector.	72
5.2 Comparing the chattering reduction and transient response performance between the Boundary Layer scheme and the LPFISMIC method in the sliding mode controller. Both methods can reduce chattering effectively. The Boundary Layer scheme has an obvious reaching phase towards the sliding surface while the LPFISMIC scheme eliminates the reaching phase.	75
5.3 Position tracking error comparison between the RMRC and SME-RMRC schemes. The SME-RMRC scheme outperformed the RMRC scheme.	76

5.4 Topologically, wheeled mobile robot is similar to multi-fingered grasping. Slip problem is considered in both wheeled mobile robots and multi-fingered grasping. Ideas on slip study of multi-fingered grasping can be borrowed for wheeled mobile robots	78
5.5 Diagram showing the rigidity condition of a rigid body motion. When applied to wheeled mobile robot, the rigidity condition describes the instantaneous relationship between the internal forces at the wheel-ground contact points and the resultant forces at the operational point of the robot. The occurrence of wheel slip implies the broken of the rigidity condition.	81
5.6 Comparing the wheel motion synchronization performance between the Augmented Object Model based control and the Augmented Object Model based control with Internal Force Minimization (IFM). When internal forces are minimized, the chance for the occurrence of wheel slip is also minimized. This diagram demonstrates the effectiveness of the proposed IFM scheme.	84

5.7 (a) Joint torque required in a straight line motion using standard Computed Torque Control scheme without internal force space control. Pseudo-inverse of the Jacobian matrix \mathbf{J} is used to compute the required joint torque. Joint torque as high as 4.2 Nm is required without joint torque limit or traction limit imposed. (b) Internal force space control is used to avoid joint torque limit or traction limit. The internal force space used in this example is that of the inverse Jacobian matrix \mathbf{J} .	86
5.8 (a) Joint torque required in a straight line motion using standard Computed Torque Control scheme without internal force space control. Pseudo-inverse of the transformation matrix \mathbf{A} is used to compute the required joint torque. Joint torque as high as 3.5 Nm is required without joint torque limit or traction limit imposed. (b) Internal force space control is used to avoid joint torque limit or traction limit. The internal force space used in this example is that of the transformation matrix \mathbf{A} .	87
5.9 Performance of the Slip Constraint Force Control (SCFC) scheme in trajectory tracking tasks. (a) Slip was detected when SCFC was not implemented; (b) Slip was eliminated when SCFC was implemented.	91

5.10 Another mobile manipulator developed in Singapore Institute of Manufacturing Technology. This mobile manipulator consists of a Mitsubishi PA10 7DOF manipulator and an omnidirectional wheeled mobile robot with 4 Powered Caster Wheels. Unified force/motion control is implemented for this mobile manipulator with the proposed slip constraint force control scheme. Image courtesy of the Singapore Institute of Manufacturing Technology.	93
5.11 Off-the-ground test for the force-guided wheeled mobile robot. (a) Wheel slip was detected when the slip constraint force control scheme was not implemented. (b) Wheel slip was eliminated when the slip constraint force control scheme was implemented.	95
5.12 On-the-ground test for the force-guided wheeled mobile robot. (a) Uneven wheel velocities were observed (implies significant wheel slip) when the slip constraint force control scheme was not implemented. (b) Even wheel velocities were observed (implies minimum wheel slip) when the slip constraint force control scheme was implemented.	96
5.13 ADAMS/Simulink co-simulation block diagram for sliding mode slip ratio control of one wheel body.	100
5.14 Slip ratio tracking performance of the sliding mode slip ratio control for one wheel body.	101

5.15 ADAMS/Simulink co-simulation block diagram for sliding mode slip ratio control with sliding mode observer for one wheel body.	102
5.16 Slip ratio tracking performance of the sliding mode slip ratio control with sliding mode observer for one wheel body.	103
5.17 Block diagram of adaptive terrain identification based on the wheel-ground interaction model. SMO: sliding mode observer. RLS: recursive least squares estimator.	104
5.18 Empirical $\lambda - \mu$ curves for different terrains.	104
5.19 Parameter estimation of the $\lambda - \mu$ curve: estimation of the critical slip ratio corresponding to the peak friction coefficient.	109
5.20 Parameter estimation of the $\lambda - \mu$ curve: estimation of the peak friction coefficient	110
D.1 Virtual Prototyping is an important step between conceptual design stage and physical prototyping stage. Image source: mscsoftware.com.	138

D.2 Usually the first step of virtual prototyping is to construct the 3D mechanical structure using CAD packages such as Solidworks, UniGraph-ics or ProEngineer. This image shows the 3D Solidworks CAD model of the tested mobile manipulator. The next step is to import the CAD model to the MSC.ADAMS package for realistic dynamic simulation. 139

D.3 Co-simulation between MSC.ADAMS (multi-body dynamics simulation package) and Matlab/Simulink (control design package) is done after the 3D CAD model of the system is imported into the MSC.ADAMS. The interface between MSC.ADAMS and Matlab/Simulink is the system inputs and outputs defined in MSC.ADAMS. 140

D.4 The interface between MSC.ADAMS and Matlab/Simulink is based on the system input/output concept. A virtual prototype is built with the close loop simulation that combines the virtual controller and the multi-body dynamic physics engine. Image source: mscsoftware.com. 141

D.5 After the virtual prototype is built, users can focus on the virtual controller design. This image shows a trajectory tracking controller designed for the tested wheeled mobile robot with Simulink. 142

Nomenclature

$\bar{\Omega}$	complementary selection matrix of the hybrid force/position control
β_i	the angle of steering point i relative to the local frame
\ddot{p}	rolling acceleration of the wheel
\ddot{x}	task space accelerations of the mobile robot
$\dot{\varepsilon}_y$	lateral slip velocity of the wheel
$\dot{\varepsilon}$	slip velocity of the wheel
$\dot{\varepsilon}_x$	longitudinal slip velocity of the wheel
\dot{p}	wheel center velocity
Γ	wheel torques
Λ	kinematic energy matrix of the mobile robot in the operational space
λ	slip ratio
λ_p	critical slip ratio
Λ_{\oplus}	augmented kinematic energy matrix of the mobile robot in the operational space

Λ_i	kinematic energy matrix of wheel i in the operational space
Λ_l	kinematic energy matrix of external loading on the mobile robot
\mathbf{g}	gravitational force vector of the mobile robot in the operational space
μ	friction coefficient between the wheel and the ground
μ_p	peak friction coefficient
Ω	selection matrix of the hybrid force/position control
ω	rotational velocity of the mobile robot
ω_{ij}	rotation axis of j -th joint of wheel i
Φ	regressor matrix of the least square estimator
ϕ	steering angle of the Powered Caster Wheel
ρ	rolling angle of the Powered Caster Wheel
σ	twisting angle of the Powered Caster Wheel
τ_ϕ	steering torque of the wheel
τ_ρ	rolling torque of the wheel
Θ	parameter vector of the least square estimator
θ	rotation angle of the task space configuration of the mobile robot's platform
\tilde{Y}	estimation error
ϑ	Coriolis/centrifugal force vector of the mobile robot in the operational space

ϑ_{\oplus}	augmented Coriolis/centrifugal force vector of the mobile robot in the operational space
ϑ_i	Coriolis/centrifugal force vector of wheel i in the operational space
ϑ_l	Coriolis/centrifugal force vector of external loading on the mobile robot
ξ_{ij}	twist of the j -th joint of wheel i
A	transformation matrix between task space velocity and contact point velocity
B	transformation matrix between joint space velocity and contact point velocity
b	offset distance of the Powered Caster Wheel
c_1	linear coefficient of the slip-traction model
c_2	linear coefficient of the slip-traction model
DOF	degree of freedom
E	transformation matrix between the contact forces and the internal forces of the wheel
e	control error
F	operational space forces of the mobile robot
f	state coefficient function of the state space equations
F_o	null space forces
F_t	forces of the main task

F_{\oplus}	augmented operational space forces of the mobile robot
F_{ε}	constraint forces associated with the wheel slip velocities
F_c	wheel contact forces
F_x	longitudinal contact force of the wheel
F_y	lateral contact force of the wheel
F_z	vertical contact force of the wheel
FK	forward displacement kinematic model of the mobile robot
g	input coefficient function of the state space equations
H	observer gains of the estimation error
h	radius of the mobile robot's platform
I_{ρ}	angular inertia of the wheel about the rolling axis
IK_i	inverse displacement kinematic model of the mobile robot for wheel i
K	observer gains of the sliding variable
M_w	mass of the wheel
P_i	center of the wheel i
p_i	position vector of P_i relative to O_L
P_x	x position of the task space configuration of the mobile robot's platform
P_y	y position of the task space configuration of the mobile robot's platform

$P_{gt}(q_i)$ position of the mobile robot's platform origin at joint configuration q_i

p_{ij} position vector of an arbitrary point on the j -th joint axis of wheel i

q_i joint space configuration of wheel i

r radius of the Powered Caster Wheel

$R_{gt}(q_i)$ rotation matrix of the mobile robot's platform at joint configuration q_i

s sliding variable

S_i steering point of the wheel i

$T_{gt}(q_i)$ homogeneous representation of joint space configuration q_i

U input variable

v translational velocity of the mobile robot measured at point O_L

v_x longitudinal velocity of the wheel

v_{i2} longitudinal direction of wheel i

X state variables

$x(q_i)$ the task space configuration of the mobile robot's platform at joint configuration q_i

$X_G O_G Y_G$ robot global frame

$X_L O_L Y_L$ robot local frame with its origin O_L at center of the mobile robot

$X_{wi} P_i Y_{wi}$ frame attached at the center of wheel i

Y output variable

z auxiliary sliding variable

CHAPTER 1

INTRODUCTION

Wheeled mobile robot (WMR) is a particular type of robot that is the focus of this research. As opposed to legged robots, WMRs are prevalent due to their high speed, high payload and ease in achieving statical stability on even surface. But generally speaking, WMRs are less flexible than legged robots and it is more difficult for WMRs to traverse rough terrains. Therefore, the goal of developing truly autonomous vehicles requires much more research efforts for improving the traversability of WMRs. Thus, the main purpose of this research is to study the slip problem that is closely related to the traversability of WMRs.

1.1 Background and Motivations

1.1.1 Traversability of Wheeled Mobile Robots (WMRs)

Wheeled mobile robots are widely used in both indoor structured environments (Fig. 1.1) and outdoor rough terrains (Fig. 1.2). The ability of WMRs to accomplish a task depends mainly on its mobility or traversability. Traversability of WMRs is the capability of the robot to move from one location to another by negotiating with the terrain. Studying the traversability of WMRs requires the analysis of the rolling motion introduced by the wheels of the mobile robot. Rolling motion of a wheel is characterized by its nonholonomic constraint and rolling friction.

The nonholonomic constraint problem has drawn the most research attention of WMRs because it introduces interesting and challenging problems for motion planning and control [1, 2, 3]. On the other hand, some researchers have developed holonomic and omnidirectional WMRs [4, 5, 6] to avoid the difficulties caused by nonholonomic WMRs.

Rolling friction is the reactive force that the terrain acts on the rolling wheel. Rolling friction is similar to the classical sliding friction but has its own characteristics. Although rolling friction is the direct force that moves WMRs, it is not explicitly considered in most existing WMR literature. This is because the assumption of “*pure rolling without slipping*” is usually made in those literature [7, 8]. Based on this assumption, rolling friction is considered as ideal constraint force that does not often appear in the system’s equations of motion. However, this assumption is not strictly correct for real rolling motion. In studying the traversability of WMRs, it is necessary to consider rolling motion with practical slip effects. Slip is part of the effects caused by the wheel-terrain interaction. Large amounts of slip would occur on certain terrains and would negatively affect the traversability of the robot.

Slip is observed as the odometry error in mobile robot localization [9]. Slip is usually compensated in high level non-realtime localization but not used for the low level realtime motion control.



Figure 1.1: Indoor planar smooth surface, one of the typical environments for wheeled mobile robots. Image of the Pioneer P3-DX mobile robot. Source: <http://www.mobilerobots.com>.

1.1.2 Vehicle Dynamics

Vehicle Dynamics is an old discipline that deals with the dynamics of ground vehicles [10]. The main concern of vehicle dynamic control is on the safety and handling issues (Fig. 1.3). Wheel-terrain interaction [10, 11] is one of the main problems in vehicle dynamics. In order to improve the traversability of WMRs in rough terrains, researchers working on WMRs have recently started to apply ideas of vehicle dynamics to WMRs. A. Ghosal [12] and S. Shekhar [13] were the first few researchers to discuss slip modelling for WMRs using the wheel-terrain interaction theory. J. Svendienius and B. Wittenmark [14] reported the wheel-terrain interaction phenomenon and summarized a few dynamic friction estimation techniques. Different from J. Svendienius' method to estimate friction, more researchers such as K. Iagnemma and

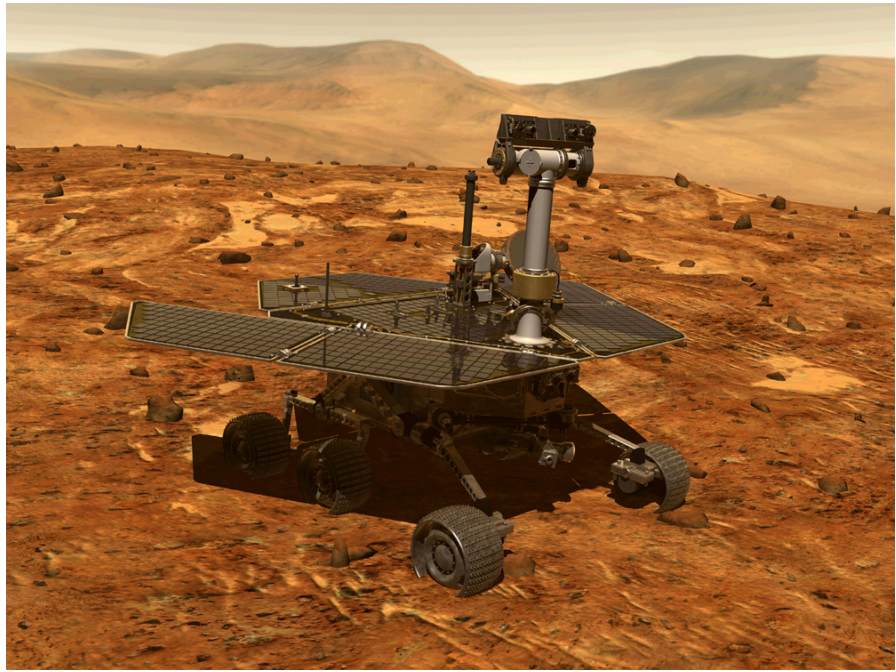


Figure 1.2: Outdoor unstructured rough terrain, another typical environment for wheeled mobile robots. Image of the Phoenix Mars rover. Source: <http://nssdc.gsfc.nasa.gov>.

S. Dubowsky [15] and J. Borenstein [16] were interested in estimating slip. In addition to the research in estimation techniques, researchers such as K. Yoshida and H. Hamano [17] and Y. Hori [18] considered the problem of slip-based traction control.

1.1.3 Multi-Fingered Grasping

Multi-fingered grasping (Fig. 1.4) is another research area that considers the slip problem. For stable grasping, it is always desirable to avoid slip in multi-fingered grasping tasks. Finger tip force distribution and internal force analysis of the grasped object are important schemes in multi-fingered grasping for slip avoidance and stable grasping. The force distribution problem of multi-fingered grasping usually requires

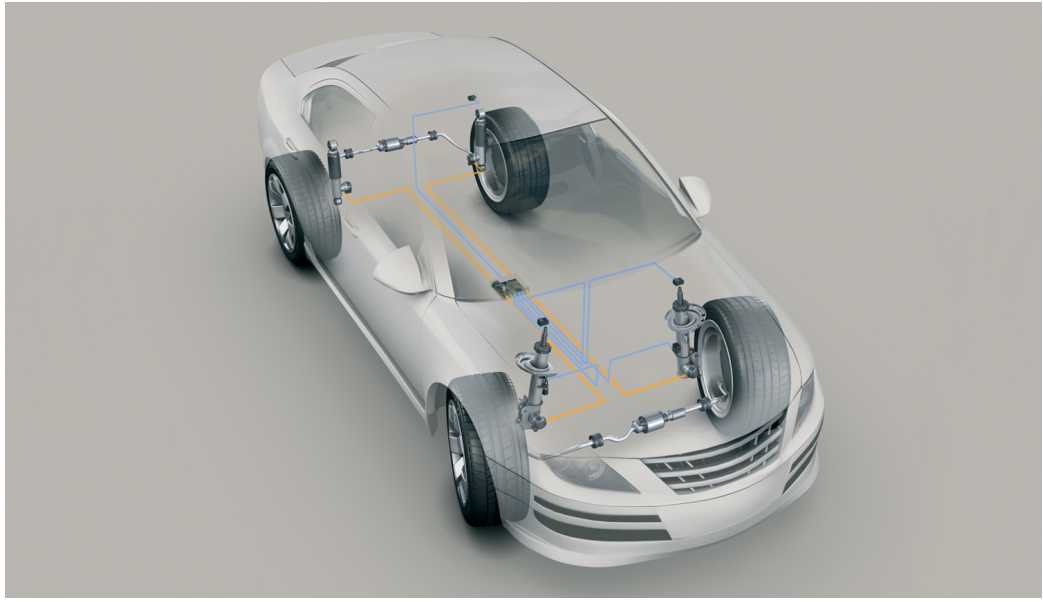


Figure 1.3: The field of vehicle dynamics studies the dynamic behavior of ground vehicles. How the wheel slip affects the dynamic behavior of the vehicle is well studied in vehicle dynamics. Image source: <http://www.zf.com>.

the robotic hand to be redundantly actuated. Redundantly actuated systems have more actuators than their degrees-of-freedom. Such systems are often found in parallel manipulators [19]. Some WMRs also adopt redundant actuation [16, 20]. J.C. Alexander [21] and T.D. Murphey [22] were the only few researchers to consider the slip effect on the dynamic model of redundantly actuated WMRs. R. Holmberg [23] was first to consider the internal force problem for WMRs by using the Virtual Linkage Model [24]. However, R. Holmberg did not introduce effective internal force control strategies for WMRs.



Figure 1.4: Slip problem also occurs in multi-fingered grasping tasks. Image of the DLR hand grasping a glass bottle. Source: <http://www.dlr.de>.

1.1.4 Mobile Manipulation

An interesting problem we discovered along the slip study of WMRs is the challenge of controlling WMRs in mobile manipulations (Fig. 1.5). To achieve full dynamic control of the whole mobile manipulator, dynamic models of both the manipulator and the mobile robot are required. Due to the parallelism characteristic of WMRs and the presence of uneven dynamics on individual wheel, controlling the mobile robot in a mobile manipulator, especially in force control tasks, is more challenging than the manipulator. Since slip affects each wheel locally, the operational

space control structure for the WMRs in mobile manipulations introduces extra difficulties for achieving satisfactory dynamic control performance.



Figure 1.5: A mobile manipulator is polishing a canopy. The interaction between the manipulator and the canopy will affect the mobile robot and may cause the wheels to slip. Image courtesy of the Singapore Institute of Manufacturing Technology.

1.2 Research Gaps

Based on above introduction and discussions, the research gaps relating the slip problem for wheeled mobile robots are addressed below.

- Most existing literatures dealing with wheeled mobile robot modelling assume “*pure rolling without slipping*”, so it is important to consider the slip dynamic effects and modeling problem for wheeled mobile robots.
- Slip is often considered in the mobile robot localization literatures. However, the concern of those literatures is mainly on slip compensation for better localization accuracy. Slip information in those literatures is not explicitly extracted for used in the low level motion control to achieve robust mobility of the robot.
- As it is stated by R. Holmberg [23] that “*Vehicle dynamics is an old discipline in which the analysis of the kinematic and dynamic properties of wheeled vehicles has evolved to embody deep and insightful knowledge of rolling mechanisms. Its fascinating that the study of rolling motion is so refined when applied to automobiles and yet very little work has been done with robots.*” Thus it is worthwhile borrowing ideas from vehicle dynamics for wheeled mobile robots.
- Slip problem is considered extensively in multi-fingered grasping tasks. Similar to wheeled mobile robot, it is always desirable to avoid slip in multi-fingered grasping tasks for stable grasping. Force distribution and internal force analysis are well studied in multi-fingered grasping tasks for slip avoidance and stable grasping. However, these problems are not well understood in wheeled mobile

robots. Therefore it is interesting to introduce the concept of force distribution and internal force analysis for wheeled mobile robots.

- Mobile manipulation is an important application for wheeled mobile robots. Full dynamic control of the whole mobile manipulator leads to extra difficulties in controlling the wheeled mobile robot, especially in force control applications. To the author's knowledge, few researchers have highlighted the practical control issues of wheeled mobile robots in mobile manipulations, especially when the manipulator is interacting with external environments.

1.3 Aims and Scope

The ultimate objective is to achieve robust mobility of wheeled mobile robots in both structured environments and rough terrains. To achieve this objective, this research focuses on developing effective slip control strategies for wheeled mobile robots.

More specifically, a systematic study of the slip problem for wheeled mobile robots is conducted by analyzing three main aspects of slip problem: modelling, detection and control. For slip modelling, we focus on the dynamic modelling of wheeled mobile robots incorporating actuation redundancy and practical vehicle dynamics. For slip detection, we highlight the utilization of observer techniques for practical real time slip detection and estimation. For slip control, internal force analysis for wheeled mobile robots is introduced to develop a general slip control structure.

Although slip issue is more critical in rough terrains than structured environments, it is not our focus to consider all aspects of rough terrain applications. Instead, we develop general slip control schemes based on analysis of planer wheeled mobile robots.

1.4 Contributions

The results of this research contribute to following research areas:

- Systematic study of slip problem for wheeled mobile robots.
- Practical slip detection and estimation schemes for wheeled mobile robots.
- General slip control structure for wheeled mobile robots.
- Robust and real time slip control techniques.
- Control of wheeled mobile robots in mobile manipulations.
- Control schemes for rough terrain mobility.

1.5 Outline

The remaining chapters are organized as follows.

Chapter 2 provides a comprehensive review of the related literatures. The existing studies on wheeled mobile robots and slip problem in different research areas are discussed.

Chapter 3 presents in detail the modelling of wheeled mobile robots that considers wheel slip effects. Slip is formally defined and explicitly expressed in the equations of motion of the system.

Chapter 4 discusses the slip detection problem. Real time slip detection and estimation techniques are introduced. Effective observer-based state estimation scheme is proposed. The performance of the proposed methods are demonstrated by both simulation and real time experiments.

Chapter 5 proposes several schemes for slip control. Internal force and its relation with slip of wheeled mobile robots is analyzed. General slip control structure for wheeled mobile robots is derived based on the internal force analysis. Simulation and experimental results are presented to validate the performance of the proposed slip control schemes. The effectiveness of the proposed schemes for mobile manipulation applications is also demonstrated. Lastly, robust slip ratio control and adaptive terrain identification are proposed for rough terrain applications.

Chapter 6 review the main work of this research, summarize the research contributions and suggests future research topics.

CHAPTER 2

LITERATURE REVIEW

In this chapter we will give a comprehensive survey on related literature. Pioneer work of wheeled mobile robots are first reviewed, followed by a literature survey on slip problems in the relevant research areas.

2.1 Modelling and Analysis of WMRs

2.1.1 Nonholonomic and Holonomic WMRs

G. Campion's pioneer work [25] is often mentioned in WMRs literature. In [25], G. Campion analyzed the structural properties of both nonholonomic and holonomic WMR configurations based on their kinematic and dynamic models. He classified WMRs into five types based on the generic structures of their motion equations. By adopting the state space methodology, he addressed the reducibility, holonomy, mobility and controllability, configuration of the motorization, and feedback equivalence of WMRs.

The nonholonomic characteristic of wheel rolling motion has attracted a large body of work in WMR research. Motion planning [26, 27, 28] and control of nonholonomic WMRs [29, 1, 2] are the main interests of many researchers. Many research activities are motivated by the important work of Bloch [30] and Brockett [31].

In order to avoid or overcome difficulties in control and planning of WMRs with nonholonomic constraints, many researchers focus on developing holonomic and omnidirectional WMRs. Usually non-conventional wheels are required for holonomic WMRs such as ball wheel [5], orthogonal wheel [4] and Swedish wheel [7, 25, 32]. To the author's knowledge, the Power Caster Wheel (PCW, also known as off-centered orientable wheel) is the only type of conventional wheel that is used to develop holonomic WMRs. More and more holonomic WMRs using PCW have been developed such as [33, 34, 6, 35, 36]. PCW-based WMRs is the main WMR configuration we are interested in in this thesis because it belongs to a general type of WMRs that is independently steered and driven.

2.1.2 Dynamic Modelling of WMRs

Dynamic modelling of WMRs is one of our main concerns because slip is part of the dynamic behavior of WMRs. Conventional rigid body dynamic modelling of WMRs are based on either the Lagrangian formalism [37, 38] or the Newton-Euler formalism [39, 40]. In [39], P. Muir developed a formalism for the dynamic modelling of multibody robotic mechanisms incorporating closed chains, higher pair joints, friction (including stiction, Coulomb, rolling and viscous friction), and unactuated and unsensed joints. Although this formulation was developed for the dynamic modelling of WMRs, the methodology is directly applicable to a spectrum of multibody robotic mechanisms.

There are other modelling methodologies developed from the aforementioned two classic formalisms. The concept of Orthogonal Complement is one of them and was applied to the dynamic modelling of WMRs in [41]. Some researchers adopted another

method called Kane's Approach (also termed Lagrange's form of d'Alembert's principle) [42] and it shown several advantages over the Newton-Euler and Lagrangian approaches. The Augmented Object Model [43], an extension of the Operational Space Formulation [44], was applied to the dynamic modelling of WMRs in [45, 36, 6]. The Augmented Object Model is computationally more efficient than other methodologies. However, it is found that of all these dynamic modelling methodologies none of them considered the wheel slipping effect.

2.1.3 Slip Modelling of WMRs

Not many of existing WMRs literatures considered the wheel slipping effect. J.C. Alexander was among the first to formulate slip in the kinematic equations of WMRs. In [21], J.C. Alexander analyzed the conditions that guarantee rolling without slipping. The questions of slippage due to misalignment of the wheels were investigated by minimization of a non-smooth convex dissipation functional derived from Coulomb friction. T.D. Murphey generalized the idea of J.C. Alexander to the cases of over-constrained WMRs, distributed manipulation and multi-fingered grasping tasks [22]. T.D. Murphey expanded the idea to a quasi-static formulation of the "Power Dissipation Principle". He also described the full Langrangian model that consists of the slip effect (represented as Coulomb friction) and unknown Langrange multipliers. However, the Coulomb friction would be too simplistic and inaccurate to represent realistic slip effects. Moreover, the challenges caused by the Langrange multipliers makes this method not attractive for practical implementation.

J. Borenstein [46] addressed the problem of severe wheel slippage caused by over-constrained WMRs and suggested the use of compliant linkages to reduce the slip

effect in over-constrained systems. Similar idea was also suggested by B.J. Choi in [47] which proposed to use the passive variable length axle to reduce the slip effect. N. Chakraborty extended the idea of B.J. Choi to the use of actuated variable length axle to avoid slip in uneven terrains [48].

By using classical results on the accessibility and controllability in nonlinear control theory, S. Shekhar derived an analytical model of the rolling motion of two linearly elastic bodies based on Kalker's simplified linear theory [13]. In [49], S. Shekhar further established the conclusion that wheel slip is inevitable under the dynamic model of motion by dynamic simulation results.

R.L. Williams et al. presented a dynamic model for omnidirectional wheeled mobile robot including slip [32]. Its objective was to model and understand the sliding dynamics problem and thus real time control was not investigated. The dynamic friction coefficient was assumed to be constant and equal to the constant static friction coefficient. Thus it was intended to just capture the gross real-world friction characteristics.

2.2 Slip in Other Areas

2.2.1 Vehicle Dynamics

Different from the rigid body dynamic modelling methodologies discussed previously, slip modelling is refined in the field of vehicle dynamics and Terramechanics [11, 10], the subdiscipline of vehicle dynamics that studies the rolling interaction between wheel and terrain. In the field of WMRs, R. Balakrishna and A. Ghosal were among the earliest researchers to formulate the dynamic model of WMRs using formal terminologies from vehicle dynamics [12]. Wheel slip dynamic modelling of

wheel-terrain interaction has been studied for WMRs in [50, 51]. Slip-based traction controllers based on wheel slip dynamic modelling have been developed for field mobile robots in [52] and [17]. We were the first to model the wheel slip dynamics for PCW-based WMRs [45, 53]. Based on the slip modelling, slip avoidance conditions were obtained and effective slip minimization control schemes were presented in [45]. New slip avoidance conditions were derived and slip estimation techniques were developed in [53].

There are a large body of techniques developed for automotive, including slip-based friction estimation, traction control and terrain identification, that are valuable and applicable for WMRs. We will review some of these techniques in specific sections of this chapter.

2.2.2 Rough Terrain Mobility

The research community of rough terrain mobility, especially the the area of planetary exploration, is active in studying the slip effects of wheel-terrain interaction due to two main reasons. First, slip critically limits the localization accuracy of mobile robots. Second, slip critically determines the traction force at the wheel-terrain interface.

Wheel slip dynamic modelling of wheel-terrain interaction has been studied for WMRs in [50, 51]. Slip compensation techniques were proposed in [54, 55]. Extended Kalman filter were adopted for slip detection and estimation in [56, 57, 58]. G. Reina et al. presented several slip detection techniques using different sensing information in [59, 60]. Slip prediction using visual information was presented in [61]. Slip-based traction control were developed in [62, 17].

2.2.3 Multiple Frictional Contact Tasks

Multiple frictional contact tasks in robotics are often referred to multi-fingered grasping, legged robot walking and cooperative manipulation tasks. When the wheel-terrain interaction and wheel slip behavior are considered, it is useful to consider WMRs moving on the ground also as a multiple frictional contact task. By this analogy, some methodologies developed for multi-fingered grasping, legged robot walking and cooperative manipulation tasks can be applied for WMRs.

In multiple frictional contact tasks, force distribution at the contact points is one of the main problems to be considered because contact forces critically determine the contact behavior as well as the slip behavior of the contacts. V.R. Kuman and K.J. Waldron analyzed an important characteristic of the Moore-Penrose Generalized Inverse solution to the contact force distribution problem in [63]. This important characteristic is applied to slip control of WMRs in this thesis.

The discussion of contact force distribution in multiple frictional contact tasks is usually involved the discussion of actuation redundancy in those tasks. Actuation redundancy is common in robotic systems with closed kinematic chains such as parallel manipulators and multiple frictional contacts. Actuation redundancy in parallel mechanisms is dual to the kinematic redundancy in serial mechanisms. Redundant actuation provides many benefits including force optimization [64], singularity avoidance [19], manipulability improvement [65], impact disturbance control [66] and internal force control [24, 67].

Internal forces in multiple frictional contact tasks are closely related to the slip behavior at the contacts. R. Holmberg was the first to analyze the internal forces in WMRs and their effects on wheel slip [6]. We further analyzed the relation between

internal force and wheel slip of WMRs and provided experimental results of reducing wheel slip by controlling the internal forces [36, 45, 53].

The force distribution flexibility provided by actuation redundancy is one of the main strategies we utilize to control the slip behavior of WMRs in this thesis. In the kinematic modelling section, we will address the importance of using actuation redundancy in the design of holonomic WMRs.

2.2.4 Mobile Manipulation

Mobile manipulation is an interesting and challenging research area. Mobile manipulation systems combine the dexterous manipulation capability offered by fixed-base manipulators and the mobility offered by mobile robots. Research group lead by Professor O. Khatib from Stanford University has made many contributions to this area. Professor O. Khatib's group has developed the framework for motion planning and obstacle avoidance of mobile manipulators [68], full dynamic modelling and control of mobile manipulators [6] and cooperative mobile manipulations [43, 24].

Research group lead by Professor Marcelo Ang from National University of Singapore has collaborated with Professor O. Khatib's group and successfully demonstrated canopy polishing using mobile manipulator [69] as well as developed unified force/motion control scheme for mobile manipulator [70].

Achieving full dynamic control of mobile manipulators using the unified force/motion control scheme is challenging because dynamic control performance of WMRs is not as good as that of manipulators, especially in torque control schemes. Wheel slip effects associated with the multiple frictional contact characteristic of WMRs is the main reason causing the low dynamic control performance for WMRs. Therefore one

objective of this research is to develop slip control techniques to improve the dynamic control performance of WMRs as well as mobile manipulators.

2.3 Slip and Friction Estimation

Control of vehicle friction is quite complex and requires reliable models and estimators of friction characteristics. Reliable and accurate information about friction force generated in contact between wheel and terrain is of significant importance in many active safety systems in modern vehicles (anti-lock brake systems, traction control, vehicle dynamic systems, etc.). Many empirical dynamic friction models for describing the wheel-terrain interaction have been developed in the vehicle dynamics community such as the well known “Pacejka-Bekker magic formula” model [11] and LuGre model [71]. In [72] and [14], different dynamic friction models have been summarized and compared. However, all the empirical models are highly nonlinear in many unknown parameters, and thus they are not well-adapted for on-line real-time friction estimation. For this reason, simplified models have been proposed in the literature such as [73].

According to vehicle dynamics and terramechanics, the frictional force at the wheel-terrain interface is directly determined by the wheel slip. So obtaining slip information is important in controlling the frictional force at the wheel-terrain interface as well as controlling the slip behavior explicitly. In vehicle dynamics, slip estimation is the common way to indirectly estimate the traction force. S. Muller et al. [74] summarized different kinds of friction estimation techniques for automotive and slip-based method is the most attractive method due to its avoidance of using

extra instrumentation for sensing. Different nonlinear observers for longitudinal velocity or slip ratio estimation have been proposed by several researchers [75, 76, 77]. However, these nonlinear observers techniques are too complex for on-line real-time slip estimation. Side slip angle estimation techniques were discussed in [78, 79].

Statistical methods such as extended Kalman filtering gain more and more popularity for slip estimation in the literature of rough terrain navigation. In [55], extended Kalman filter was used to process measurements from an inertial measurement unit and visual odometry and then compared to the kinematic estimate to determine whether slippage has occurred, taking into account estimate uncertainties. Slip information was described as the difference between the extended Kalman filter estimate and the kinematic estimate. Similar techniques were presented in [80, 56, 57, 58] but different sensing information were used.

Robust estimation techniques using sliding mode observer were proposed in [81, 53]. Sliding mode observer were chosen due to its robustness to parametric uncertainty and external disturbances. Moreover, sliding mode observer was shown to provide better performance than extended Kalman filter [81].

2.4 Slip Reduction and Slip-based Traction Control

Wheels are usually independently controlled in WMRs and the problem of synchronizing and coordinating the motion of each wheel is closely related to slip effects. When the motion of different wheel is not consistent with the kinematic constraints of the system, the wheels are “fighting” with each other and thus leads to slippage. In order to reduce slippage caused by wheel motion inconsistency, wheel synchronization techniques have been proposed. The Cross-Coupling method introduced by J.

Borenstein [9] is one of the most well known methods. This method was originally introduced for differential drive WMRs and was then applied to a four-wheel-steering WMR by M. Makatchev [82]. Another method for wheel synchronization control is the concept of Pseudo-Velocity and Constraint Force Control, which was typically used to control mechanical systems with constrained motion. This method has been applied to the control of a WMR with multiple steerable wheels in [83]. The benefit of this method is that it decouples the position control and constraint force control of the system and thus provides the flexibility of constraint force control for the purpose of slip reduction.

Optimization methods for traction control and slip minimization were presented in [84, 85, 62, 52]. Researchers in the field of electric vehicle suggested to use voltage control mode of DC motors instead of current control mode to reduce slip [86, 18]. The main idea of this method is to make use of the fast torque response characteristic of voltage controlled DC motors for slip reduction. However, this method would be only effective for automotive in high driving speed conditions.

Due to the dependence of traction force on wheel slip, slip-based traction control is the main methodology in controlling the dynamic behavior of vehicles. K. Yoshida and H. Hamano presented a slip ratio regulation scheme based on the slip-traction vehicle model using standard PI controller [17]. This regulation scheme was implemented on a planetary rover for rough terrain exploration. The Research group lead by Professor Y. Hori from the University of Tokyo has developed a series of slip-based traction control techniques for electric vehicles. For longitudinal vehicle dynamics control, model following control and optimal slip ratio control were proposed to control the slip ratio of the wheels both implicitly and explicitly [87]. For lateral vehicle dynamics

control, a novel dynamic yaw-moment control and a new skid detector were presented in [88]. For terrain identification problem, road condition estimation schemes were developed using disturbance observer and recursive least square techniques in [89]. All these techniques were integrated and tested on an electric vehicle [90]. The main problem of all these slip-based traction control methods is that they are pure model-based methods and thus the accuracy of the slip-traction model has critical effects on the traction control performance.

In order to overcome the disadvantages of the previous pure model-based traction control methods, robust control techniques have been reported in the literatures. Sliding mode control [91, 92] is the most popular robust control technique applied for vehicle traction control. C. Unsal and P. Kachroo applied sliding mode techniques for both velocity observer and slip-based traction controller [81]. Observability and stability of the system were also analyzed. However, the chattering problem of sliding mode was addressed by using standard boundary layer method and only simulation results were presented. K.R. Buckholtz proposed a similar strategy as C. Unsal and P. Kachroo in [93]. Again, boundary layer method was used to solve the chattering problem and only simulation results were shown. Sliding mode techniques have been found to provide good potential in many vehicle control applications. I. Haskara et al. summarized the wide applications of sliding mode techniques in automotive control including functional optimization, disturbance estimation and compensation, state observation, friction compensation as well as slip-based traction control [94].

Although sliding mode control is robust to parametric uncertainties, previous sliding mode-based traction controllers would not perform well if terrain characteristics have severe roughness. For this reason, traction controllers are desirable to be able

to adapt to different terrains. H. Lee and M. Tomizuka have proposed an adaptive sliding mode traction controller [95] that combines adaptive on-line road condition estimation and slip-based traction control using sliding mode.

For practical use of sliding mode control, the chattering problem must be addressed. Besides the well known boundary layer method, A. Kawamura et al. presented a new chattering reduction scheme that combined disturbance observer and feed-forward control [96]. U. Utkin and J.X. Shi proposed an effective chattering reduction scheme called “integral sliding mode with low pass filtering” in [97]. The main advantage of this scheme is that the robustness of the system can be guaranteed throughout the entire response starting from the initial time instance. That is, the reaching phase in conventional sliding mode control is eliminated by applying integral sliding mode. In [98], U. Utkin summarized and compared different chattering reduction schemes for sliding mode control existing in the literature.

Previous literatures of traction control mainly discussed the longitudinal vehicle dynamics. For automotive control, lateral force as well as side slip angle control are critical for vehicle stability and safety during high speed driving conditions. Therefore many results on lateral control were also reported in literatures [99, 100, 101]. However, due to the significantly lower speed of WMRs compared to automotive, the problem of lateral slip control is not significant for WMRs except that lateral skidding situation should be avoided for steerable wheels such as powered caster wheel. Therefore we will focus on the longitudinal slip control for WMRs in this thesis.

2.5 Slip-based Terrain Identification

The purpose of terrain identification is to provide the traction controller with updated terrain information so that the controller can regulate its parameters for changing terrains. Since the slip curve describes the main characteristics of a particular terrain, most literature investigating terrain identification focus on the slip-based method. Researchers have reported different terrain identification methods using different slip model representations. K. Yi et al. presented observer-based terrain identifiers using the “Bekker-Pacejka Magic Formula” [102]. The identifiers developed by C. Canudas-De-Wit et al. utilized the LuGre model [103, 104]. The main drawback of these two approaches is that the high computational load undermines real-time applications. For achieving tractable real-time terrain identification, simplified slip models are preferred. B. Kwak and Y. Park presented an adaptive friction estimator [105] using the modified Dugoff tire model that was much simpler than the “Bekker-Pacejka Magic Formula” and LuGre model. Another well known simplified model adopted is the Kinecke model [73] which involved only two parameters. Another even simpler model was proposed based on the observation that the initial slip slope is co-related to the terrains. The slope of the slip can be used for categorizing different terrain conditions. This method has been experimentally verified to be able to distinguish different terrains for certain road conditions by F. Gustafsson [106, 107].

There are several types of estimation techniques used in terrain identification literature. Nonlinear observer techniques were used in [103, 104]; Recursive least-square techniques were used in [73, 102, 105] while extended Kalman filter were adopted

in [106, 107, 105]. In [74] and [108], several recent common terrain identification techniques were summarized.

Previous literature mainly discussed the problem of on-line terrain estimation. It would be more useful for slip avoidance if a particular terrain information was obtained before the robot enters that terrain. Terrain prediction based on visual information was proposed in [61].

CHAPTER 3

SLIP MODELLING OF WMRS WITH POWERED CASTER WHEELS (PCWS)

Slip modelling of wheeled mobile robots in both kinematics and dynamics is studied in this chapter. In both kinematic and dynamic cases, we start with deriving the non-slip models and then extend to the slip ones. One important technique we used for slip modelling and analysis is the introduction of local longitudinal and lateral coordinates besides the classical joint coordinates and operational coordinates in each wheel. As it will be seen in this and later chapters, local wheel coordinates are useful in relating the non-slip models with the slip-based wheel-ground interaction model and internal force model.

Due to the existence of different configurations for wheeled mobile robots, different modelling methodologies may be chosen. In order to show the generality of our method, we choose WMRs with PCW as our study platform. WMRs with PCW is chosen because it is a general WMR configuration in both of mobility and mechanical configuration. As it has been mentioned in previous chapters, WMRs with PCW is holonomic. Any non-holonomic WMRs can be obtained by applying extra non-holonomic constraints onto the holonomic ones. In terms of mechanical configuration, WMR with PCWs is the most general case because of its independent steering and driving characteristic in each wheel.

Another interesting problem of studying WMRs with PCWs is its actuation scheme. Either redundant or non-redundant actuation can be used in powering this type of robot. As it has been mentioned in previous chapter, redundant actuation provides many benefits over non-redundant actuation. In this chapter, we will show one of the important benefits provided by redundant actuation in WMRs with PCWs based on the derived kinematic model. Regarding the slip problem, actuation redundancy also provides the flexibility to avoid or reduce slip effects. One of the main contributions of this research is the effective utilization of actuation redundancy in slip control.

For the study of wheel slip problem, a holonomic WMR with four PCWs has been developed. Fig. 3.1 shows the actual robot and Fig. 3.2 shows the compact design of one PCW module of the robot. Each PCW module contains both steering and rolling actuators. The design is modular and thus a holonomic WMR is easily constructed by mounting several PCW modules onto a chassis. The holonomic WMR is characterized by its omnidirectional mobility, singularity free design and actuation redundancy. These characteristics of WMRs with PCWs will be analyzed through the modelling of the robot as presented in the following.

3.1 Mobility Analysis

Kinematically, the planar wheeled mobile robot with n Powered Caster Wheels is equivalent to a planar fixed base parallel manipulator with n legs and each leg consists of an RPR (revolute-prismatic-revolute) serial manipulator as shown in Fig. 3.3. The three joints in each leg are: the revolute joint (represented as σ in Fig. 3.3) connecting the wheel disk body to the ground; the prismatic joint (represented as ρr



Figure 3.1: An omnidirectional wheeled mobile robot with **4** Powered Caster Wheels. This mobile robot was developed in the Singapore Institute of Manufacturing Technology and it was the main test-bed for this research. Image courtesy of the Singapore Institute of Manufacturing Technology.



Figure 3.2: The compact design of the Powered Caster Wheel (PCW) module used in the mobile robot shown in Fig. 3.1. Every PCW module is powered by two actuators. One is for steering and the other one for rolling. The rolling axis and the steering axis of the PCW are perpendicular to each other and there is a non-zero offset distance between these two axes. The offset is critical in generating the omnidirectional motion for WMRs with PCWs.

in Fig. 3.3) connecting the wheel disk body to the steering fork link; the revolute joint (represented as ϕ in Fig. 3.3) connecting the steering fork link to the moving platform of the mobile robot.

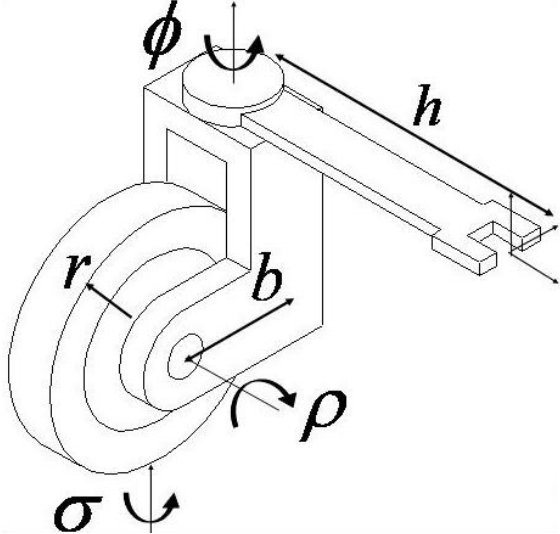


Figure 3.3: A Powered Caster Wheel can be considered as a serial manipulator with **3** joints in each instance. The **3** joints are: the instantaneous revolute joint (σ) whose rotation axis is the vertical axis at the contact point between wheel and ground; the virtual prismatic joint (ρr) whose translational axis is the forward direction of the wheel caused by the wheel rolling motion; the revolute joint (ϕ) that represents the steering motion of the wheel.

The purpose of deriving the *Mobility* of the mobile robot with Powered Caster Wheels is to show its omnidirectional capability. As we only consider planar wheeled mobile robots, it is expected that the mobility of the mobile robot should be 3 for it to be omnidirectional. For mechanical systems that are subjected to independent constraints by the joints, the mobility of the system can be computed using the Grubler formula [109].

$$DOF = 3(m - 1) - 2l_1 - l_2 \quad (3.1)$$

where F is the mobility of the system, m is the number of rigid bodies, l_1 is the number of joints that have 1 degree-of-freedom while l_2 is the number of joints that have 2 degrees-of-freedom. In the case of wheeled mobile robots with n Powered Caster Wheels, those parameters are given as

$$m = 2 + 2n$$

$$l_1 = 3n$$

$$l_2 = 0$$

There are two rigid bodies for every Powered Caster Wheel: the wheel disk body and the steering fork link. The ground is also counted as a rigid body in the mobility computation. Together with the moving platform of the mobile robot, the total number of rigid bodies in the system is $2 + 2n$. As each Powered Caster Wheel module can be considered as a 3DOF serial manipulator (Fig. 3.3), the number of 1DOF joint is $3n$. There is no 2DOF joint in the system, thus the number of 2DOF joint is zero.

With the above values, the total mobility of planar wheeled mobile robots with n powered caster wheels is computed from Eq. 3.1 as

$$DOF = 3(2 + 2n - 1) - 2 \times 3n - 0 = 3 \quad (3.2)$$

The result is as expected to be 3 and this confirms the robot is omnidirectional. Theoretically, it can be seen from Eq. 3.2 that the mobility of WMRs with PCWs are independent of the number of wheels. However, as each PCW module has only two actuators, one wheel is not sufficient to provide all the 3DOF mobility for planar motion. Therefore, minimum two PCWs are needed for designing WMRs with PCWs.

3.2 Kinematic Modelling

3.2.1 Displacement Kinematic Model

R. Holmberg, one of the inventors of Powered Caster Wheel (PCW), commented that “Because of the nonholonomic constraints at the wheels, it is not possible to get a relationship between the joint positions and the robot positions” [23]. However, since the mobile robot being analyzed is omnidirectional, we can model the wheeled mobile robot as a planar parallel manipulator with fixed base that has equivalent instantaneous kinematics as the wheeled mobile robot. Therefore, in each instance, we can still make use of the displacement kinematic model of the equivalent fixed base parallel manipulator to compute the small displacement in each control sample period. The integration of these small displacements forms the position and orientation trajectory of the moving platform in Cartesian coordinate. This is an alternative to computing the odometry of the wheeled mobile robot using the Jacobian matrix of the robot and it should provide more accurate odometry. In this case, it is meaningful to derive the displacement kinematic model of the wheeled mobile robot.

Different methods can be used to model the displacement kinematics of parallel manipulators. In follows, we will adopt **PoE** [110] to derive the displacement kinematic model for the wheeled mobile with Powered Caster Wheels. As the displacement kinematic model for the wheeled mobile robot is valid only instantaneously, it is convenient to choose the spatial frame to be the same as the body frame fixed at the center of the moving platform at each instance. Another reason for this treatment is that it is natural to describe the motion of wheeled mobile robots in the instantaneous spatial frame that has the same orientation as the body frame. In order to

simplify the **PoE** equations for the robot, the reference configuration is chosen such that the instantaneous spatial frame coincident with the body frame (Eq. 3.3).

It is noted that although the motion of planar robots can be represented as the **SE(2)** displacement group, we will derive the general **SE(3)** representation to make the equations applicable for the case of 3 dimensional space.

$$T_{gt}(0) = \begin{bmatrix} I & \begin{pmatrix} 0 \\ 0 \\ 0 \end{pmatrix} \\ 0 & 1 \end{bmatrix} \quad (3.3)$$

The twist of each joint in leg i ($i = 1, 2, \dots, n$) are given as

$$\xi_{i1} = \begin{bmatrix} -\omega_{i1} \times p_{i1} \\ \omega_{i1} \end{bmatrix} \quad (3.4)$$

$$\xi_{i2} = \begin{bmatrix} v_{i2} \\ 0 \end{bmatrix} \quad (3.5)$$

$$\xi_{i3} = \begin{bmatrix} -\omega_{i3} \times p_{i3} \\ \omega_{i3} \end{bmatrix} \quad (3.6)$$

The subscript $(i1)$ represents the first joint of leg i which is the instantaneous twist joint at the contact point between the wheel and the contact surface. Similarly, $(i2)$ represents the second joint of leg i which is the instantaneous prismatic joint generated by the rolling motion of the wheel; $(i3)$ represents the third joint of leg i which is the steering revolute joint of the wheel.

The twist axes of those revolute joints and the selected reference points on the rotation axes of revolute joints are given as follows.

$$\omega_{i1} = \omega_{i3} = [0, 0, 1]^T$$

$$v_{i2} = \begin{bmatrix} \cos(\sigma_i) \\ \sin(\sigma_i) \\ 0 \end{bmatrix}$$

$$p_{i3} = h \begin{bmatrix} \cos(\beta_i) \\ \sin(\beta_i) \\ 0 \end{bmatrix}$$

$$p_{i1} = p_{i3} - bv_{i2}$$

Finally, the instantaneous configuration of the body frame in the instantaneous spatial frame is derived for each leg of the parallel mechanism using the **PoE** formula as follows.

$$T_{gt}(q_i) = e^{\hat{\xi}_{i1}} e^{\hat{\xi}_{i2}} e^{\hat{\xi}_{i3}} T_{gt}(0) \quad (3.7)$$

After simplifying the analytical form of the above **PoE** equations, we obtain the instantaneous rotation matrix and position vector of the body frame relative to the instantaneous spatial frame as follows.

$$R_{gt}(q_i) = \begin{bmatrix} \cos(\phi_i + \sigma_i) & -\sin(\phi_i + \sigma_i) & 0 \\ \sin(\phi_i + \sigma_i) & \cos(\phi_i + \sigma_i) & 0 \\ 0 & 0 & 1 \end{bmatrix} \quad (3.8)$$

$$P_{gt}(q_i) = \begin{bmatrix} h(\cos(\beta_i) - \cos(\beta_i + \phi_i + \sigma_i)) + (b + r\rho_i)\cos(\phi_i + \sigma_i) - b\cos(\sigma_i) \\ h(\sin(\beta_i) - \sin(\beta_i + \phi_i + \sigma_i)) + (b + r\rho_i)\sin(\phi_i + \sigma_i) - b\sin(\sigma_i) \\ 0 \end{bmatrix} \quad (3.9)$$

We define the joint space configuration q_i for leg i and the task space configuration $x(q_i)$ as

$$q_i = \begin{bmatrix} \sigma_i \\ \rho_i \\ \phi_i \end{bmatrix}$$

$$x(q_i) = \begin{bmatrix} P_x \\ P_y \\ \theta \end{bmatrix}$$

In planar case, we can represent $R_{gt}(q_i)$ and $P_{gt}(q_i)$ in a simplified form with $Xx(q_i)$ and q_i as

$$x(q_i) = \begin{bmatrix} h(\cos(\beta_i) - \cos(\beta_i + \phi_i + \sigma_i)) + (b + r\rho_i)\cos(\phi_i + \sigma_i) - b\cos(\sigma_i) \\ h(\sin(\beta_i) - \sin(\beta_i + \phi_i + \sigma_i)) + (b + r\rho_i)\sin(\phi_i + \sigma_i) - b\sin(\sigma_i) \\ \phi_i + \sigma_i \end{bmatrix} \quad (3.10)$$

The loop closure constraints imposed by all the wheels can be represented as

$$x(q_1) = x(q_2) = \dots = x(q_n) \quad (3.11)$$

As the instantaneous of the twist angle σ_i is not measurable, it is required to compute this angle from the measurable joint angles ρ_i and ϕ_i assuming there is no slip on the wheels. Based on the loop closure equation 3.11, we can compute the instantaneous twist angle σ_i with the measurable joint angles from any two wheels i and j . After simple algebraic calculation by making use of following two trigonometric sum-difference formulas

$$\begin{aligned} \sin(\alpha \pm \beta) &= \sin(\alpha)\cos(\beta) \pm \cos(\alpha)\sin(\beta) \\ \cos(\alpha \pm \beta) &= \cos(\alpha)\cos(\beta) \mp \sin(\alpha)\sin(\beta) \end{aligned}$$

we obtain following equations

$$a(\phi_i, \rho_i, \phi_j, \rho_j)\cos(\sigma_i) + b(\phi_i, \rho_i, \phi_j, \rho_j)\sin(\sigma_i) = c(\phi_i, \rho_i, \phi_j, \rho_j) \quad (3.12)$$

for $i \neq j$ and $i, j = 1, \dots, n$.

The coefficients $a(\phi_i, \rho_i, \phi_j, \rho_j)$, $b(\phi_i, \rho_i, \phi_j, \rho_j)$ and $c(\phi_i, \rho_i, \phi_j, \rho_j)$ are all algebraic formulations of the trigonometric functions of those measurable joint angles. With the unmeasurable instantaneous twist joint angles from Eq. 3.12 and the loop closure

equations 3.11, the *forward displacement kinematic model* of the robot can be written in the following form

$$x = FK(\phi_i, \rho_i, \phi_j, \rho_j) \quad (3.13)$$

and by similar algebraic and trigonometric manipulations, the *inverse displacement kinematic model* of the robot can be written in the following form

$$\begin{bmatrix} \phi_i \\ \rho_i \end{bmatrix} = IK_i(x) \quad (3.14)$$

where $FK(\cdot)$ and $IK_i(\cdot)$ are common algebraic and trigonometric formulations. It is noted that both Eq. 3.13 and Eq. 3.14 are only valid instantaneously.

3.2.2 Differential Kinematic Model

The “Pure Rolling Without Slipping” Condition

The “pure rolling without slipping” condition describes the ideal rolling motion of a wheel relative to the ground. The kinematic modelling of the “pure rolling without slipping” condition is derived as follows. We define the frames and variables on the wheel as shown in Fig. 3.4. P and C denote respectively the wheel center and the wheel-ground contact point. X_wPY_w is a wheel frame whose origin is at the wheel center. The x axis points towards the forward direction of wheel motion while the y axis aligns with the rolling axis of the wheel. Following the terminologies of vehicle dynamics, the x axis of wheel frame X_wPY_w is called *longitudinal* axis and its y axis is called *lateral* axis. The velocity of wheel center P is defined as $\dot{p} = [v_x, v_y]^T$ while the velocity between wheel and ground at contact point C is defined as $\dot{\varepsilon} = [\dot{\varepsilon}_x, \dot{\varepsilon}_y]^T$ and both of these two velocity vectors are expressed in the wheel frame.

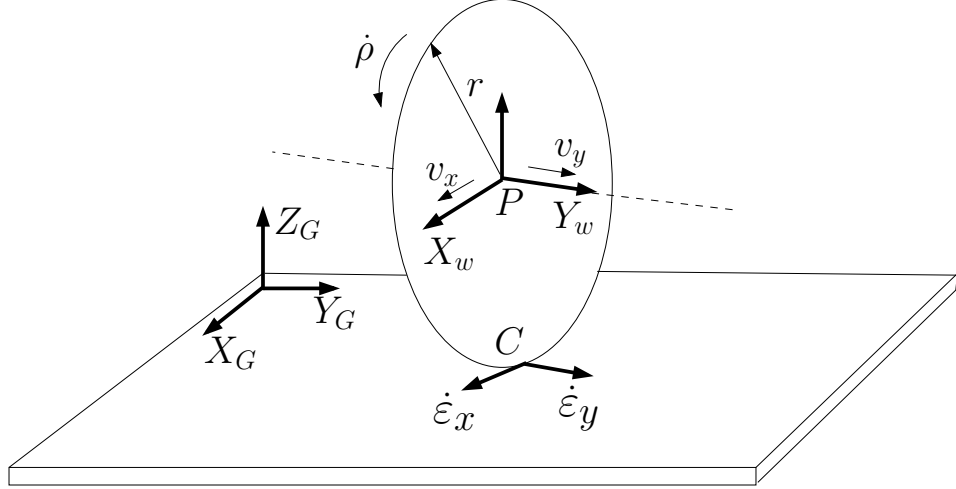


Figure 3.4: Velocity of wheel center and slip velocity of the contact between wheel and ground.

The “pure rolling without slipping” condition can be mathematically described as two separate conditions:

$$\begin{aligned}\dot{\varepsilon}_x &= 0 \\ \dot{\varepsilon}_y &= 0\end{aligned}\tag{3.15}$$

In vehicle dynamics terminologies, $\dot{\varepsilon}_x$ is called *longitudinal slip* and $\dot{\varepsilon}_y$ called *lateral slip*. Among these two conditions, it should be noted that an equivalent and more useful representation of the zero longitudinal slip condition is given as the “pure rolling” relation:

$$v_x = r\dot{\rho}\tag{3.16}$$

where $\dot{\rho}$ is the angular velocity of the wheel and r is the wheel radius. This relation also implies that

$$\dot{\varepsilon}_x = r\dot{\rho} - v_x\tag{3.17}$$

Now we apply the “pure rolling without slipping” condition to derive a general kinematic model of a WMR with n PCWs.

Robot Model

Table 3.1: Definition of parameters and variables in Fig. 3.5

$X_G O_G Y_G$	robot global frame
$X_L O_L Y_L$	robot local frame with its origin O_L at center of the mobile robot
$X_{wi} P_i Y_{wi}$	frame attached at the center of wheel i
S_i	steering point of the wheel i
P_i	center of the wheel i
p_i	position vector of P_i relative to O_L
v	translational velocity of the mobile robot measured at point O_L
ω	rotational velocity of the mobile robot
$\dot{\rho}_i$	angular velocity of wheel i
$\dot{\phi}_i$	steering velocity of wheel i
ϕ_i	steering angle of wheel i
β_i	the angle of steering point i relative to the local frame
θ	orientation of the mobile robot relative to the global frame
r	wheel radius
b	offset between steering point and center of the wheel
h	distance between steering point and center of the mobile robot

The planar diagram of a mobile robot with n PCWs is shown in Fig. 3.5. Table 3.1 lists the definitions of the frames, parameters and variables.

The steering velocity of a PCW will generate a lateral motion at the wheel center if seen from the chassis of the mobile robot. Based on this observation, we can derive a similar relation as Eq. 3.17 for the lateral slip:

$$\dot{\varepsilon}_y = b\dot{\phi} - v_y \quad (3.18)$$

Ideally, each wheel's center velocity $\dot{p}_i = [v_{xi}, v_{yi}]^T$ can be obtained from the robot center velocity $[v, \omega]^T$ by the relationship:

$${}^L \dot{p}_i = {}^L v - {}^L p_i \times {}^L \omega$$

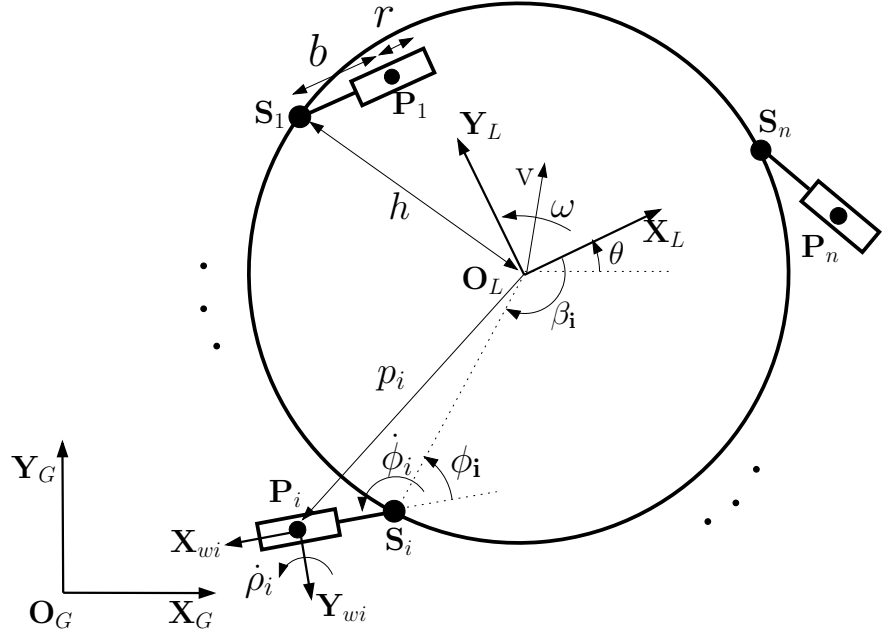


Figure 3.5: Frame assignments, parameter and variable definitions of a mobile robot with n Powered Caster Wheels. See Table 3.1 for the detailed explanations of the notations.

where the left-superscript L of the variables denote that the corresponding variable expressed in the local frame of the robot.

By defining \hat{p}_i as the cross product operator associated with p_i , cross product $p_i \times \omega$ is simplified as: $\hat{p}_i \omega$. Above equation can now be rewritten in matrix form:

$${}^L\dot{p}_i = \begin{bmatrix} I_{2 \times 2} & -{}^L\hat{p}_i \end{bmatrix} \begin{bmatrix} {}^Lv \\ {}^L\omega \end{bmatrix} \quad (3.19)$$

To express wheel center velocities in individual wheel frame, pre-multiplying Eq. 3.19 with the rotation matrix ${}^{wi}R_L$ where

$$^{wi}R_L = \begin{bmatrix} \cos(\beta_i - \phi_i) & \sin(\beta_i - \phi_i) \\ -\sin(\beta_i - \phi_i) & \cos(\beta_i - \phi_i) \end{bmatrix}$$

The velocity of each wheel center expressed in wheel local frame can be written as:

$${}^{wi}\dot{p}_i = [{}^{wi}R_L \quad -{}^{wi}R_L {}^L\hat{p}_i] \begin{bmatrix} {}^L\boldsymbol{v} \\ {}^L\boldsymbol{\omega} \end{bmatrix} \quad (3.20)$$

For the convenience of analysis, we will ignore left-superscripts in subsequent analysis.

In order to describe equations derived above for the case of **n**-wheeled robot, we define the following variables:

- slip $\dot{\varepsilon}$:

$$\dot{\varepsilon} = [\dot{\varepsilon}_{x1}, \dot{\varepsilon}_{y1}, \dots, \dot{\varepsilon}_{xn}, \dot{\varepsilon}_{yn}]^T$$

- wheel center velocity \dot{p} :

$$\dot{p} = [v_{x1}, v_{y1}, \dots, v_{xn}, v_{yn}]^T$$

- joint velocity \dot{q} :

$$\dot{q} = [\dot{\rho}_1, \dot{\phi}_1, \dots, \dot{\rho}_n, \dot{\phi}_n]^T$$

- operational velocity \dot{x} :

$$\dot{x} = [v, \boldsymbol{\omega}]^T$$

Extension of Eq. 3.20 for n -wheeled robot using matrix representation can now be given as

$$\dot{p} = A\dot{x}$$

where:

$$\mathbf{A} = \begin{bmatrix} {}^{w1}R & -{}^{w1}R\hat{p}_1 \\ \vdots & \vdots \\ {}^{wn}R & -{}^{wn}R\hat{p}_n \end{bmatrix}_{2n \times 3} \quad (3.21)$$

In actual case, we have measurements of the joint velocities \dot{q} . The wheel center velocities \dot{p} can be *sensed* by following equations

$$\dot{p}_{sensed} = B\dot{q}$$

where:

$$\mathbf{B} = \begin{bmatrix} r & 0 & \dots & 0 & 0 \\ 0 & b & \dots & 0 & 0 \\ \vdots & 0 & \ddots & 0 & 0 \\ 0 & 0 & \dots & r & 0 \\ 0 & 0 & \dots & 0 & b \end{bmatrix}_{2n \times 2n} \quad (3.22)$$

Combining Eq. 3.17 and 3.18, we obtain

$$\dot{\varepsilon} = \dot{p}_{sensed} - \dot{p} \quad (3.23)$$

Based on condition 3.15, the “pure rolling without slipping” kinematic model of the robot can be given as

$$A\dot{x} = B\dot{q} \quad (3.24)$$

Inverse Differential Kinematic Model

Since matrix B is a diagonal matrix and always invertible, the inverse differential kinematic model is obtained as follows.

$$\dot{q} = B^{-1}A\dot{x} \quad (3.25)$$

It is noted that the inverse kinematics is useful for the motion controller to compute the desired trajectory for individual joint.

Forward Differential Kinematic Model

Even without considering the slip effect, the derivation of forward kinematics for mobile robots is not as straight-forward as their inverse kinematics due to the parallelism characteristic of mobile robots. In general, the forward kinematics of parallel

mechanisms is a under-determined problem as can be seen from the non-square size of matrix \mathbf{A} . A common way to resolve this problem is the use of generalized inverse of non-square matrix. When the pseudo-inverse of matrix \mathbf{A} is used, the forward kinematics of the mobile robot can be derived as:

$$\dot{x} = \mathbf{A}^\dagger \mathbf{B} \dot{q} \quad (3.26)$$

where pseudo-inverse of matrix A is given as

$$\mathbf{A}^\dagger = (\mathbf{A}^T \mathbf{A})^{-1} \mathbf{A}^T \quad (3.27)$$

By using the pseudo-inverse, Eq. 3.26 leads to a solution of \dot{x} that minimizes, in a least-square manner, the differences between the sensed wheel center velocity \dot{p}_{sensed} and the actual wheel center velocity \dot{p} .

Besides the generalized inverse method discussed here, many other methods such as optimization method [111] and statistical method [112] have been reported for resolving the forward kinematics of parallel mechanisms. For the case of wheeled mobile robots, statistical method has been claimed to be promising solution when there are slip and other uncertainties in the task.

Kinematic Slip Model

When the “pure rolling without slipping” condition 3.15 is not satisfied, the kinematic model of WMRs will have to take into account the slip effect. Based on Eq. 3.23 and 3.24, the kinematic model that takes into account the slip defined as $\dot{\varepsilon}$, can be written as

$$\dot{\varepsilon} = \mathbf{B} \dot{q} - \mathbf{A} \dot{x} \quad (3.28)$$

3.2.3 Odometry

In the case of wheeled mobile robots, *odometry* (also called *dead-reckoning*) refers to the estimation of absolute configuration of the wheeled mobile robot in Cartesian coordinates from the wheel motion measurements with sensors on the wheels. Due to the nonholonomic constraints of wheel rolling motion, the odometry can only be calculated by accumulating the wheel motion through numerical integration. The absolute configuration of the wheeled mobile robot represented in a selected global frame G is updated in every sampling period by the following equations

$$P_{gt}(k) = P_{gt}(k-1) + R_{gt}(\theta(k), z)\Delta P_{gt}(k) \quad (3.29)$$

$$\theta(k) = \theta_o + \sum_{j=1}^k \Delta\theta(j) \quad (3.30)$$

There are different ways of updating the $\Delta P_{gt}(k)$ and $\Delta\theta(k)$ that will affect the precision of the odometry. In below we present two odometry algorithms that are based on the displacement kinematic model and the differential kinematic model derived in the previous sections, respectively.

Odometry with Displacement Kinematic Model

The first odometry method is based on the forward displacement kinematic model 3.13 and $\Delta P_{gt}(k)$ and $\Delta\theta(k)$ are computed as follows.

$$\Delta P_{gt}(k) = FK(\Delta\phi_i(k), \Delta\rho_i(k), \Delta\phi_j(k), \Delta\rho_j(k)) \quad (3.31)$$

$$\Delta\theta(k) = \Delta\phi_i(k) + \Delta\sigma_i(k) \quad (3.32)$$

where

$$\Delta\phi_i(k) = \phi_i(k) - \phi_i(k-1)$$

$$\Delta\rho_i(k) = \rho_i(k) - \rho_i(k-1)$$

$$\Delta\sigma_i(k) = \sigma_i(k) - \sigma_i(k-1)$$

Odometry with Differential Kinematic Model

The second odometry method is based on the forward differential kinematic model 3.26 and $\Delta P_{gt}(k)$ and $\Delta\theta(k)$ are computed as follows.

$$\begin{bmatrix} \Delta P_{gt}(k) \\ \Delta\theta(k) \end{bmatrix} = A^\dagger B \Delta q \quad (3.33)$$

where Δq is also computed from the backward difference of the measurable joint angles.

3.2.4 Singularity Analysis

The purpose of this section is to show the necessity of using redundant actuation scheme to address the singularity avoidance problem for WMRs with PCWs.

Modelling the kinematics of parallel mechanisms in the form of Eq. 3.24 is often adopted in parallel mechanism literatures. This form of modelling is especially useful for singularity analysis of parallel mechanisms because it is easily seen, from this structure of kinematic equations, the three types of singularities for parallel mechanisms that can be described in following conditions:

- Type I: **A** is rank deficient.
- Type II: **B** is rank deficient.

- Type III: \mathbf{A} and \mathbf{B} are both rank deficient.

As mentioned previously that matrix \mathbf{B} is always square and invertible for both non-redundant and redundant actuators. This implies that Type II and Type III singularities do not exist for WMRs with PCW. Thus it is only left with Type I singularity for consideration. Type I singularity analysis requires the evaluation of the rank of matrix \mathbf{A} . This evaluation is done in the following two cases.

Case 1: Full Actuation

Full actuation means all actuators of the robot (all \mathbf{n} wheels with 2 actuators in each wheel) are powered.

For the trivial case when $\mathbf{n} = 1$, it is obvious that even though matrix \mathbf{A} is full rank, it does not have enough actuators to perform 3DOF motion for planar mobile robot.

For the case when $\mathbf{n} \geq 2$, the determinant of $\mathbf{A}^T \mathbf{A}$ is

$$\det(\mathbf{A}^T \mathbf{A}) = n^2 \sum_{i=1}^n \hat{p}_i^T \hat{p}_i - n \left(\left(\sum_{i=1}^n \hat{p}_i \right)^T \left(\sum_{i=1}^n \hat{p}_i \right) \right) \quad (3.34)$$

It is noted that the rotation matrix ${}^{wi}R_L$ does not appear in the above equation. This is due to the fact that rotation matrix ${}^{wi}R_L$ is orthonormal.

It is a known property that the sum of the magnitude of vectors is larger than or equal to the magnitude of the sum:

$$\sum_i \|\hat{p}_i\| \geq \left\| \sum_i \hat{p}_i \right\| \quad (3.35)$$

Therefore $\det(\mathbf{A}^T \mathbf{A}) > 0$. This means that full actuation for two PCWs is enough to guarantee a singularity-free omnidirectional mobile robot design using PCW. This proof confirms the findings in [25] where this actuation scheme was cited as one of the “admissible arrangements” for a singularity-free mobile robot.

Case 2: Selective Actuation

While powering all the 4 actuators of two PCWs is enough to guarantee singularity-free design for PCW-based mobile robots, the same number of actuators when utilized to power only the steering or rolling actuator of the wheels (selective actuation) are not enough to be singularity-free. It is difficult to prove this case through the symbolical expression for $\det(\mathbf{A}^T \mathbf{A})$ as the expression is complex. However, singular configurations can be found for all cases of selective actuation where there are no two fully powered wheels. Without loss of generality, we show examples of singular configurations in Fig. 3.6 for the case of mobile robot with three PCWs: one wheel is actuated for both steering and rolling, while the other two has either steering or rolling actuation.

These singular configurations, resulting from the rank deficiency of matrix \mathbf{A} , cause the robot to be uncontrollable in the singular direction(s). This means that even though all the active joints are locked, for example, the mobile robot is not able to resist force/moment in the singular direction [113]. In our examples, the mobile platform cannot resist external force/moment that causes it to rotate around wheel-ground contact point C_1 (Fig. 3.6).

Based on the above analysis, the conclusion drawn here is: to guarantee singularity-free omnidirectional mobile robot with PCWs, the minimum number of PCW is 2 and their 4 actuators have to be powered. Since utilization of minimal 4 actuators implies the use of redundant actuation, this result supports the choice of redundant actuation for PCW-based WMRs. In the later chapters of this thesis, we will further demonstrate the benefits of adopting redundant actuation for the purpose of slip control.

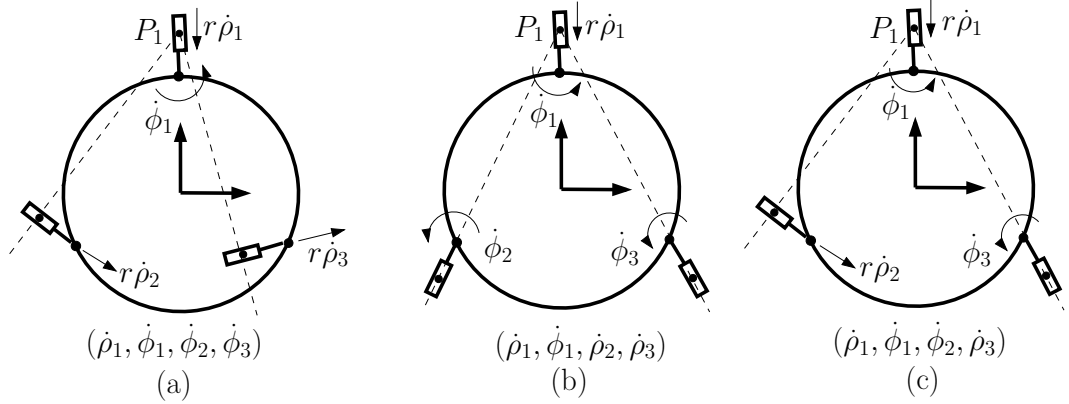


Figure 3.6: Examples of a singular configuration in the mobile robot with Powered Caster Wheels for different selective actuation situations. In (a), only one rolling actuator from one of the wheels is active. In (b), only one steering actuator from one of the wheels is active. In (c), only one wheel is fully actuated and the rest of wheels are selectively actuated.

The main results of the singularity analysis presented in this section have been published in our previous works [114] and [115].

3.3 Dynamic Modelling

We separate the dynamic modelling of wheeled mobile robots into two different parts: one is the whole vehicle rigid body dynamics and the other is the interaction dynamics between individual wheel and the ground. The entire vehicle rigid body dynamics can be modelled using classical Newton-Euler or Lagrangian formulation while the wheel-ground interaction can be modelled using the ideas from vehicle dynamics and terramechanics.

Most literature only consider the whole vehicle rigid body dynamics based on the assumption that there is no slippage on the wheel-ground interaction. In this section, we will first derive the rigid body dynamic model of WMRs without considering the slip effect. Different from classical modelling methodologies, a novel method is

adopted to model the rigid body dynamics of the robot without explicitly imposing the closed-chain constraints on the dynamic equations. Next, we will introduce the slip-based wheel-ground interaction model following ideas from the area of vehicle dynamics.

3.3.1 Augmented Object Model

Since WMRs belong to closed-chain mechanism, the closed-chain constraints must be considered when modelling their dynamics. Those closed-chain constraints are explicitly described in the dynamic equations when classical Newton-Euler or Lagrangian formulation is used. For example, when modelling WMRs dynamics using Lagrangian formulation with joint angles as the generalized coordinates, Lagrangian multipliers are used to describe the closed-chain constraints. This would make the dynamic computation inefficient for real time implementation.

In order to obtain an efficient dynamic model for WMRs, the *Augmented Object Model (AOM)* ([43]) is adopted. The **AOM** was originally introduced to model the dynamics of multiple cooperative manipulators using the well known *Operational Space Formulation (OSF)* [44]. The **OSF** is based on the classical Lagrangian formulation but it chooses the operational coordinates as generalized coordinates for the dynamic equations. The mobility of the robot is generally equal to the number of generalized coordinates. With the same characteristic, the **AOM** is able to model the dynamics of closed-chain mechanisms (such as multiple cooperative manipulators) without the need to explicitly impose the closed-chain constraints on the dynamic equations. Since WMR is also closed-chain mechanism, we can adopt the **AOM** for its dynamic modelling.

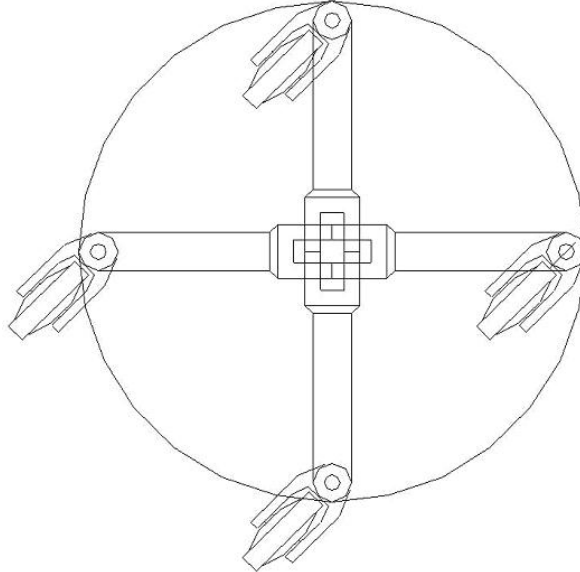


Figure 3.7: By considering each Powered Caster Wheel (PCW) as a serial manipulator with **3** joints as shown in Fig. 3.3, a mobile robot with PCWs can be considered as cooperative serial manipulators grasping a common object at the end-effectors of each manipulator. By this consideration, the Augmented Object Model can be used to model the dynamics of WMRs with PCWs.

In order to adopt the **AOM**, we consider a PCW module as a 3-DOF serial manipulator (Fig. 3.3) and PCW-based WMR as a cooperative manipulator system (Fig. 3.7).

The operational space dynamic model of a serial manipulator is given as:

$$F = \Lambda \ddot{x} + \vartheta + g \quad (3.36)$$

where **F** and **x** are the operational forces and operational coordinates of the system. **Λ**, **ϑ** and **g** are respectively the kinematic energy matrix, Coriolis/centrifugal force vector and gravitational force vector represented in the operational space.

Since we only consider mobile robots in planar space, the gravitational force vector **g** will be ignored in subsequent discussion.

The Augmented Object Model states that the dynamics of the cooperative system is obtained by summing the operational space dynamics of each robot and the load [43]. The augmented kinetic energy matrix, augmented Coriolis/centrifugal force vector are given as:

$$\Lambda_{\oplus} = \sum_{i=1}^n \Lambda_i + \Lambda_{\ell} \quad (3.37)$$

$$\vartheta_{\oplus} = \sum_{i=1}^n \vartheta_i + \vartheta_{\ell} \quad (3.38)$$

where Λ_i denotes the kinetic energy matrix of manipulator \mathbf{i} in the cooperative system while Λ_{ℓ} denotes the kinetic energy matrix of the load “grasped” by all the manipulators of the cooperative system. Similarly, ϑ_i and ϑ_{ℓ} denote the Coriolis/centrifugal force vector of manipulator i and the load, respectively.

The dynamics of the augmented system in operational space can then be written as:

$$F_{\oplus} = \Lambda_{\oplus} \ddot{x} + \vartheta_{\oplus} \quad (3.39)$$

Appendix B explains the detail of deriving the dynamic model for the robot shown in Fig. 3.1 using the Augmented Object Model.

Define

$$F_c = [F_{x1}, F_{y1}, \dots, F_{xn}, F_{yn}]^T$$

as the wheel contact forces and

$$\Gamma = [\tau_{\rho 1}, \tau_{\phi 1}, \dots, \tau_{\rho n}, \tau_{\phi n}]^T$$

as the joint torques. Based on the force/velocity duality, the relations between the augmented operational forces \mathbf{F}_{\oplus} , wheel center force \mathbf{F}_c and joint torque $\mathbf{\Gamma}$ are given

as:

$$F_{\oplus} = A^T F_c \quad (3.40)$$

and

$$\Gamma = B^T F_c \quad (3.41)$$

Since $B^T = B$, Eq. 3.41 is equivalent to:

$$\Gamma = BF_c \quad (3.42)$$

R. Holmberg was the first to use the Augmented Object Model to model the dynamics of WMRs ([6]). However, he divided the chassis of the mobile robot into a number of links that is equal to the number of wheels. He then summed the dynamics of each wheel modules with a “zero” mass load to compute the augmented dynamics. Since the dynamic parameters are dependent on the mass distribution of the rigid bodies, modelling the chassis as a sperate link will decrease the model accuracy. We modify R. Holmberg’s modelling by considering the third link in each PCW “manipulator” as zero mass rigid body. We then treat the chassis body as the common body grasped by the PCW “manipulators”. With this modification, the accuracy of the dynamic model is improved.

3.3.2 Slip-based Wheel-Ground Interaction Model

Modelling the wheel-ground interaction is very different from the case of modelling rigid body dynamics. There is no solid and fully established dynamic formulation as in the case of rigid body dynamic modelling using Newton-Euler or Lagrangian formulation. Wheel-ground interaction is a very complex dynamic behavior depending on material properties of both the ground and the wheel as well as the contact conditions. Vehicle dynamics [10] and Terramechanics [11] are the main areas that study

the wheel-ground interaction. However, the results are mainly based on empirical results. Most empirical models, such as distributed models, “Bekker-Pacejka’s Magic Formula” [11], LuGre model [71], are based on their own experimental results. In mobile robotics community, researchers working on rough terrain mobility or planetary exploration also consider the wheel-ground interaction problem. However, there is no systematic study on using wheel-ground interaction for slip control in mobile robotics community.

In this research, we consider the wheel-ground interaction effects from vehicle dynamics point of view to facilitate the analysis of wheel slip. Regarding the empirical characteristic of most wheel-ground interaction models, simplified model for the ease of real time implementation is adopted and robust control techniques for slip control are proposed.

If we consider the ground and the mobile robot as a whole system, the contact forces generated at each contact point are, in fact, the constraint forces between the ground and the mobile robot. According to the principle of virtual work, when the non-slip kinematic constraints are satisfied, the virtual work done by the constraint forces is zero. Under the ‘pure rolling without slipping’ assumption, the dynamic modelling ignores the ideal constraint forces and only describes the relationship between joint torques (input forces) and operational space forces (inertial forces and other external forces). However, when wheel slip occurs, the virtual work done by the constraint forces is no longer zero, thus the dynamic modelling needs to consider the contact forces to account for the wheel slip effects.

Since wheel-ground interaction is mainly introduced by the wheel rolling motion, only the longitudinal dynamics and longitudinal slip effect of the wheel is considered.

In longitudinal dynamics, an important quantity that describes the slip behavior of the wheel is the *Slip Ratio* defined as

$$\lambda = \frac{r\dot{\rho} - v_x}{\max(r\dot{\rho}, v_x)} \quad (3.43)$$

The full wheel-ground interaction model includes the vehicle rigid body dynamics and the wheel-ground interaction dynamics. In follows we derive these two models separately.

Vehicle Dynamics

The vehicle dynamics is the relationship between contact forces \mathbf{F}_c and operational forces \mathbf{x} . The equations of motion can be obtained using the Augmented Object Model as follows.

$$\Lambda_{\oplus}\ddot{x} + \vartheta_{\oplus} = A^T F_c \quad (3.44)$$

Wheel Dynamics

As only longitudinal wheel dynamics is considered, the equations of motion describing the rolling dynamics of the wheel are as follows.

$$I_{\rho}\ddot{\rho} = \tau_{\rho} - F_x r \quad (3.45)$$

where I_{ρ} is the inertia of the wheel body.

Since lateral wheel dynamics is not considered, the lateral forces F_y are computed based on the system statics as

$$\tau_{\phi} = F_y b$$

In classical vehicle dynamics, other effects such “rolling resistance” and “aligning torque” are considered. They are ignored in this research as these effects are trivial for WMRs with PCWs working in indoor planar grounds.

Slip-Friction Model

The longitudinal contact forces F_x can be described in the form of classical frictional force representation as

$$F_x = \mu F_z \quad (3.46)$$

where μ is the friction coefficient that depends on the material properties of the wheel and ground and the relative motion between the wheel and ground.

Variations of friction coefficient μ with slip ratio λ is an important characteristic curve [10] in vehicle dynamics (Fig. 3.8). In a typical $\lambda - \mu$ curve, μ increases with λ until it reaches its peak value μ_p which corresponds to slip ratio λ_p . Further increase of the slip ratio beyond λ_p results in rapid decrease of μ and the wheel slides or spins on the ground unstably [116].

Most of the reported $\lambda - \mu$ curves for different terrains were determined by experiments. There are also many analytical models reported in the literatures that aim to formulate the slip-friction model. However, those models are usually too complicated to be used in practice. In this research, we adopt the simple Kinecke Model [73] (Eq. 3.47) to describe the $\lambda - \mu$ curve.

$$\mu = \frac{2\mu_p \lambda_p \lambda}{\lambda_p^2 + \lambda^2} \quad (3.47)$$

The Kinecke Model is chosen because it models the $\lambda - \mu$ curve using only the two important parameters of the terrain: the peak friction coefficient μ_p and the critical slip ratio λ_p corresponding to μ_p .

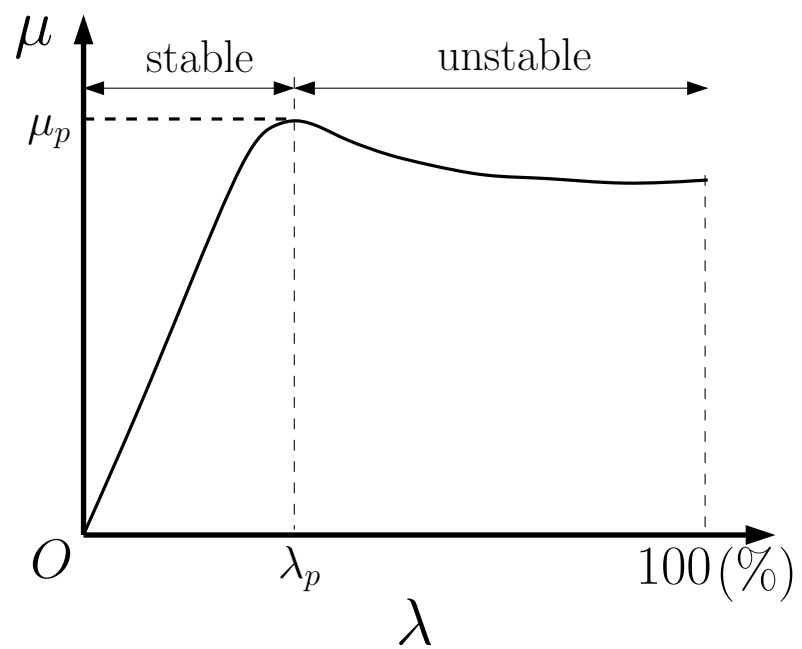


Figure 3.8: Relationship between the longitudinal friction coefficient and the slip ratio. In the stable region of this curve, the friction coefficient increases with the slip ratio. In the unstable region of this curve, the wheel slips significantly and the wheel loses traction.

CHAPTER 4

REAL TIME SLIP DETECTION AND ESTIMATION

In order to control the slip behavior of the system explicitly or implicitly, it is necessary to obtain the information of slip quantitatively or qualitatively. Sensor measurement and system model are required for slip detection and estimation. The objective is to obtain slip information in real time using limited and cost effective sensors. Slip detection and estimation are useful for the purpose of improving the odometry accuracy of WMRs. It is also useful for the servo controller to determine the control or adjust its control parameters in order to reduce the slip effects.

4.1 Slip Detection with Cost Effective Sensors

We present an effective slip detection technique using two types of inexpensive sensors that are commonly available for WMRs. The two types of sensors are encoder and Inertia Measurement Unit (IMU). This technique is known as dead reckoning or proprioceptive navigation with internal sensing as opposed to exteroceptive navigation with external sensing.

4.1.1 Slip Detection with Encoder

In WMRs, internal sensing is referred to the use of position or velocity sensors in the wheels to estimate the robot position or velocity in the global frame. Estimating the global position of the robot using only internal sensors is the simplest and common localization method for mobile robotics. This method is called odometry or dead-reckoning in localization literature. For the purpose of slip detection, velocity information is more important than position information.

Common internal sensors for WMRs are encoders, resolvers and tachometers. Angular encoder and resolver are angular position sensors but are also usually used to estimate angular velocity by backward difference method combined with suitable low pass filters. Tachometer is direct angular velocity measuring sensor and can generally provide more accurate angular velocity information than encoder or resolver. In this thesis, however, we assume that the velocity estimation using encoder or resolver or the direct velocity measurement from tachometer are both accurate enough for the purpose of slip detection.

We assume each wheel of WMRs is equipped with either position or velocity sensors. For PCW-based WMRs, since these robots are redundantly actuated, each actuator must be equipped with position or velocity sensor for servo control. In this case, by comparing the internal sensing information between wheels, slip information on particular wheel could be detected.

Slip detection based on internal sensing mainly makes use of the kinematic model of the robot. The principle of this slip detection method can be described as below:

The “sensed” wheel center velocities are computed from the internal sensing of joint velocities \dot{q}_{int} :

$$\dot{p}_{int} = B\dot{q}_{int} \quad (4.1)$$

Then operational velocities of the robot are estimated based on the forward kinematics using the pseudo-inverse of matrix \mathbf{A} :

$$\dot{x}_{int} = \mathbf{A}^\dagger \dot{p}_{int} \quad (4.2)$$

With the operational velocities of the robot \hat{x}_{int} that are estimated from internal sensor information, the corresponding actual wheel center velocities \dot{p} are also estimated using the internal sensor information:

$$\hat{\dot{p}}_{int} = \mathbf{A}\hat{x}_{int} \quad (4.3)$$

Although the slip is defined as the difference between the “sensed” and the actual wheel center velocity, we obtained an estimated slip using only internal sensor information:

$$\hat{\varepsilon} = \dot{p}_{int} - \hat{\dot{p}}_{int} \quad (4.4)$$

All these equations can be written in one as:

$$\hat{\varepsilon} = (I - \mathbf{A}\mathbf{A}^\dagger)B\dot{q}_{int} \quad (4.5)$$

With the “internally sensed” operational velocities based on pseudo-inverse, we share information between wheels to detect the outliers which are slipping.

This internal sensing based slip detection method is effective even in indoor environments as shown in Fig. 4.1. This figure shows a scenario where all the wheels were not slipping except wheel 3 that was slipping during the period between 1.5 sec

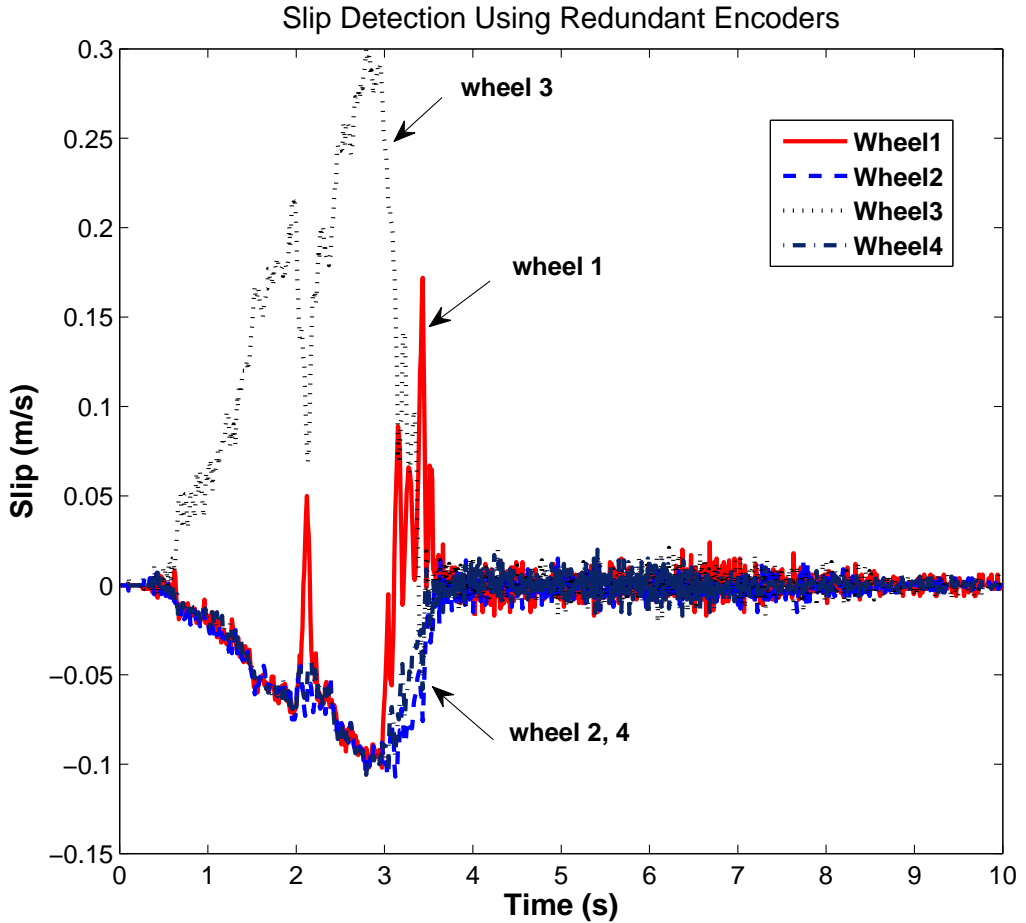


Figure 4.1: Wheel slip can be detected using the redundant wheel encoders. For those wheels that are slipping, the calculated slip velocities of them are not consistent with those of the rest of wheels. This detection scheme becomes invalid if all wheels are slipping simultaneously.

and 3.5 sec. It can be seen that the estimated slip of the slipping wheel (Wheel 3 in the figure) is positive while those of the rest are negative. The magnitude of the estimated slip actually provides a useful hint to determine the slip behavior of the wheel. In vehicle dynamics, positive slip is sometimes called *slipping* while negative slip is called *skidding*.

However, a reliable slip detection procedure using internal sensing is not as simple as just observing the sign of the estimated slip. We have developed a systematic procedure [117] in detecting wheel slip as follows.

1. If all rolling (steering) joints satisfy condition:

$$|\hat{\varepsilon}| < \dot{\varepsilon}_{thres} \quad (4.6)$$

where $\dot{\varepsilon}_{thres}$ is the threshold to reject the effects of sensing noise and numerical error, then no wheel is slipping or skidding.

2. If there exists at least one rolling (or steering) joint that doesn't satisfy Condition 4.6, find the two wheels i and j that satisfy:

$$\begin{aligned} \hat{\varepsilon}_i \hat{\varepsilon}_j &> 0 \\ \hat{\varepsilon}_i - \hat{\varepsilon}_j &\leq \dot{\varepsilon}_{thres} \end{aligned} \quad (4.7)$$

- If such a pair of wheels cannot be found, it implies that all the wheels are slipping/skidding or there is only one wheel that is not slipping/skidding but it cannot be recognized by this procedure.
- If more than one such pair of wheels are found, the pair with smallest estimated slip magnitude is considered non-slipping. Consider a third wheel k : if

$$\begin{aligned} \hat{\varepsilon}_i \hat{\varepsilon}_k &> 0 \\ \hat{\varepsilon}_i - \hat{\varepsilon}_k &\leq \dot{\varepsilon}_{thres} \end{aligned} \quad (4.8)$$

then wheel k is not slipping/skidding, otherwise wheel k is slipping if its estimated slip is positive or skidding if its estimated slip is negative.

3. Recompute the “correct” operational velocities:

$$\hat{x}_{cor} = A_{ij}^\dagger B_{ij} \dot{q}_{ij}$$

and the “correct” slip for slipping/skidding wheels:

$$\hat{\varepsilon}_{cor} = (I - A_{ij}A_{ij}^\dagger)B_{ij}\dot{q}_{ij}$$

It can be seen that this procedure not only recognizes the slipping/skidding wheels but also computes the “correct” slip information of those slipping or skidding wheels.

It is noted that above procedure should be evaluated separately for the rolling and steering joints in case of independently steered and driving WMRs such as PCW-based WMRs. It should also be noted that this procedure is not reliable for some trivial cases. For example, if there are about the same “amount” of slip on all the wheels except one non-slipping wheel, this procedure will result in wrong detection. In the following, we address this issue.

4.1.2 Slip Detection with Inertia Measurement Unit

The main problem of internal sensing based slip detection lies in the fact that it estimates the actual wheel center velocity using internal sensor information. In this case, both the “sensed” and actual wheel center velocities are obtained from internal sensing. So the estimated slip is, in principle, not realistic. In case where all wheels are slipping, internal sensing based slip detection method cannot work or it may lead to wrong detection in some trivial cases. Combining external sensing and internal sensing can overcome the problem by obtaining the operational velocities directly from external sensors. The principle of this slip detection method can be described as below:

The “sensed” wheel center velocities are still computed from internal sensing of joint velocities:

$$\dot{p}_{int} = B\dot{q}_{int} \tag{4.9}$$

while the “actual” wheel center velocities are now computed from external sensing of operational velocities:

$$\dot{p}_{ext} = A\dot{x}_{ext} \quad (4.10)$$

The estimated slip is thus computed as:

$$\begin{aligned} \hat{\dot{\varepsilon}} &= \dot{p}_{int} - \dot{p}_{ext} \\ \hat{\varepsilon} &= B\dot{q}_{int} - A\dot{x}_{ext} \end{aligned} \quad (4.11)$$

A threshold is still desirable to be used in the case of external sensing to reject sensing noise and numerical errors. The condition to determine whether a wheel is slipping/skidding or not is given as:

$$|\hat{\dot{\varepsilon}}| < \dot{\varepsilon}_{thres} \quad (4.12)$$

If this condition is satisfied, the wheel is not slipping/skidding, otherwise the wheel is slipping/skidding.

Combining internal sensing and external sensing is ideal for slip detection and estimation. However, this method requires the extra external sensors and the external sensors are required to have as fast response as the internal sensors so that real time slip detection and estimation is realized. A desirable solution is the availability of cost effective and yet fast feedback rate external sensors. Among the existing sensors, MEMS-based Inertial Measurement Unit (IMU) sensor is probably the most suitable external sensor to fulfill our requirements. Due to the advancement of MEMS technology in recent years, IMU sensors become cost effective and their sensing rate is fast enough that they are suitable for real time sensing. Moreover, thanks to its inertia-based sensing, IMU sensors are self-contained.

We have tested the performance of a IMU sensor for real time velocity sensing and compared it with the velocity computed from the encoder sensing. The tested results

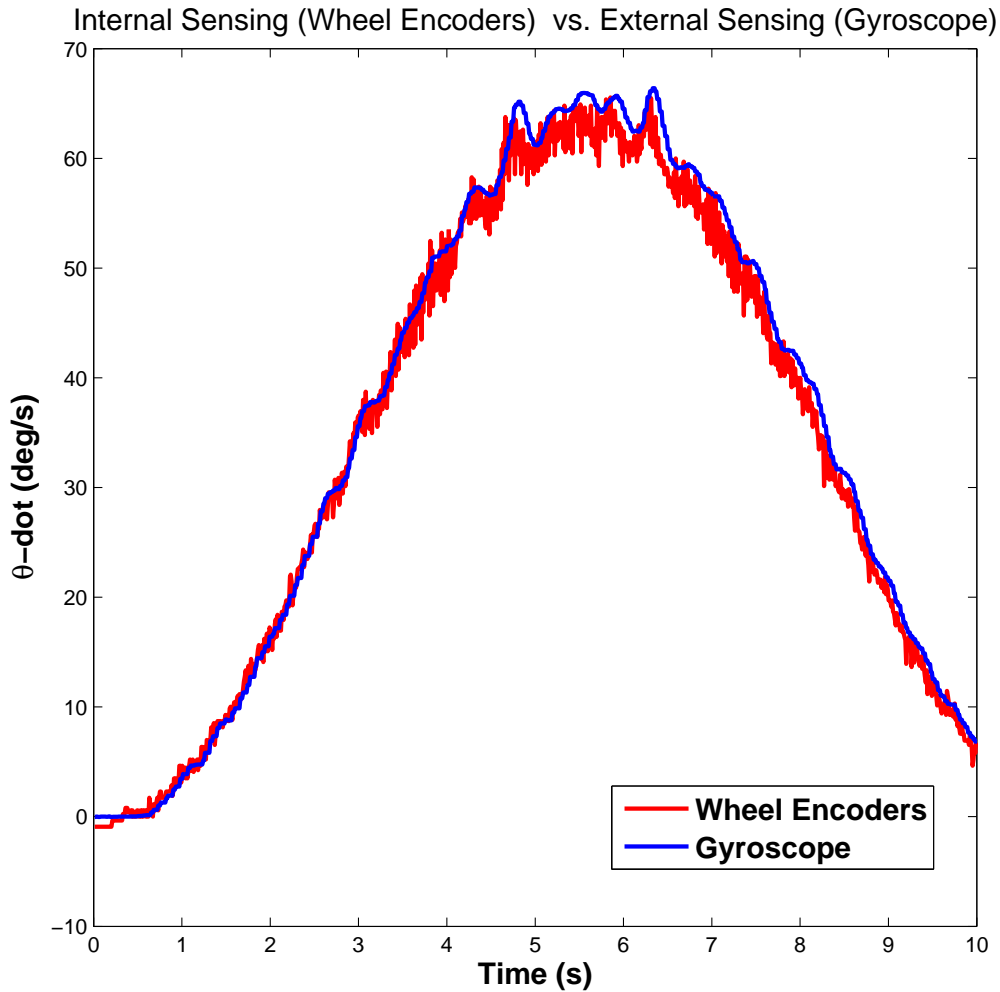


Figure 4.2: With the assist of external sensors such as Inertia Measurement Unit (IMU), wheel slip can be detected by comparing the velocities sensed by the wheel encoders and the IMU.

are shown in Fig. 4.2. The sensing rate of the IMU sensor used in this experiment was as high as **1000** Hz, it is sufficient for real time sensing. Since Gyroscope is absolute sensor, the wheel slip can be reliably detected by comparing the velocities sensed by the wheel encoders and the Gyroscope sensor.

4.2 Slip Estimation with Sliding Mode Observer

Internal sensing is not always reliable while external sensing requires extra sensors. Moreover, external sensors such as IMU suffer the drift problem. The drift problem will be even more significant in the case of accelerometer due to integration error. An alternative sensing technique is to construct state observers based on the information about the system model.

State observers can be considered as virtual sensors. Ideally, with the system model and limited output/input information, state observers can always be constructed. However, conventional state observers are designed for linear systems. In our case, the full dynamic model consists of the vehicle rigid body dynamics and the wheel-ground interaction model. This makes the system model highly nonlinear. A solution to this is to linearize the system model and then use conventional linear state observers such as Kalman filters [118]. Another solution is to directly use nonlinear state observers. In a similar application, [81] has compared the performances between extended Kalman filter and sliding mode observer. Sliding mode observer was found to outperform the extended Kalman filter. Sliding mode observer is preferred also due to its simplicity for implementation and its robustness characteristic [91]. Therefore we adopt sliding mode observer to estimate the mobile robot's operational velocities.

Below we construct two sliding mode observers based on either joint velocity measurement or joint angle measurement.

4.2.1 Velocity Observer with Joint Velocity Measurement

The evaluation of slip ratio requires the information of the wheel angular velocity and the actual velocity of the mobile robot. Usually, only the wheel angular velocity

is directly available using measurement from tachometer or numerical differentiation from encoder. The actual velocity of the mobile robot is usually not directly measured and can be estimated using the sliding mode observer.

For the convenience of analysis, we formulate the system in state space for one wheel. We define the following variables:

- States X :

$$X = \begin{bmatrix} \dot{\rho} \\ v_x \end{bmatrix}$$

States of the system are chosen as the wheel angular velocity $\dot{\rho}$ and the longitudinal velocity of the wheel v_x .

- Output Y :

$$Y = \dot{\rho}$$

- Input U :

$$U = \tau_\rho$$

Based on Eqs. 3.45 to 3.47, the state space equations of the one wheel system can be written as

$$\dot{X} = f(X) + gU \quad (4.13)$$

In Eq. 4.13, $f(X)$ and g are given as

$$f(X) = \begin{bmatrix} -\mu(X)F_zr/I_\rho \\ \mu(X)F_z/M_w \end{bmatrix}$$

$$g = \begin{bmatrix} 1/I_\rho \\ 0 \end{bmatrix}$$

where F_z is the vertical force acting on the wheel and M_w is the mass of the wheel. The fact that the friction coefficient $\mu(X)$ is an implicit function of the state vector X

can be seen from Eq. 3.47 which shows the relationship between the friction coefficient μ and the slip ratio λ .

We define the sliding mode observer as follows

$$\dot{\hat{X}} = \hat{f}(\hat{X}) + \hat{g}U - H\tilde{Y} - K\text{sgn}(\tilde{Y}) \quad (4.14)$$

where \hat{X} , \hat{f} and \hat{g} are estimates of X , f and g respectively. $\tilde{Y} \equiv \dot{\rho} - \hat{\rho}$ is defined as the estimation error. In the structure of the sliding mode observer, estimation error \tilde{Y} acts as the *Sliding Variable* \mathbf{s} .

Readers are referred to [119] for the details of the observer derivation and its analysis as well as techniques to choose the gains H and K for matching the estimated states to their actual values.

Fig. 4.3 shows the simulation performance of the sliding mode observer in estimating the wheel's longitudinal velocity v_x with the wheel angular velocity measurement. It can be seen that the estimated states \hat{v}_x successfully converged to the actual states v_x .

4.2.2 Velocity Observer with Joint Angle Measurement

The sliding mode observer presented in previous section assumes the joint velocities are measurable. However, in most cases, position sensor such as encoder and resolver are used instead of velocity sensor such as tachometer. Although joint velocities can be obtained using backward difference of position measurement with low pass filter, the accuracy is limited. Due to the robustness of SMO, we will show in this section that, even with only the joint position measurement, SMO is still capable of estimating the unmeasurable states of the system.

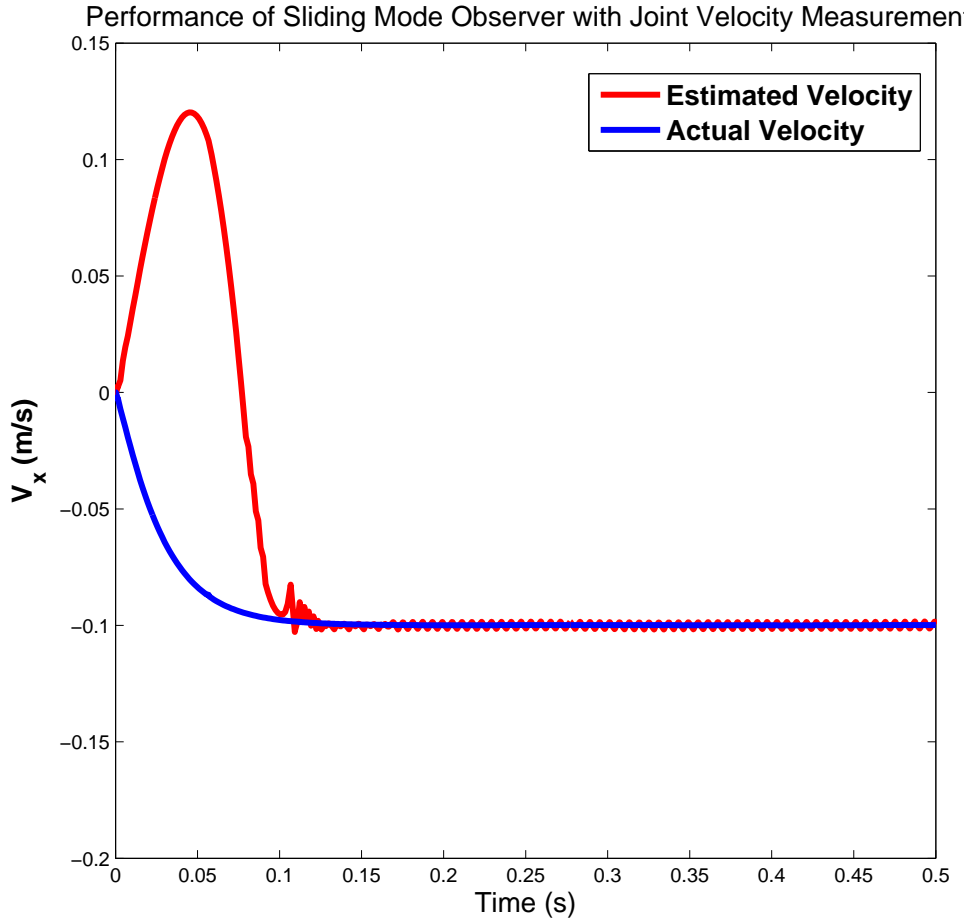


Figure 4.3: In the simulation of one wheel motion, wheel velocity estimated using the sliding mode observer with joint velocity measurement is plotted versus the actual velocity of the wheel. The settling time for convergence is about **0.12** second.

The same SMO structure can be used. The only difference is the order of the observer has been increased. We modify the previous observer as follows:

- States X :

$$X = \begin{bmatrix} \rho \\ \dot{\rho} \\ v_x \end{bmatrix}$$

- Output Y :

$$Y = \rho$$

- Input U :

$$U = \tau_\rho$$

The two terms $f(X)$ and g shown in Eq. 4.13 are now given as

$$f(X) = \begin{bmatrix} \dot{\rho} \\ -\mu(X)F_z r/I_\rho \\ \mu(X)F_z/M_w \end{bmatrix}$$

$$g = \begin{bmatrix} 0 \\ 1/I_\rho \\ 0 \end{bmatrix}$$

The observer has the same structure as the previous one:

$$\hat{X} = \hat{f}(\hat{X}) + \hat{g}(\hat{X})U - H\tilde{Y} - K\text{sgn}(\tilde{Y}) \quad (4.15)$$

Fig. 4.4 shows the performance of this sliding mode observer in simulation. Similar to the result shown in Fig. 4.3, the estimated states converged to the actual states successfully.

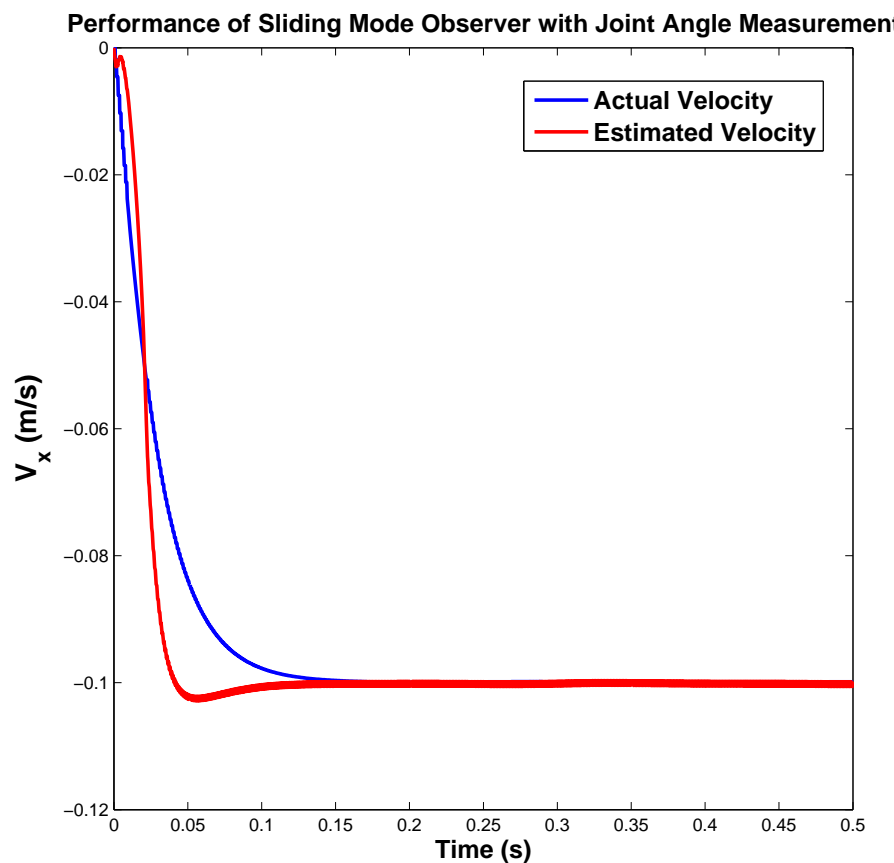


Figure 4.4: In the simulation of one wheel motion, wheel velocity estimated using the sliding mode observer with only joint angle measurement is plotted versus the actual velocity of the wheel. The settling time for convergence is about **0.15** second.

CHAPTER 5

SLIP CONTROLLERS: DESIGN AND IMPLEMENTATION

In the previous chapters, we have extended both kinematic and dynamic models to the ones that take slip into account. Several slip detection, measurement and estimation schemes were presented to obtain slip information in real time. It has been shown that classical robotic controllers are not capable of handling the slip problem. In this chapter, we will make use of all the results from previous chapters to design controllers that aim to reduce slip or to control the dynamic behavior of slip explicitly. Our slip controller design is based on the main effects that are relevant to the slip behavior of WMRs.

There are three main effects relevant to slip behavior of WMRs. The most direct effect of slip phenomenon is the incompatibility of wheel motion with the non-slip kinematic constraints of the system. Therefore, from the control point of view, high performance motion controller with disturbance rejection is expected to reduce the slip effect.

The second effect is that slip generates internal forces within the mechanism. When slip occurs, wheel motion violates the ‘rigidity’ condition of rigid body motion and internal forces are generated within the mechanism. On the other hand, increased

internal forces will further amplify the occurrence of slip. Therefore effectively controlling the internal forces will be beneficial for slip reduction.

Lastly, slip effect is directly related to the traction forces that the ground acts on the mobile robot. It can be seen from the wheel-ground interaction model presented in Chapter 3 that traction force is a function of slip ratio. So by explicitly controlling the slip ratio, we can control the traction forces that drive the mobile robot.

In this chapter, we will propose several control algorithms to handle the three main effects that are related to slip. For the motion incompatibility effect, we modify the standard kinematic controller by incorporating with the sliding mode control technique to achieve better trajectory tracking and disturbance rejection. For the internal force effect, we derive a controller that describes the contact forces in terms of task space forces and internal forces. Actuation redundancy of the system is used to achieve desired internal forces. For the traction force effect, we propose a slip ratio controller that controls explicitly the slip behavior of system. Along with all the controller design, comprehensive results of all the proposed control algorithms are demonstrated in both simulation and real time experiments.

5.1 Sliding Mode Slip Compensation

In most existing WMRs, the well known *Resolved Motion Rate Control (RMRC)* is prevalent for their controller design. In **RMRC**, desired task space trajectory is first mapped to desired joint space trajectory based on the kinematic model of the robot and then each joint is controlled independently. Due to its kinematic-based and individual joint control characteristic, different tracking performance exists for each joint. Uneven tracking performance of each wheel will be more significant in

the case of WMRs due to the varying loading and contact conditions between wheel and ground. Strictly speaking, slip occurs as long as tracking error of any wheel is different and not zero. Thus, a fast and accurate trajectory tracking controller is a basic strategy for slip reduction. Due to the fact that dynamics is not accounted for in **RMRC**, dynamics effects act as disturbances to the controller during motion. So a controller that is insensitive to the un-modelled dynamics and disturbances will also be effective in slip reduction.

A simple PID controller taking Eq. (5.1) as input can be implemented.

$$e = A\dot{x}_d - (B\dot{q} - \dot{\varepsilon}) \quad (5.1)$$

In order to achieve higher performance, the slip should be compensated in a fast manner so that the “fighting” between wheels can be eliminated quickly to achieve better wheel synchronization. For this case, we choose sliding mode controller. Sliding mode controller is well known to be robust to un-modelled dynamics and other disturbances.

In this section, we incorporate sliding mode control with standard **RMRC** to achieve high trajectory tracking performance with the capability of dynamics compensation and disturbance rejection.

5.1.1 Sliding Mode Kinematic Control

Sliding Mode Control is a simple and effective robust nonlinear control technique thanks to its robustness to parametric uncertainty and external disturbances [91]. The basic idea of sliding mode is that with replacing n^{th} -order tracking problem with an equivalent 1^{st} -order regulation problem, high performance can be in principle

achieved in the presence of arbitrary bounded parameter uncertainty and external disturbances. Details on the design procedure and stability analysis of sliding mode controller is presented in Appendix C. Fig. (5.1) shows a control diagram that incorporates **RMRC** with **SMC** and we called this scheme the *Sliding Mode Enhanced Resolved Motion Rate Control (SME-RMRC)*. The control algorithm of the **SME-RMRC** scheme is formulated in Table 5.1.

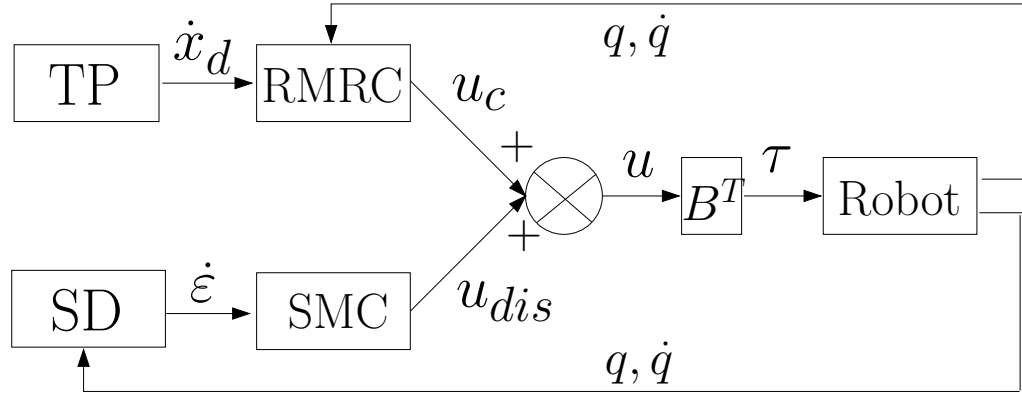


Figure 5.1: Control diagram of the Sliding Mode Enhanced Resolved Motion Rate Control (SME-RMRC) scheme. TP: trajectory planner, SD: slip detector.

In the **SME-RMRC** scheme as shown in Fig. 5.1, the one-to-one mapping between the joint torques τ and the control signal u is obtained through the transformation matrix B^T . Treating the contact point forces as the control signal is an important scheme for developing slip control algorithms in this research. The control signal u consists of two terms: one is the continuous control u_c and the other one the discontinuous control u_{dis} . The continuous control u_c is computed using the

Table 5.1: Control algorithm of the *Sliding Mode Enhanced Resolved Motion Rate Control (SME-RMRC)* scheme.

(1) Control Input
$\tau = B^T u$ (wheel torque)
$u = u_c + u_{dis}$ (controller output)
(2) Continuous Control with Resolved Motion Rate Control
$u_c = k_p(\dot{p}_d - \dot{p}) + k_i \int_{t_o}^t (\dot{p}_d - \dot{p}) dt$ (PI controller)
$\dot{p}_d = Ax_d$ (desired wheel center velocity)
$\dot{p} = B\dot{q}$ (actual wheel center velocity)
(3) Discontinuous Control with Low Pass Filtered Integral Sliding Mode Control
$u_{dis} = \frac{K}{\epsilon p + 1} sgn(s)$ (low pass filtered sliding mode control)
$s = -\dot{\varepsilon} + z$ (sliding variable)
$\dot{z} = u - K sgn(s)$ (auxiliary sliding variable)

conventional **RMRC** scheme. In the **RMRC** scheme, we adopted a simple PI controller as described in Table 5.1. The discontinuous control u_{dis} is computed using a sliding mode controller. In order to reduce the negative effects of the chattering issue of sliding mode controller, we adopted the integral sliding mode with low pass filtering scheme as described in Table 5.1. This special sliding mode control scheme is explained in detail in the next section.

5.1.2 Chattering Reduction

Chattering problem remains the main obstacle for practical implementation of sliding mode control. There are mainly three factors that cause chattering in sliding mode control. First, perfect switching across the *sliding plane* $s = 0$ is not possible in practice (for instance, switching is not actually instantaneous, and the value of s is only known with finite precision) [91]. Second, fast dynamics neglected in the system modelling is often excited by the fast switching of sliding mode controllers [98]. Third, digital implementation with fixed sampling rates leads to discretization error [98].

Many schemes dealing with chattering problem of sliding mode control have been proposed in the literature such as **boundary layer** method [91], **disturbance observer** method [96] etc. Although all these schemes can handle the chattering problem with certain performance, none of these schemes can eliminate the reaching phase of sliding mode control. As stated in [98], “the robustness property of conventional sliding mode control with respect to variations of system parameters and external disturbances can only be achieved after the occurrence of sliding mode. During the reaching phase, however, there is no guarantee of robustness”. In order to solve the chattering problem as well as the reaching phase elimination problem, a scheme called *Low Pass Filtered Integral Sliding Mode Control (LPFISM C)* is adopted in our sliding mode controller. The formulation of the **LPFISM C** scheme is shown in Table 5.1. The reason of integral sliding mode control being able to eliminate the reaching phase is due to the fact that the order of the motion equation in integral sliding mode is equal to the order of the original system. Incorporating with a fine tuned low pass

filter, integral sliding mode control can achieve robustness starting from the initial time instance without chattering.

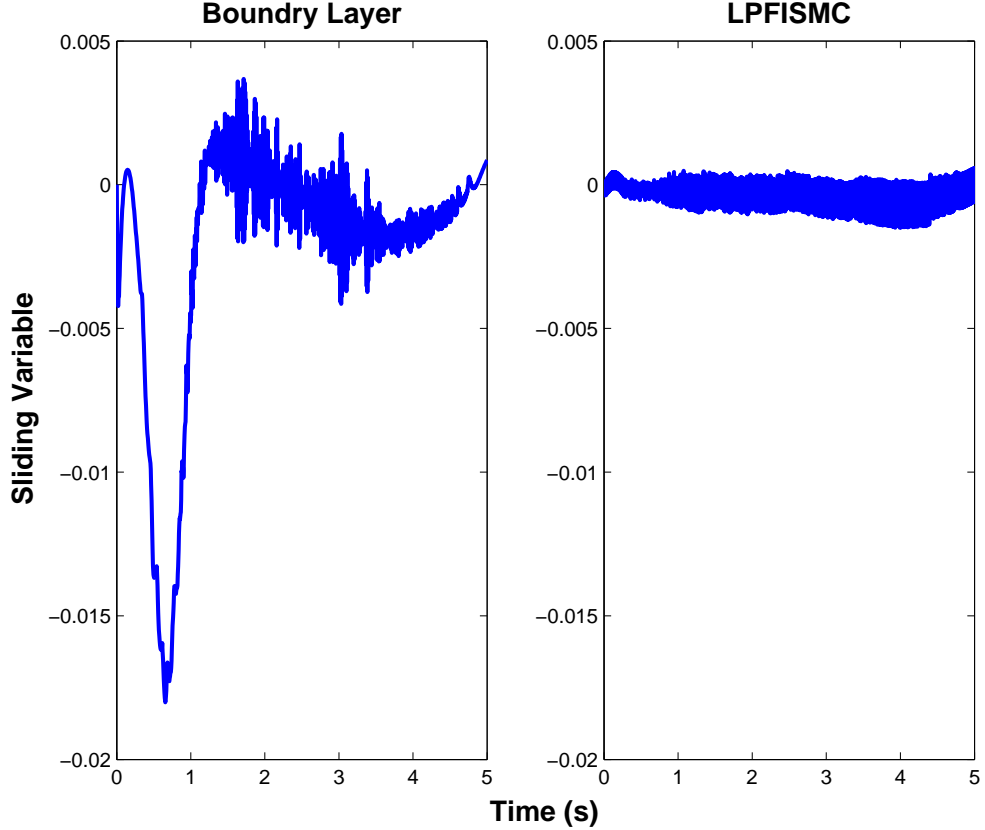


Figure 5.2: Comparing the chattering reduction and transient response performance between the Boundary Layer scheme and the LPFISM method in the sliding mode controller. Both methods can reduce chattering effectively. The Boundary Layer scheme has an obvious reaching phase towards the sliding surface while the LPFISM scheme eliminates the reaching phase.

Fig. (5.2) shows a comparison between the boundary layer method and the **LP-FISM** method. It can be seen from these two figures that both methods rejected the chattering. However, the boundary layer method experienced a reaching phase

before the sliding mode while the **LPFISM**C reached the sliding mode almost instantaneously without any reaching phase.

The idea of **LPFISM**C was originated from Utkin's work [98] and was called the *disturbance rejection* method. However, to our best understanding, this is the first time that **LPFISM**C is used for WMR control.

Fig. 5.3 shows the tracking performance comparison between the **LPFISM**C scheme and the standard **RMRC** scheme in real time experiments.

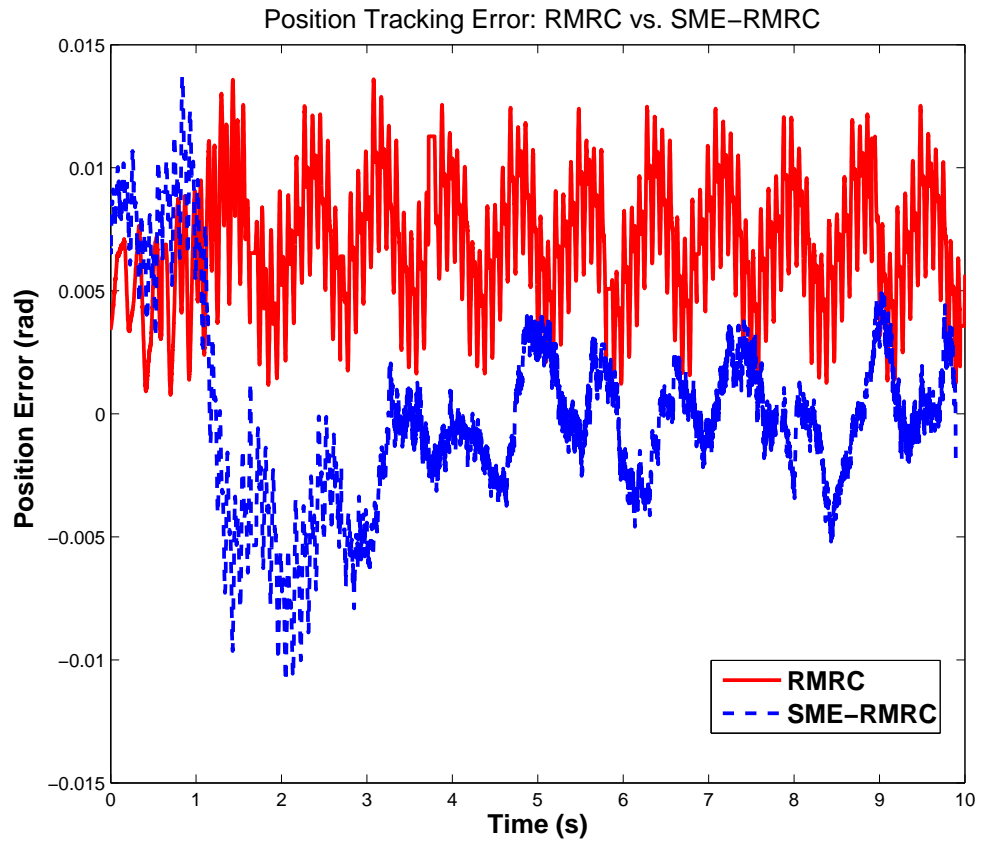


Figure 5.3: Position tracking error comparison between the RMRC and SME-RMRC schemes. The SME-RMRC scheme outperformed the RMRC scheme.

Noted that only the angular position tracking error for one wheel is shown in Fig. 5.3 as the robot was commanded to move in straight line. In this experiment, the position tracking error is taken as the performance criteria. The position error, which was computed based on the assumption that the inverse kinematic model is accurate, was taken as the ground true for this experiment. It can be seen that the tracking performance was improved significantly after incorporating the sliding mode control with the **RMRC** scheme. The slip information is required for the sliding mode control and it can be obtained either by direct sensing or estimation using those slip estimation schemes developed in Chapter 4. Sliding mode is chosen for its fast response and robustness to compensate for the unmodelled dynamics.

5.2 Internal Force Control

In Chapter 3, we have presented the dynamic modelling of wheeled mobile robots (WMRs) based on the Augmented Object Model (AOM). The AOM concept considers the WMR as instantaneous fixed base multiple manipulators (the wheels) grasping a common object (the chassis). Another similar observation of WMRs is to consider WMRs as multi-fingered hand system grasping a object (the ground). In this observation, the contact forces that the ground acts on the WMR result in the resultant motion of the WMR. In the multi-fingered grasping tasks, an object (the ground in the WMRs case) is grasped by the fingers (the wheels in WMRs case). The similarity between WMRs and multi-fingered grasping tasks are demonstrated in Fig. 5.4. By this observation, the ideas from multi-fingered grasping (MFG) tasks can be used for the case of WMRs.

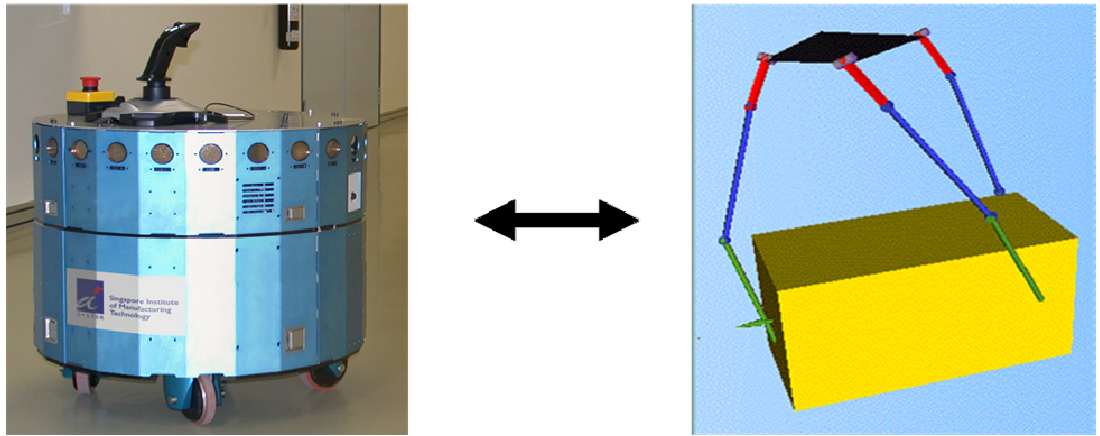


Figure 5.4: Topologically, wheeled mobile robot is similar to multi-fingered grasping. Slip problem is considered in both wheeled mobile robots and multi-fingered grasping. Ideas on slip study of multi-fingered grasping can be borrowed for wheeled mobile robots

In multi-fingered grasping tasks, *internal force* (or interaction force) is an important effect to be considered. Internal force between two contact points of a multiple points contact is defined as *the difference between the contact forces along the line joining the two contact points*. Internal force is closely related to the slip phenomenon in multi-fingered grasping tasks (the finger tips slip on the object) in following four cases:

1. zero internal force but non-zero slip.

This case is trivial for both MFG and WMR because it represents a rare situation where slip occurs but it generates zero relative motion between any pair of contact points.

2. non-zero internal force and non-zero slip.

This case is not desirable for both MFG and WMR. However, this case is also the most common situation for both tasks.

3. non-zero internal force but zero slip.

This case is ideal for MFG since non-zero internal force is required to ensure a stable grasp. For the case of WMR, zero slip is desired but non-zero internal force is harmful because the existence of internal force increases the chance of slipping.

4. zero internal force and zero slip.

Zero internal force is not preferred for MFG because internal force is required for stable grasping. However, this case is ideal for WMR.

For WMRs, our main objective is to achieve zero slip. Therefore, Case 3 and 4 are desirable. Generally, the mobile robot is in situations of Case 2. Therefore, the control scheme should try to drive the robot from Case 2 to Case 3 or the ideal situation of Case 4.

Standard controller design for mobile robots is to determine joint torques τ (rolling and steering motor torques) directly in terms of operational forces \mathbf{F} . However, such design does not describe the internal forces of the system and it is possible that significant internal forces may be generated. It is desirable to design controllers that

are able to specify the internal forces. Since internal forces describe the relationship among the contact forces of each pair of contact points, controllers directly describing contact forces are possible to reveal the internal force generated in the system. The concept of relating contact forces to operational space forces is well known in areas of multi-fingered grasping tasks, multi-arms manipulation tasks and legged robots walking tasks. In these areas, the relationship between contact forces and operational space forces are described as *equilibrium equations* [63, 64]. In what follows, we first propose a control scheme that aims to minimize the internal forces.

5.2.1 Internal Force Minimization

Fig. 5.5 shows the diagram that describes the relationship between the internal forces $F_{int} = [F_{int}^{ij}, F_{int}^{jk}, F_{int}^{ki}]^T$, contact forces $F_{con} = [F_{con}^i, F_{con}^j, F_{con}^k]^T$ and operational space forces $F_t = [f, m]^T$.

We have previously derived the relationship between operational space velocities and contact point velocities in Chapter 3 as

$$\dot{p} = A\dot{x}$$

In the case of Fig. 5.5, matrix A is given as

$$A = \begin{bmatrix} 1 & \hat{p}_i \\ 1 & \hat{p}_j \\ 1 & \hat{p}_k \end{bmatrix}$$

From the velocity/force duality, it is straight-forward to derive following equations relating the contact forces to operational space forces

$$F_t = A^T F_{con} \quad (5.2)$$

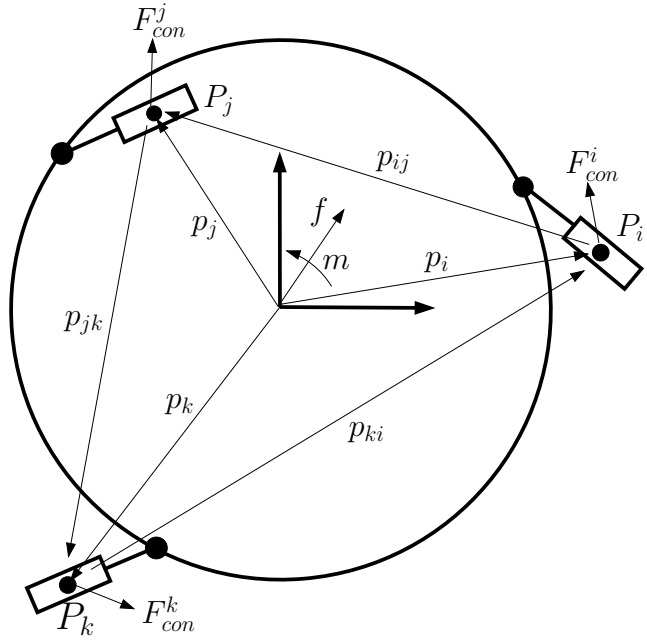


Figure 5.5: Diagram showing the rigidity condition of a rigid body motion. When applied to wheeled mobile robot, the rigidity condition describes the instantaneous relationship between the internal forces at the wheel-ground contact points and the resultant forces at the operational point of the robot. The occurrence of wheel slip implies the broken of the rigidity condition.

Based on the definition of internal force, the relationship between contact forces and internal forces is described as follows.

$$F_{int} = EF_{con} \quad (5.3)$$

where \mathbf{E} is given as

$$E = \begin{bmatrix} p_{ij} & -p_{ij} & 0 \\ 0 & p_{jk} & -p_{jk} \\ -p_{ki} & 0 & p_{ki} \end{bmatrix}$$

and

$$p_{ij} = p_j - p_i$$

It can be verified that

$$EA = 0$$

This relation implies that internal forces lie in the null space of resultant forces acted on the object.

A general solution to the contact forces based on Eq. (5.2) is given as

$$F_{con} = (A^T)^\# F_t + (I - (A^T)^\# A^T) f_o \quad (5.4)$$

where $(A^T)^\#$ is any generalized inverse of A^T .

If we choose the generalized inverse $(A^T)^\#$ to be the pseudo-inverse (Moore-Penrose Generalized Inverse), Eq. (5.4) can be written as

$$F_{con} = (A^T)^\dagger F_t + (I - (A^T)^\dagger A^T) f_o \quad (5.5)$$

where $(A^T)^\dagger = A(A^T A)^{-1}$ is the pseudo-inverse of A^T .

It can be seen that when the pseudo-inverse is used, the internal forces are given as

$$\begin{aligned} F_{int} &= E(A^T)^\dagger F_t + E(I - (A^T)^\dagger A^T) f_o \\ &= EA(A^T A)^{-1} F_t + Ef_o - EA(A^T A)^{-1} A^T f_o \\ &= 0 + Ef_o - 0 \\ &= Ef_o \end{aligned}$$

This implies that a solution to the contact forces that generates zero internal forces is given as

$$F_{con} = (A^T)^\dagger F_t \quad (5.6)$$

We called this solution the *Minimal Internal Force* solution for the contact force distribution problem.

A control algorithm based on the Minimal Internal Force solution is formulated in Table 5.2 and we refer to this as the *Internal Force Minimization (IFM)* scheme.

Table 5.2: Control algorithm of the *Internal Force Minimization (IFM)* scheme.

$\tau = B^T F_{con}$ $F_{con} = (A^T)^\dagger F_\oplus$ $F_\oplus = \hat{\Lambda}_\oplus(\ddot{x}_d + k_p(x_d - x) + k_d(\dot{x}_d - \dot{x})) + \hat{\vartheta}_\oplus$
--

Fig. 5.6 shows the results of comparing the wheel motion synchronization performance between the Augmented Object Model based control and the Augmented Object Model based control with the Internal Force Minimization (**IFM**). When internal forces are minimized, the chance for the occurrence of wheel slip is also minimized. This graphs demonstrate the effectiveness of the proposed **IFM** scheme.

The fact that the pseudo-inverse leads to a minimum internal force solution has already been revealed in literature of multi-fingered grasping tasks [63]. This idea was recently applied to wheeled mobile robots by R. Holmberg [6]. However, R. Holmberg has considered only the scheme to achieve zero internal force. The actuation redundancy of the system was not actively utilized in R. Holmberg's scheme. However, the actuation redundancy of the system introduces a null space where the internal forces can be actively controlled. We call this null space the “*Internal Force Space*”. In follows, we propose two slip control schemes that actively make use of the internal force space of the robot. The internal force space of the robot is actively utilized in the two schemes (Traction Limit Avoidance and Slip Constraint Force Control) aiming to achieve minimum wheel slip.

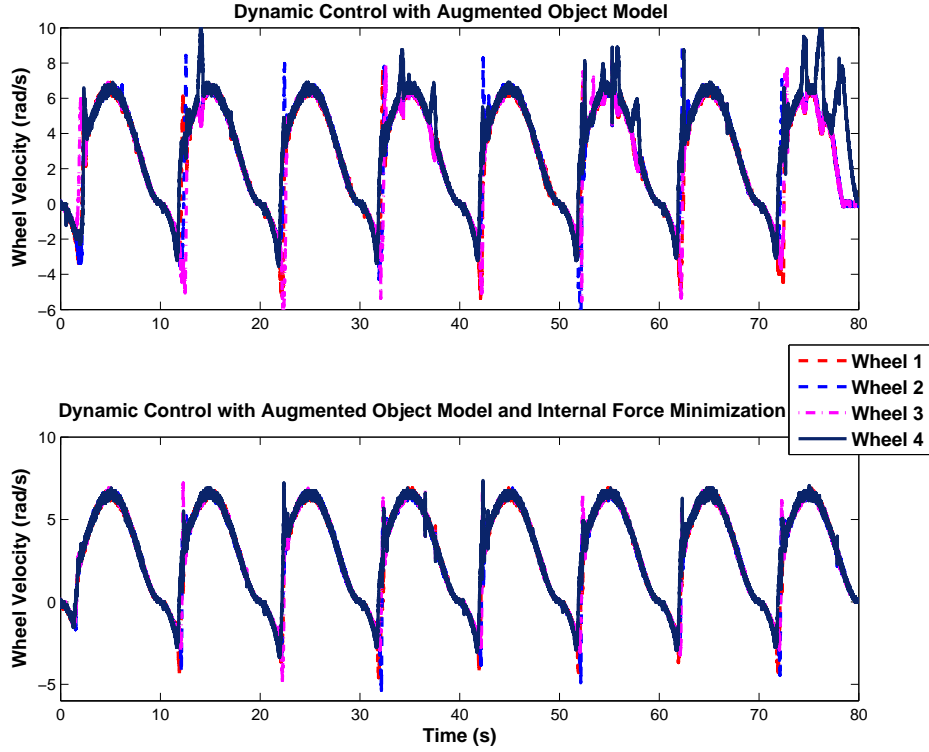


Figure 5.6: Comparing the wheel motion synchronization performance between the Augmented Object Model based control and the Augmented Object Model based control with Internal Force Minimization (IFM). When internal forces are minimized, the chance for the occurrence of wheel slip is also minimized. This diagram demonstrates the effectiveness of the proposed IFM scheme.

5.2.2 Traction Limit Avoidance

From the previous vehicle dynamics analysis, it can be seen that there exists a traction limit between the wheel and the contact surface. The traction limit can be decomposed into the longitudinal traction limit F_{mx} and lateral traction limit F_{my} . If the required contact force computed based on the augmented operational forces F_{\oplus} exceeds the traction limit F_{mx} or F_{my} , the wheel will slip/skid in the longitudinal direction or the lateral direction. Therefore a traction limit avoidance control scheme

should be developed. By actively making use of the internal force space of the robot, we propose a control scheme called *Traction Limit Avoidance (TLA)* and its control algorithm is summarized in Table 5.3. In this algorithm, contact point desired force F_{con} is computed with two parts: one is the operational force F_{\oplus} that represents the motion control task and the other one is the null space control f_o that ensures the contact force is limited to be a certain percentage of the traction limit f_m . If the calculated contact force is less than the traction limit, the calculated value will be taken as the required contact force command. This decision making rule as described by the last equation of Table *Tb-TLAvoid* guarantees the control objective of traction limit avoidance.

Table 5.3: Control algorithm of the *Traction Limit Avoidance (TLA)* scheme.

$\tau = B^T F_{con}$ $F_{con} = (A^T)^\dagger F_{\oplus} + (I - (A^T)^\dagger A^T) f_o$ $F_{\oplus} = \hat{\Lambda}_{\oplus}(\ddot{x}_d + k_p(x_d - x) + k_d(\dot{x}_d - \dot{x})) + \hat{\vartheta}_{\oplus}$ $f_o = [f_{con} \leq a f_m : f_{con}, a f_m], (0 < a < 1)$

Fig. 5.7 and 5.8 compare the torque distribution and traction limit avoidance capabilities of the Jacobian matrix J and the transformation matrix A . By comparing Fig. 5.7 (a) and Fig. 5.8 (a), it can be seen that use of transformation matrix A results in less joint torque compared to the use of Jacobian matrix J . By comparing Fig. 5.7

(b) and Fig. 5.8 (b), it can be seen that use of transformation matrix A distributes the joint torque more evenly than the case when Jacobian matrix J is used.

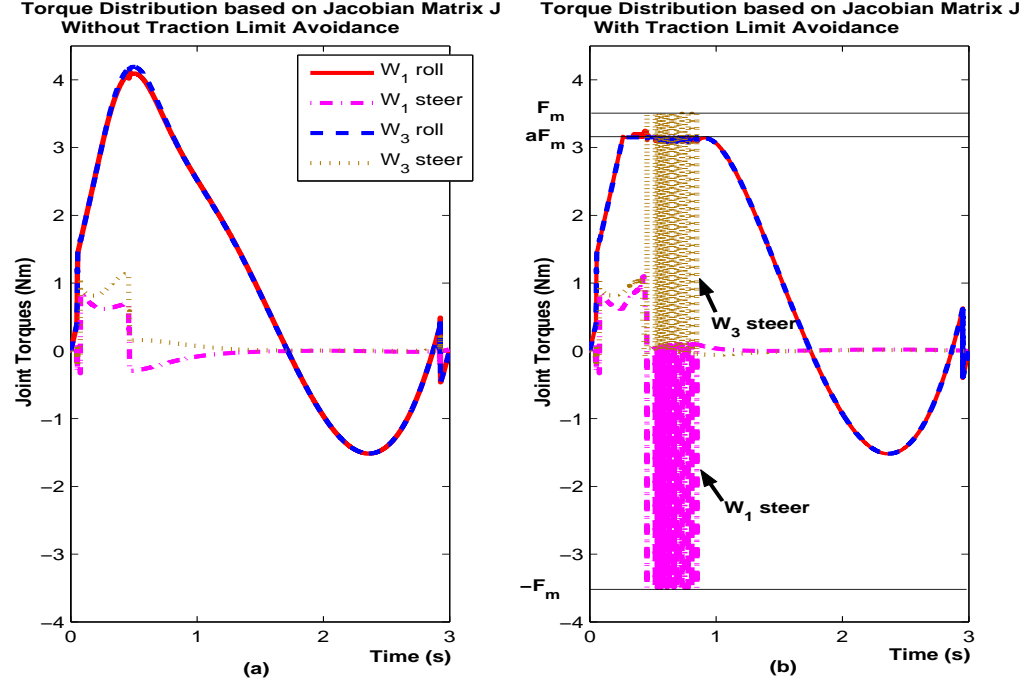


Figure 5.7: (a) Joint torque required in a straight line motion using standard Computed Torque Control scheme without internal force space control. Pseudo-inverse of the Jacobian matrix \mathbf{J} is used to compute the required joint torque. Joint torque as high as 4.2 Nm is required without joint torque limit or traction limit imposed. (b) Internal force space control is used to avoid joint torque limit or traction limit. The internal force space used in this example is that of the inverse Jacobian matrix \mathbf{J} .

Besides the objective of traction limit avoidance, actuation redundancy of the wheeled mobile robot can also be used for other objectives such as singularity avoidance and joint limit avoidance. In case of WMRs with PCWs that power all actuators, singularity avoidance problem is not needed as the robot is singularity free (recall from

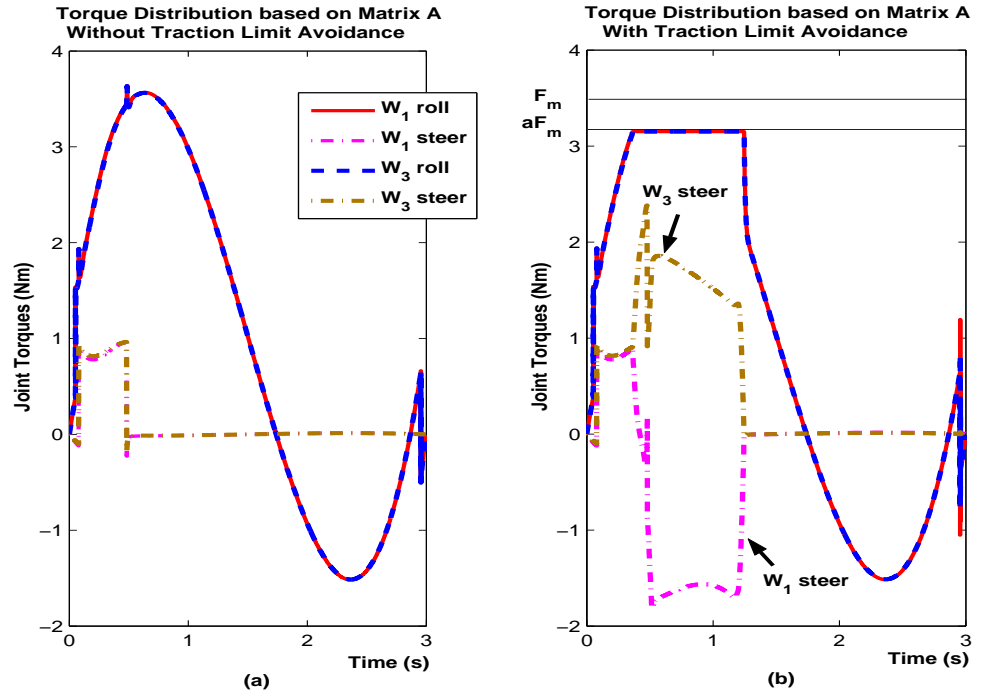


Figure 5.8: (a) Joint torque required in a straight line motion using standard Computed Torque Control scheme without internal force space control. Pseudo-inverse of the transformation matrix \mathbf{A} is used to compute the required joint torque. Joint torque as high as **3.5 Nm** is required without joint torque limit or traction limit imposed. (b) Internal force space control is used to avoid joint torque limit or traction limit. The internal force space used in this example is that of the transformation matrix \mathbf{A} .

the singularity analysis presented in Chapter 3). For the joint limit avoidance problem, since traction limit is usually stricter than the joint limit, avoidance of traction limit implies avoidance of the joint limit.

The Traction Limit Avoidance (**TLA**) control scheme is basically a “limit condition check”. However, the traction limit check does not explicitly utilize wheel slip information. Avoiding the traction limit does not guarantee zero wheel slip. An active slip control scheme should utilize wheel slip information to drive the slip towards zero. In the following we propose such a control scheme.

5.2.3 Slip Constraint Force Control

The internal force analysis presented previously motivates us to develop slip control scheme through the internal force space control. The concept of using internal force control for WMRs is of important research value. R. Holmberg [6] was the first to propose the scheme of minimum internal force distribution for WMRs with the Virtual Linkage Model [24]. However, he did not specify any criteria on the non-zero internal force control problem for WMRs. In this research, we characterize the internal forces in WMRs as the constraint forces associated with wheel slip. Based on the principle of virtual work, we propose a control scheme to minimize the slip constraint forces in the internal force space. This scheme is desirable as it decouples the operational forces with the internal forces by controlling wheel slip in the internal force space. This scheme is similar to Khatib's task/posture behavior control structure [120].

In the following we analyze an important relationship between the constraint forces and wheel slip. This relationship is important in our subsequent control schemes development. The relationship is basically the fact that the constraint forces associated with wheel slip are lying in the internal force space of the system.

Based on the principle of virtual work, following relation is derived.

$$F_\varepsilon^T \delta\varepsilon = F_p^T \delta p - F^T \delta x$$

where F_ε is the constraint forces associated with the virtual wheel slip displacement $\delta\varepsilon$.

Based on the fact that $\dot{\varepsilon} = B\dot{q} - A\dot{x}$, the above equation is re-written as

$$F_\varepsilon^T (B\delta q - A\delta x) = F_p^T B\delta q - F^T \delta x$$

Similarly, based on the fact that $\dot{x} = A^\dagger B \dot{q}$, the above equation is re-written as

$$F_\varepsilon^T (B \delta q - AA^\dagger B \delta q) = F_p^T B \delta q - F^T A^\dagger B \delta q$$

The above equation is satisfied for any δq , therefore

$$F_\varepsilon^T (B - AA^\dagger B) = F_p^T B - F^T A^\dagger B$$

By taking the transpose of both sides of the above equation, we obtain

$$(B - AA^\dagger B)^T F_\varepsilon = B^T F_p - (A^\dagger B)^T F$$

These equations are satisfied for any \mathbf{B} , therefore

$$F_p = (A^\dagger)^T F + (I - AA^\dagger)^T F_\varepsilon$$

From this equation, it can be seen that the constraint forces associated with wheel slip lie exactly in the internal force space. This relationship enables us to utilize the wheel slip information to control the slip-associated constraint forces.

By intuition, the slip-associated constraint forces achieve zero when wheel slip achieves zero. Thus we can construct a potential field function of the wheel slip to represent the slip-associated constraint forces and control this potential field function to drive the wheel slip to zero. To do this, we construct following relation

$$F_\varepsilon = k_p(0 - \hat{\varepsilon}) + k_i(0 - \int \hat{\varepsilon} dt) \quad (5.7)$$

The control algorithm of the *Slip Constraint Force Control (SCFC)* scheme is summarized in Table 5.4. Different from the **TLA** scheme, where the contact force command is checked against the traction limit so that avoidance of the traction limit is achieved, the slip velocity information is used explicitly in the **SCFC** scheme such

Table 5.4: Control algorithm of the *Slip Constraint Force Control* (**SCFC**) scheme.

$\tau = B^T F_p$
$F_p = (A^T)^\dagger F_\oplus + (I - (A^T)^\dagger A^T) f_\varepsilon$
$F_\oplus = \hat{\Lambda}_\oplus(\ddot{x}_d + k_p(x_d - x) + k_d(\dot{x}_d - \dot{x})) + \hat{\vartheta}_\oplus$
$f_\varepsilon = k_p(0 - \hat{\varepsilon}) + k_i(0 - \int \hat{\varepsilon} dt)$

that the slip velocity is driven towards zero by using control scheme described in Eq. 5.7.

In the following we present experimental results to demonstrate the effectiveness of the Slip Constraint Force Control scheme. These results have been published in [117].

Slip Constraint Force Control for Trajectory Tracking

This experiment tests the effectiveness of the **SCFC** scheme in trajectory tracking of the wheeled mobile robot. The basic controller structure used in this experiment was a computed torque scheme based on the dynamic model formulated with the Augmented Object Model. The robot was commanded to move in a straight line for two cases: one without the **SCFC** scheme implemented and the other with the **SCFC** scheme implemented. Fig. 5.9 (a) shows that slip was detected when the **SCFC** scheme was not implemented while Fig. 5.9 (b) shows that slip was maintained at zero when the **SCFC** scheme was implemented. Since the desired velocity of the

robot is quintic polynomial with initial and final velocities to be zero, Fig. 5.9 also shows that slip was more significant when the robot moved with faster speed.

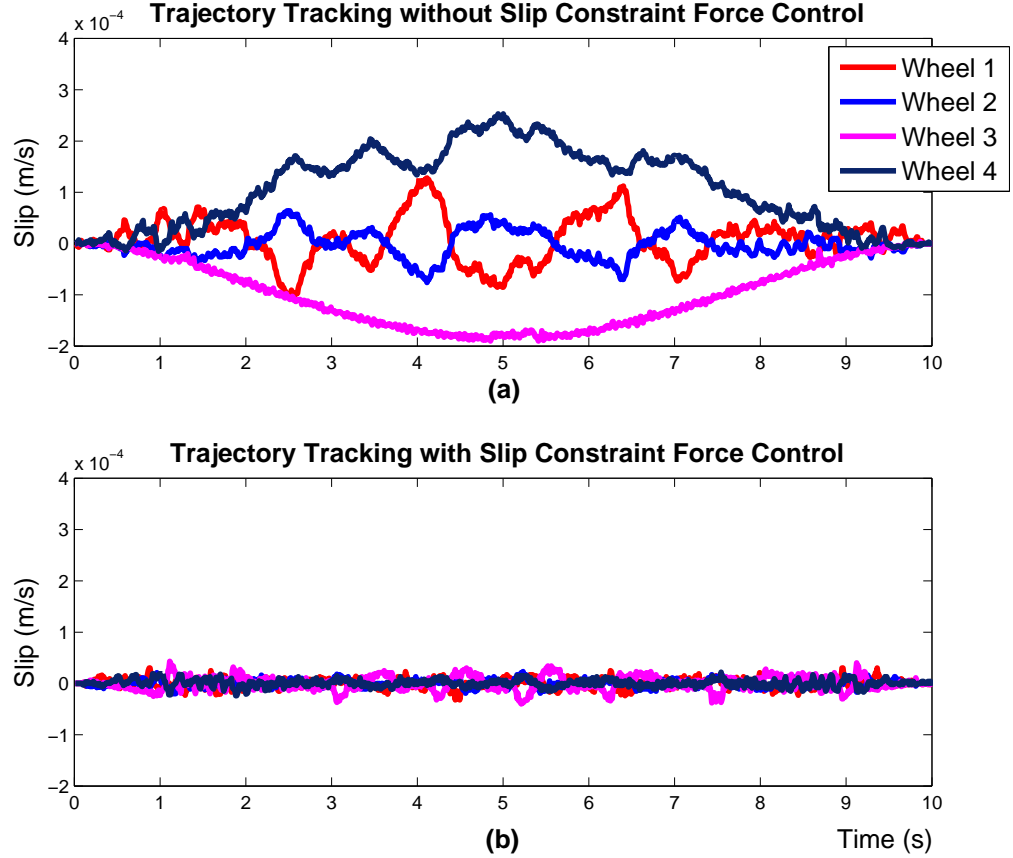


Figure 5.9: Performance of the Slip Constraint Force Control (SCFC) scheme in trajectory tracking tasks. (a) Slip was detected when SCFC was not implemented; (b) Slip was eliminated when SCFC was implemented.

Slip Constraint Force Control for Force-Guided Wheeled Mobile Robots

This PhD research is part of an on-going collaborative project between Singapore Institute of Manufacturing Technology and National University of Singapore. The

main objective of the collaborative project is to achieve robust mobile manipulation in human unstructured environments. To achieve this objective, a mobile manipulator system with high performance unified force/motion control [44] capabilities is critical for the mobile manipulator system to interact with humans and unstructured environments. This objective also acts as the main motivation for developing an omnidirectional wheeled mobile robot with dynamic control and slip control capabilities. Fig. 5.10 shows another mobile manipulator developed in Singapore Institute of Manufacturing Technology. This mobile manipulator consisted of a Mitsubishi PA10 7DOF manipulator and the omnidirectional wheeled mobile robot with 4 Powered Caster Wheels. Most of the experimental results presented in this dissertation was obtained from the mobile robot of this mobile manipulator. We have modified the **SCFC** scheme to adapt to the unified force/motion control framework of the mobile manipulator. Table 5.5 summarizes the control algorithm of the modified **SCFC** scheme and we call this modified algorithm the **UFM-SCFC** scheme. As seen from Table 5.5, the unified force F_u is computed using the conventional unified force/motion control framework that unifies force control F_f and motion control F_m with the selection matrix Ω . The special feature of this scheme is mainly in the computing of the null space control f_o . Instead of using the estimated slip velocity in the **SCFC** scheme, a virtual slip velocity is computed in the **UFM-SCFC** scheme as $(A \int \bar{\Omega} F_f dt - B \dot{q})$. This virtual slip velocity will generate extra control effort (besides the effort generated within F_u) to achieve better active force control F_f .

Before testing the **UFM-SCFC** scheme in the mobile manipulator system, we first implemented force control for the mobile robot to validate the slip constraint force control concept. The force-guided wheeled mobile robot was implemented with

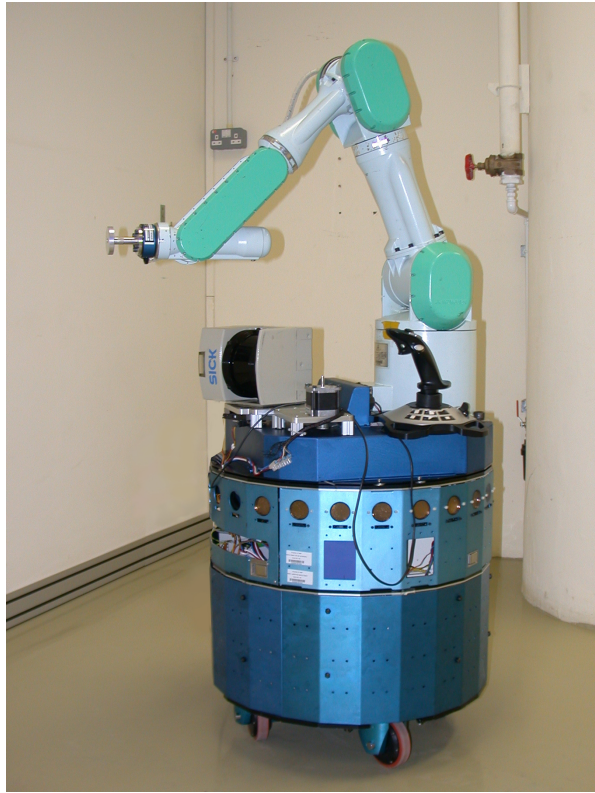


Figure 5.10: Another mobile manipulator developed in Singapore Institute of Manufacturing Technology. This mobile manipulator consists of a Mitsubishi PA10 7DOF manipulator and an omnidirectional wheeled mobile robot with 4 Powered Caster Wheels. Unified force/motion control is implemented for this mobile manipulator with the proposed slip constraint force control scheme. Image courtesy of the Singapore Institute of Manufacturing Technology.

a JR3 6DOF force/torque sensor mounted on the mobile robot. Two experimental results were obtained from the force-guided tasks of the mobile robot.

Fig. 5.11 shows off-the-ground test of proposed controller in Table 5.5. The evenness of individual wheels' driving speeds during two force-guided motions of the mobile robot were captured. In order to repeat the same motions as much as possible, the operator has tried to apply the same force commands. When slip constraint force control scheme was not incorporated as shown in Fig. 5.11 (a), wheel speeds were

Table 5.5: Control algorithm of the *Unified Force/Motion with Slip Constraint Force Control (UFM-SCFC)* scheme.

$\tau = B^T F_p$ $F_p = (A^T)^\dagger F_u + (I - (A^T)^\dagger A^T) f_o$ $F_u = \hat{\Lambda}_\oplus (\Omega F_m + \bar{\Omega} F_f) + \hat{\vartheta}_\oplus + F_{sensor}$ $F_m = \ddot{x}_d + k_{mp}(x_d - x) + k_{md}(\dot{x}_d - \dot{x})$ $F_f = k_{fp}(f_d - f) + k_{fi} \int (f_d - f) dt$ $f_o = k_{op}(A \int \bar{\Omega} F_f dt - B \dot{q}) + k_{oi} \int (A \int \bar{\Omega} F_f dt - B \dot{q}) dt$
--

not even which implied more slip occurs on the wheels. On the other hand, the evenness of wheel speeds was much better when slip constraint force control scheme was incorporated as shown in Fig. 5.11 (b).

Fig. 5.12 shows on-the-ground test of proposed controller in Table 5.5. The evenness of individual wheels' driving speeds during two force-guided motions of the mobile robot were captured. In order to repeat the same motions as much as possible, the operator has tried to apply the same force commands and moved the robot at the same location for the two guided motions. When slip constraint force control scheme was not incorporated as shown in Fig. 5.12 (a), wheel speeds were not even which implied more slip occurs on the wheels. On the other hand, the evenness of wheel speeds was much better when slip constraint force control scheme was incorporated as shown in Fig. 5.12 (b).

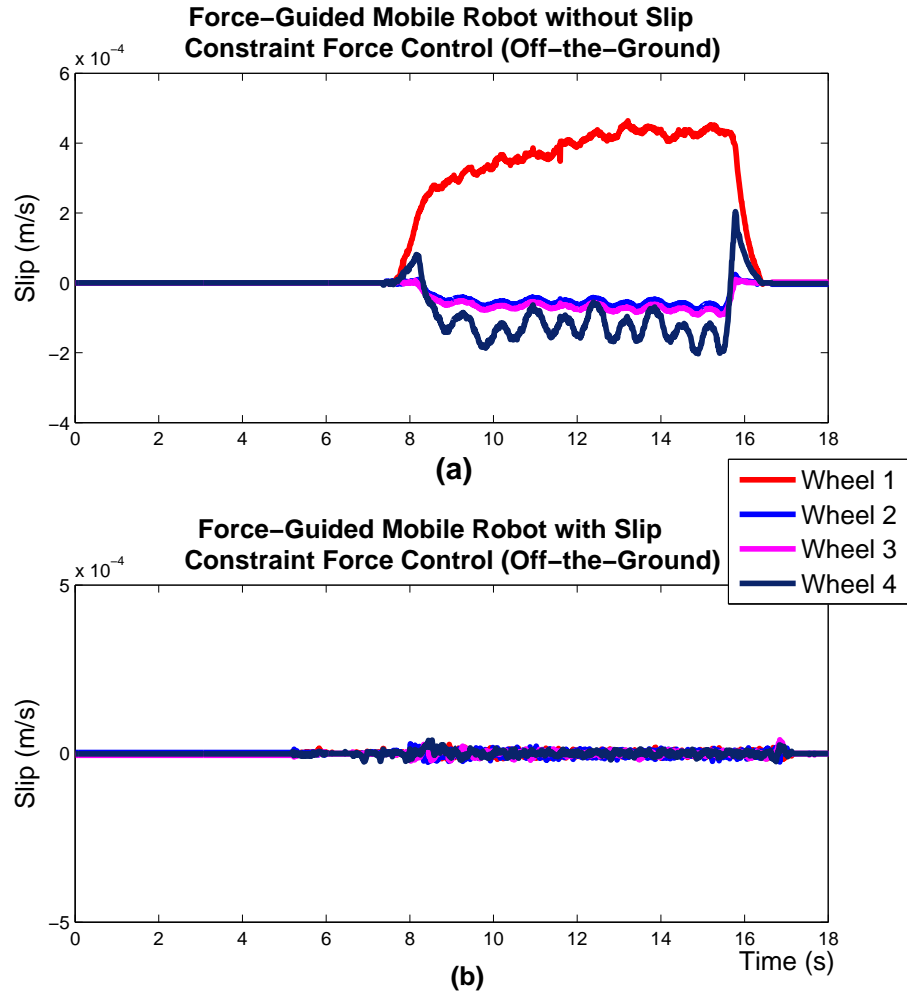


Figure 5.11: Off-the-ground test for the force-guided wheeled mobile robot. (a) Wheel slip was detected when the slip constraint force control scheme was not implemented. (b) Wheel slip was eliminated when the slip constraint force control scheme was implemented.

The above experimental results obtained for the force-guided wheeled mobile robot have been published in [117]. Two video clips demonstrate part of the research results of the aforementioned mobile manipulation project: one is the force-guided wheeled mobile robot with slip constraint force control (<http://ams.simtech.a-star.edu.sg/robot/uploads/MobileBase-WalkThrough.wmv>) and the other one is the

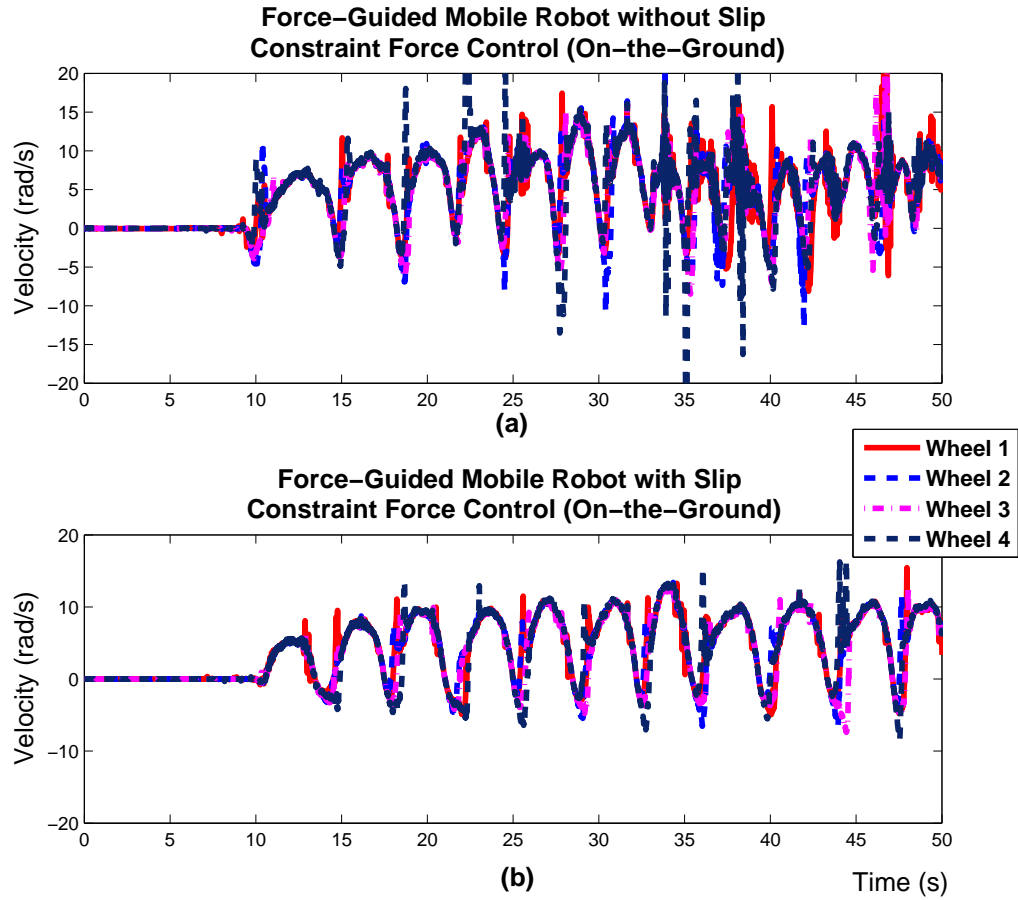


Figure 5.12: On-the-ground test for the force-guided wheeled mobile robot. (a) Uneven wheel velocities were observed (implies significant wheel slip) when the slip constraint force control scheme was not implemented. (b) Even wheel velocities were observed (implies minimum wheel slip) when the slip constraint force control scheme was implemented.

lead-through motion of the full mobile manipulator (<http://ams.simtech.a-star.edu.sg/robot/uploads/CombinedForceMotion-mobile-manip.mpg>) shown in Fig. 5.10.

5.3 Slip Control for Rough Terrain Navigation

In general, the slip problem of WMRs is not serious in structured environments such as rigid flat surfaces or indoor environments. The purpose of slip control in these

environments is mainly to achieve better localization accuracy in applications such as navigation or to ensure the success of a task in task-critical applications such as planetary exploration. However, in rough terrain navigation tasks, the critical mission of WMRs is to reliably move from the current location to the goal location. Thus wheel slip control becomes critical because wheel slip critically determines the traction performance of the system. For robust navigation on rough terrains, slip control becomes an important element of the system controller. The wheel-ground interaction model, which describes the relation between slip and traction force, becomes the critical dynamics to be considered.

Although we have presented the wheel-ground interaction model that complements the rigid body dynamic model, this model is not explicitly utilized in our slip control schemes presented in previous chapters. In rough terrain navigation tasks, the wheel-ground interaction dynamics becomes significant due to the highly time varying characteristic of the system dynamics in rough terrains. Therefore the controller should take the wheel-ground interaction dynamics into account for rough terrain navigation tasks.

In the following we present two schemes for achieving rough terrain navigation. One is the slip ratio control using sliding mode and the other one is the adaptive terrain parameter identification using the Recursive Least Squares estimator.

5.3.1 Sliding Mode Slip Ratio Control

As can be seen from the $\lambda - \mu$ curves (Fig. 3.8), the maximal traction force occurs at non-zero slip. In order to achieve the best tractive performance, it is desirable to

control the slip ratio at a desired value so that the tractive performance of the wheel-ground contact is optimized. One objective of slip ratio control is to drive the actual slip ratio towards the optimal traction force. Another objective of slip ratio control is to maintain the slip ratio within the stable region of the $\lambda - \mu$ curve, that is, the $(0, \mu_p)$ region of the curve. In below we will first derive the state space representation of the equations of motion of the wheel with the slip ratio as the state. Sliding mode controller will then be designed to form a explicit slip ratio control scheme.

Wheel Dynamics in Terms of Slip Ratio

By differentiating the slip ratio as described in Eq. 3.43, we obtain:

$$\dot{\lambda} = \frac{(1 - \lambda)\dot{\rho}r - \dot{v}_x}{\dot{\rho}r} \quad (5.8)$$

It is noted that Eq. 5.8 is for the acceleration case where $\dot{\rho}r > v_x$. The model for the deceleration case can be easily derived similarly.

As we only consider the wheel body dynamics, the longitudinal wheel dynamic model is simply

$$F_x = m\dot{v}_x \quad (5.9)$$

where m is the mass of the wheel body.

Combining Eq. 5.8, Eq. 5.9, the wheel dynamic model Eq. 3.45 and the slip-friction model Eq. 3.46, The dynamics of the wheel body taken into account the slip ratio is given as

$$\dot{\lambda} = f + gu \quad (5.10)$$

where

$$f = -\frac{(3 - 2\lambda)F_z\mu}{\dot{\rho}mr}$$

$$g = \frac{(1 - \lambda)}{I_\rho \dot{\rho} r}$$

$$u = \tau_\rho$$

Sliding Mode Controller

Denote λ as the state and λ_d the desired state, the sliding variable is defined as

$$s = \lambda_d - \lambda \quad (5.11)$$

The sliding variable s is used by the sliding mode control to change the structure of the control law.

The sliding mode slip ratio controller can be written as:

$$u = \frac{-f + \dot{\lambda}_d + k sgn(s)}{g} \quad (5.12)$$

where k is the sliding control gain.

Eq. (5.12) is the conventional structure of sliding mode controller. However, the notorious chattering problem makes it impractical to directly adopt the conventional sliding mode control structure. Therefore, instead of applying Eq. (5.12), the Low Pass Filtered Integral Sliding Mode Control (LPFISM) scheme developed in Section 5.2.1 was adopted to reduce the chattering problem.

Fig. 5.13 shows the block diagram of the ADAMS/Simulink co-simulation block diagram of the sliding mode slip ratio control for one wheel. Fig. 5.14 shows the simulation result of block diagram 5.13. The desired slip ratio is set to be 0.2. It can be seen the slip ratio tracked the desired slip ratio successfully with the proposed sliding mode slip ratio control scheme.

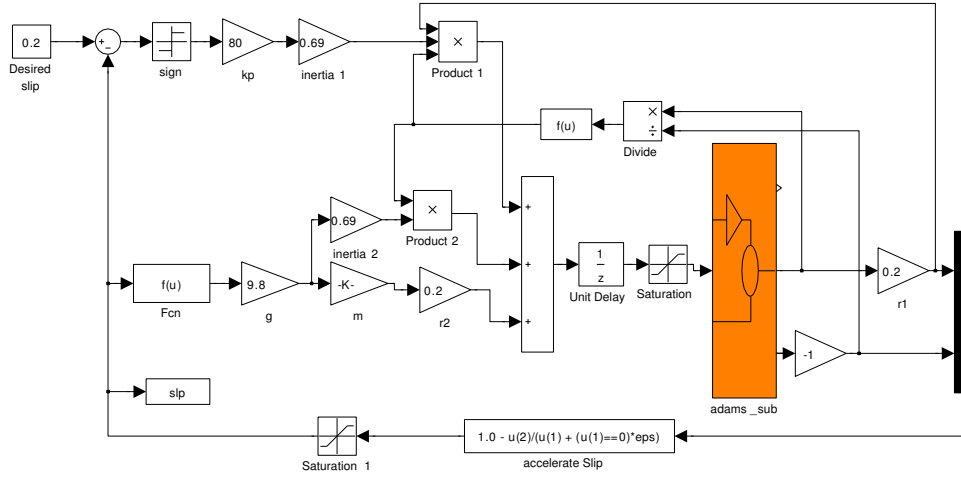


Figure 5.13: ADAMS/Simulink co-simulation block diagram for sliding mode slip ratio control of one wheel body.

Fig. 5.15 shows the ADAMS/Simulink co-simulation block diagram of the sliding mode slip ratio control for one wheel with the wheel linear velocity estimated by a sliding mode observer proposed in Chapter 4. Fig. 5.16 shows the slip ratio tracking result of the simulation. The simulation setup in this experiment is same as Fig. 5.13. It can be seen from Fig. 5.13 that, with the combination of sliding mode controller and sliding mode observer, the slip ratio tracking performance is comparable to that of the sliding mode controller (Fig. 5.14).

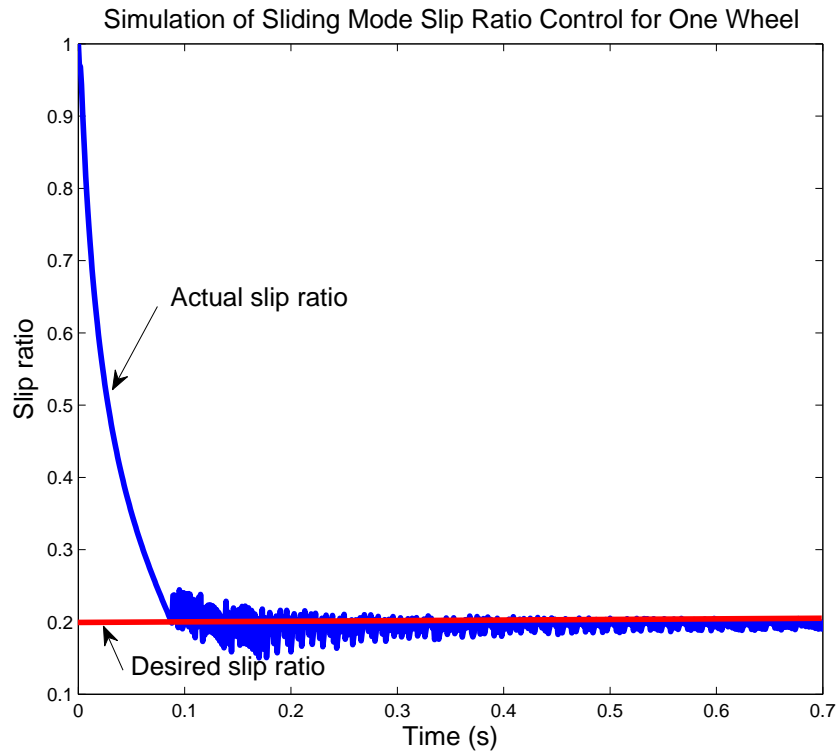


Figure 5.14: Slip ratio tracking performance of the sliding mode slip ratio control for one wheel body.

5.3.2 Adaptive Terrain Identification

In rough terrain environments, the characteristics of the changing terrains may be significantly different. So the controller of the mobile robot is required to perform normally in different terrains. That is, the controller is required to be adaptive. Since the wheel-ground interaction model is critical in rough terrain mobility, the characteristics of different terrain are the critical parameter that needs to be adapted.

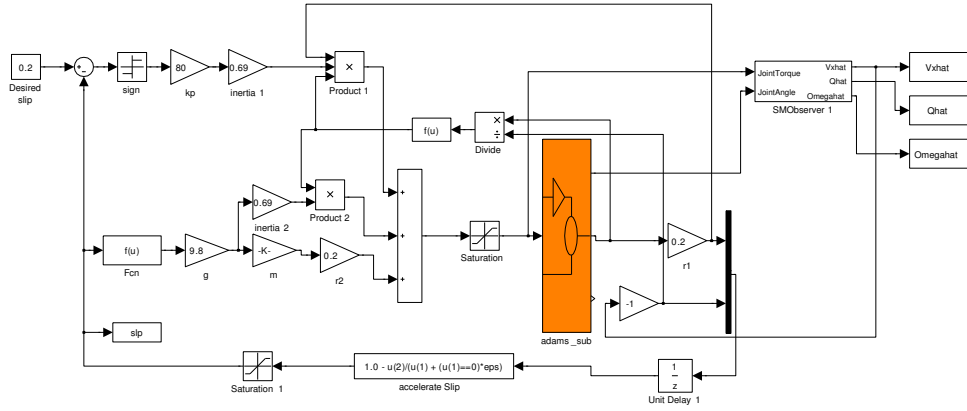


Figure 5.15: ADAMS/Simulink co-simulation block diagram for sliding mode slip ratio control with sliding mode observer for one wheel body.

In order to utilize the sliding mode slip ratio controller effectively, it is necessary to know about the optimal friction coefficient of different terrains. Since the optimal slip ratio is different for different types of terrain, it is essential to obtain this optimal slip ratio information for a particular type of terrain. In follows we propose a scheme to adaptively identify the terrain type combining a sliding mode observer for estimating the wheel linear velocity and a recursive least squares estimator for estimating the slowly changing terrain parameters. The advantage of this scheme is its ease for real time implementation. The proposed adaptive terrain identification is shown in the block diagram in Fig. 5.17. The inputs of the scheme are the joint angle ρ and

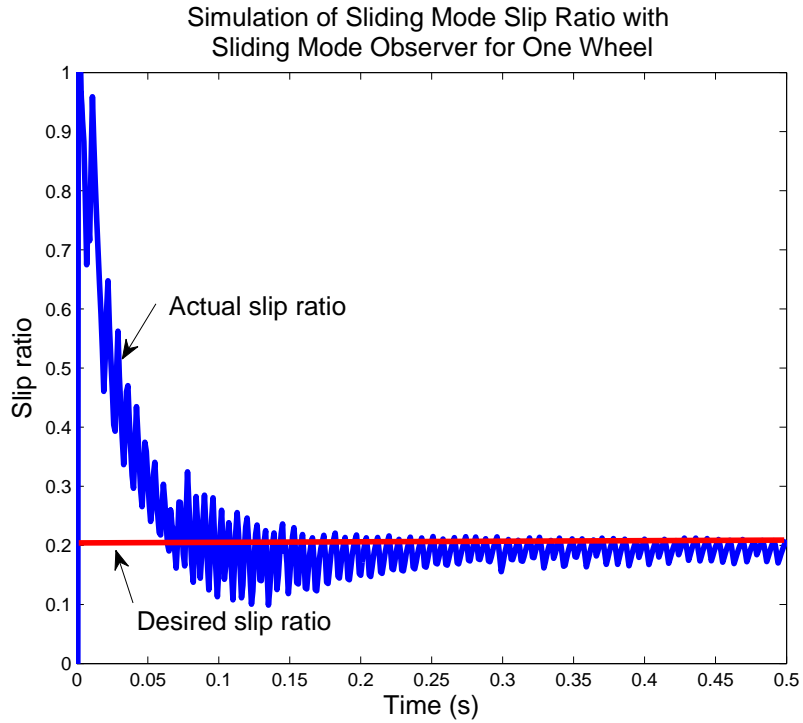


Figure 5.16: Slip ratio tracking performance of the sliding mode slip ratio control with sliding mode observer for one wheel body.

the joint torque τ . Both wheel angular velocity $\dot{\rho}$ and wheel longitudinal velocity \dot{p}_x are estimated using the sliding mode observer as proposed in Chapter 4. With the wheel-ground interaction model, the friction coefficient μ and slip ratio λ are computed. The computed friction coefficient and slip ratio will be input into the recursive least-squares estimator to estimate the parameters c_1 and c_2 of the $\lambda - \mu$ curve.

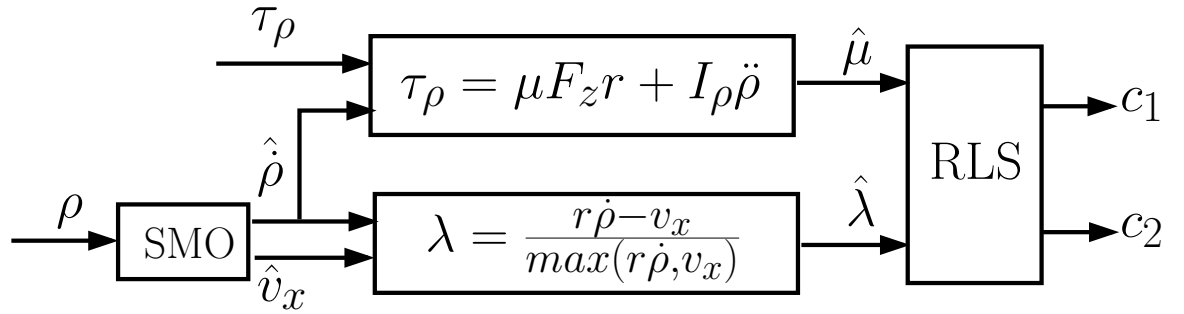


Figure 5.17: Block diagram of adaptive terrain identification based on the wheel-ground interaction model. SMO: sliding mode observer. RLS: recursive least squares estimator.

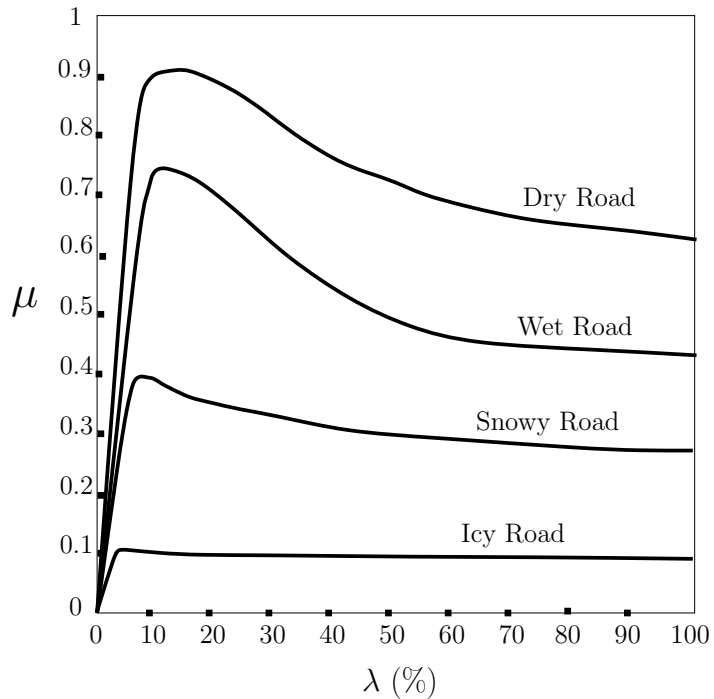


Figure 5.18: Empirical $\lambda - \mu$ curves for different terrains.

Model-Based Terrain Identification

Fig. 5.18 shows that empirical $\lambda - \mu$ curves for different terrains. As presented in Chapter 3, the $\lambda - \mu$ curves for different terrains can be approximated using the Kinecke Model [73] as given by Eq. 3.47104

By observation, this equation is a 2nd-order system with respect to the slip ratio. For convenience of deriving a linear form for this equation, we define two coefficients c_1 and c_2 for this 2nd-order system with respect to the slip ratio. Replacing λ_p and μ_p with c_1 and c_2 , Eq. 3.47 can be re-written as

$$\mu(\lambda) = \frac{c_1 \lambda}{c_2 + \lambda^2} \quad (5.13)$$

where:

$$\lambda_p = \sqrt{c_2}$$

$$\mu_p = \frac{c_1}{2\sqrt{c_2}}$$

For the convenience of estimation, we re-write the above model into the linear-in-the-parameters form as follows.

$$Y = \Phi \Theta \quad (5.14)$$

where:

- **Output**

$$y(k) = \mu(k) \lambda^2(k)$$

$$Y = [y(1), y(2), \dots, y(k)]^T$$

- **Regressor**

$$\varphi(k) = \begin{bmatrix} \lambda(k) \\ -\mu(k) \end{bmatrix}$$

$$\Phi = \begin{bmatrix} \varphi^T(1) \\ \vdots \\ \varphi^T(k) \end{bmatrix}$$

- **Parameter**

$$\Theta = \begin{bmatrix} c_1 \\ c_2 \end{bmatrix}$$

It can be seen from above model equations that the friction coefficient μ is required in identifying the known parameters. We have studied two methods for obtaining the friction coefficient. The first method is, in the case of a recursive identifier, we update both the parameters being identified and the friction coefficient in a similar recursive manner. The recursive updating law for the friction coefficient is chosen as

$$\hat{\mu}(k) = \frac{\hat{c}_1(k-1)\lambda(k)}{\hat{c}_2(k-1) + \lambda^2(k)} \quad (5.15)$$

However, it is verified through numerical simulation that this method cannot guarantee the convergence of the both friction coefficient and the unknown parameters being identified. Therefore, an alternative method was adopted to obtain the friction coefficient. The alternative method is, once again, a model-based method. We rewrite the wheel dynamic model 3.45 and 3.46 here

$$I_\rho \ddot{\rho} = \tau_\rho - F_x r$$

$$F_x = \mu F_z$$

It can be seen that the friction coefficient can be computed with the availability of wheel torque and wheel angular acceleration. Wheel torque is assumed be available from the motor current measurement. However, wheel angular acceleration is not directly measured. It is natural that we can obtain wheel angular acceleration through numerical differentiation of the wheel angular velocity. However, it is well known that acceleration estimation using position or velocity signals is usually difficult due to noise issues. A low pass filtering technique call *torque filtering* as studied in [121] helps overcoming this problem. Applying a low pass filter to both sides of Eq. 5.14

yields

$$(Y)_l = (\Phi)_l \Theta \quad (5.16)$$

where

$$(\cdot)_l = L^{-1} \left[\frac{l}{l+s} L(\cdot) \right]$$

where $L()$ and $L^{-1}()$ represent the Laplace transformation and the inverse Laplace transformation respectively, and l is the parameter for the first order low pass filter.

Although adopting the torque filtering technique eliminates the requirement of wheel angular acceleration, wheel angular velocity and wheel longitudinal velocity are still needed for successfully identifying the terrain characteristics. This problem has already be studied in the previous chapter where sliding mode observer has been introduced to obtain these velocities.

Recursive Least Squares with Exponential Forgetting

Recursive least squares (RLS) estimator is widely used for on-line parameter estimation applicable to systems that are linear-in-the-parameters. This method has the capability of estimating time-varying parameter, and it is known to have good robustness with respect to noise and disturbance [122]. The use of forgetting factor discounts the influence of the past data in the estimation of the current parameter. This property is very useful in dealing with time-varying parameter. Since RLS is for linear systems, we need to first describe the system in a linear discrete form. In order to form a linear system of equations, we need to re-construct the original Kiencke model as follows.

$$\hat{\Theta}(k) = \hat{\Theta}(k-1) + P(k)(y(k) - \varphi(k)^T \hat{\Theta}(k-1)) \quad (5.17)$$

$$P(k) = Q(k-1)\varphi(k)(\lambda I + \varphi^T(k)Q(k-1)\varphi(k))^{-1} \quad (5.18)$$

$$Q(k) = Q(k-1)(I - P(k)\varphi^T(k))/\lambda \quad (5.19)$$

where λ is a parameter such that $0 < \lambda < 1$. The parameter λ is called the *forgetting factor*. The most recent data is given unit weight, but data that is n time units old is weighted by λ^n . This method is called *exponential forgetting* [122]. $P(k)$ and $Q(k)$ are two gain matrices that drive the estimator to converge. The inputs of the estimator are the initial guess of the parameters $\hat{\Theta}(t_0)$ and gain matrix $Q(t_0) = (\Phi^T(t_0)\Phi(t_0))^{-1}$. To obtain an initial condition for Q , it is thus necessary to choose $k = t_0$ such that $\Phi^T(t_0)\Phi(t_0)$ is nonsingular.

In order to validate the effectiveness of this method, numerical simulation is conducted. As we decompose the operational forces into the lateral and longitudinal forces, the longitudinal wheel dynamics can be considered independently. Therefore, simulation with one wheel is chosen to test the effectiveness of *Recursive least Squares with Exponential Forgetting (RLSEF)*.

In the simulation, random noise of plus minus 10 percents were added to the velocity signals. Forgetting factor in the simulation is chosen to be 0.8. Low pass filter parameter is chosen as $l = 1$. The wheel torque input is chosen as sinusoidal. High frequency harmonics was added to the signal to simulate the noise in the wheel torque signal. The low pass filter used two purposes: firstly, it improves the signal-to-noise ratio by filtering the wheel torque as well as the regression matrix; secondly, with the low pass filter, measurement of the wheel angular acceleration or linear acceleration is not required. The results are shown in Figs. 5.19 and 5.20.

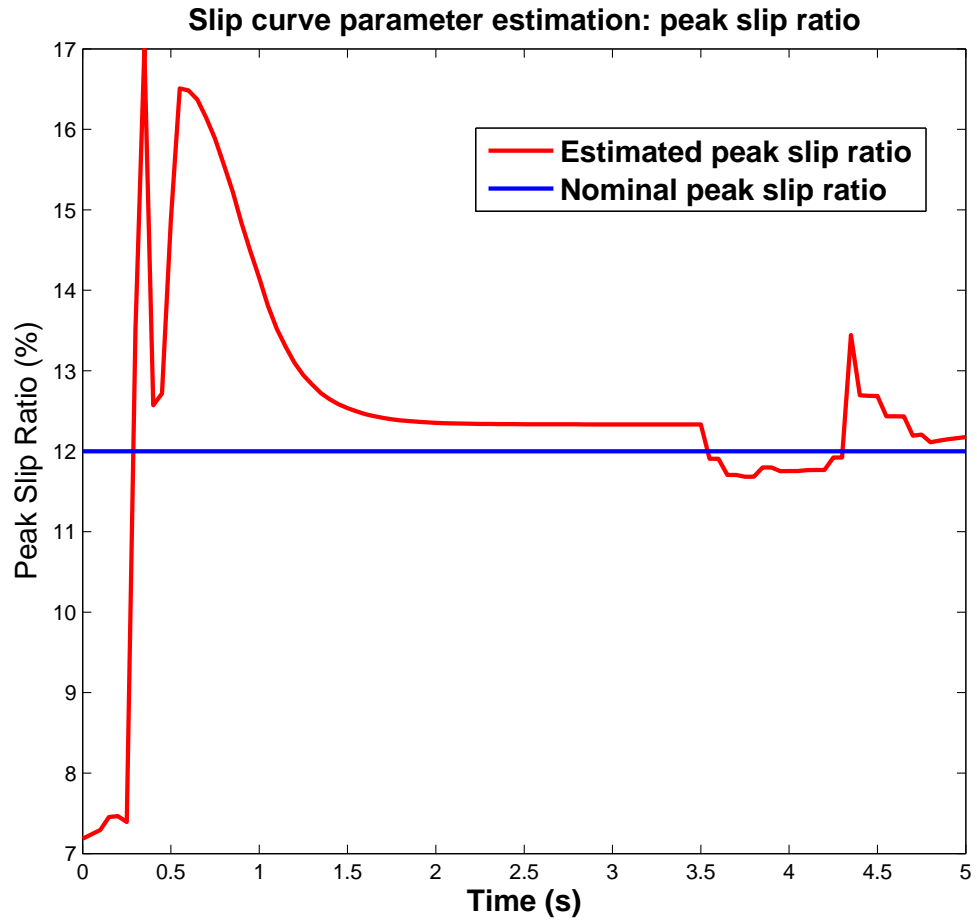


Figure 5.19: Parameter estimation of the $\lambda - \mu$ curve: estimation of the critical slip ratio corresponding to the peak friction coefficient.

5.4 Summary: Multi-Objective Controller Design

With the combination of the controllers proposed in this chapters, we achieve the following multiple objectives simultaneously

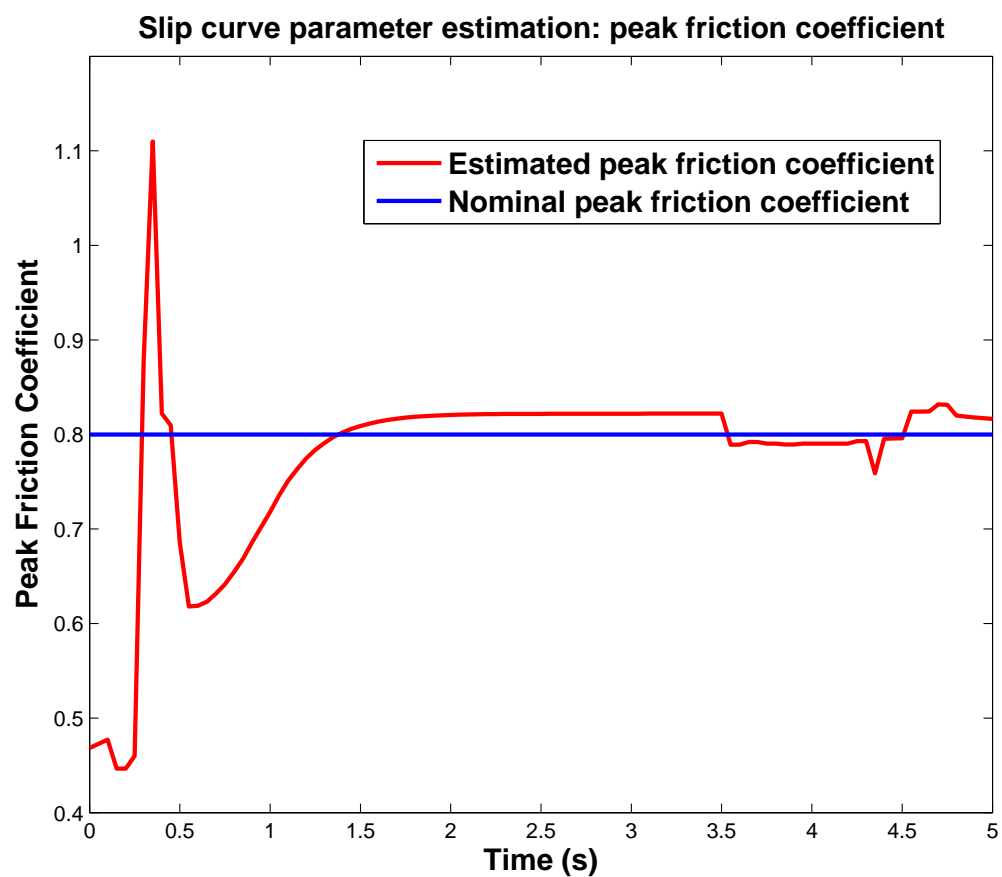


Figure 5.20: Parameter estimation of the $\lambda - \mu$ curve: estimation of the peak friction coefficient

- **operational space control.**

The adoption of the operational space formulation provides an unified and powerful control framework for different control modes such as trajectory tracking and hybrid force/motion control, and such control framework is applicable to almost any mechanism configurations such as serial manipulators, parallel manipulators, mobile robot and mobile manipulators.

- **internal force control.**

The proposed slip minimization by regulating the internal forces in the wheel-ground interaction thanks to the actuation redundancy of the mobile robot with powered caster wheels. The internal force controller can be integrated into the operational space control framework through null space torque projection.

- **slip ratio control.**

The proposed sliding mode slip ratio controller is aggressive control strategy in cases when wheel slip dynamics is significant in the wheel-ground interaction. It is expected that this controller would be more significant for outdoor vehicles where compliant pneumatic tire wheel moving high speed on unstructured road conditions. However, this technique is studied in this research as well. If wheel slip is successfully detected in indoor wheeled mobile robots, sliding mode controller could effectively regulate the wheel slip behavior. Sliding slip control can also be integrated into the operational space control framework through generating compensating wheel torque to account for the wheel-ground interaction dynamics.

- **adaptive terrain identification.**

Sensing or estimating the external environment is an important research problem in robotics. It is always effective to study a problem through the mathematical modeling of the problem. As wheel slip dynamic model represents the interaction between terrain characteristic and wheel motion, identifying terrain characteristics should be feasible by accurately measuring the wheel motion and reliable signal processing techniques. The developed recursive least squares estimator in this chapter represents a practical and yet effective strategy for achieving the objective of terrain identification.

CHAPTER 6

CONCLUSIONS

6.1 Research Review

A systematic study of the slip problem for wheeled mobile robots has been conducted in this research. Three main aspects of the slip problem are addressed: slip modelling, slip detection and slip control. The collective objective of this research is to develop effective slip control strategies for achieving robust mobility of wheeled mobile robots in both structured and unstructured environments.

In this research, wheel-ground interaction model is introduced and this complements the conventional rigid body dynamic model. By taking the longitudinal and lateral velocities of each wheel as the generalized velocities of the system, both kinematic and dynamic equations of the system are described explicitly in terms of slip.

Real time slip detection and estimation schemes have been presented. The effectiveness of the proposed schemes are verified. Robust estimating technique based on sliding mode is shown effective with a simplified wheel-ground interaction model.

The main work of this research is on the proposition of several slip control schemes. The proposed internal force based control schemes is effective for slip control of

wheeled mobile robots. Thanks to the actuation redundancy of the system, operational space control is decoupled from the internal force space control. The performance of the proposed slip control schemes is validated by both simulation and real time experiments.

The internal force based control structure has also been applied to force-controlled wheeled mobile robots. The proposed slip control scheme has also been combined with the unified force/motion control framework for a mobile manipulator. Experimental results confirm the slip reduction effect of the proposed scheme for both force-controlled WMRs and the mobile manipulator.

Explicit slip ratio control and real time adaptive terrain identification, which are suitable for rough terrains, are proposed. Simulation and experimental results show the potential of combining these two techniques together with the internal force control structure to achieve rough terrain mobility.

6.2 Contributions

The main contributions of this research are summarized as follows.

- **Systematic study of slip problem for wheeled mobile robots is conducted.**

Main aspects of slip problem for wheeled mobile robots have been researched respectively. With all these main aspects studied, general and complete slip control framework for wheeled mobile robots can be developed.

- **Physically meaningful and general slip control structure is developed based on internal force analysis for wheeled mobile robots.**

The proposed slip control scheme is physically meaningful as it is based on the

internal force analysis of the system. The internal force slip control scheme is also general as internal force analysis can always be conducted for wheeled mobile robots.

- **Slip control for both force-controlled wheeled mobile robot and mobile manipulator is achieved.**

Controlling wheeled mobile robots in mobile manipulation systems with unified force/motion control capability is challenging. The proposed slip control schemes have been successfully implemented for mobile manipulation.

- **Robust slip control and adaptive terrain identification are developed towards rough terrain mobility.**

Combining these schemes with the internal force control structure provides a flexible and reliable slip control scheme for rough terrain negotiations of wheeled mobile robots.

6.3 Limitations

This research is limited to planar WMRs due to the fact that the experimental setup without suspension system is mainly for indoor environments. Limitations of this research related to the planar constraint are summarized as follows.

- The simplified wheel-ground interaction model presented in this research is not sufficient to model the complex slip behavior of the wheel in rough terrains.
- The internal force analysis for planar WMRs presented in this research becomes invalid in the case of rough terrains.

- The vertical forces acted on the wheel is same for all wheels for planar WMRs.

However, this is not valid for WMRs working in rough terrains. The effective radius of each becomes varying for changing vertical forces acting on the wheel. Slip estimation for varying effective wheel radius is challenging.

6.4 Future Work

Interesting future work for this research is to overcome the limitations discussed above. In order to achieve robust rough terrain mobility, some recommended future research topics are summarized as follows.

- Robust rough terrain mobility requires more sensing information and more advanced state estimation techniques than those used in this research. Real time visual sensing has good potential for motion estimation and terrain classification. Due to the highly uncertain feature of wheel-ground interaction in rough terrains, sensor fusion techniques and statistical estimation techniques, such as extended Kalman filter or particle filter, are worthwhile for future work of this research.
- Fault detection and identification (FDI) and fault tolerant control (FTC) are important strategies for robust rough terrain mobility. The structure of sliding mode observer makes it suitable for FDI and the switching characteristic of sliding mode controller makes it feasible for FTC. It is worthwhile applying the sliding mode techniques used in this research to FDI and FTC.
- The omnidirectional mobility, singularity-free and redundant actuation characteristics of PCW-based WMRs make this type of robot suitable for rough

terrain applications such as planetary exploration. It is interesting to develop PCW-based WMRs to work in rough terrains.

BIBLIOGRAPHY

- [1] B. Thuiilot, B.D. Novel, and A. Micaelli, “Modelling and feedback control of mobile robots equiped with several steering wheels,” *IEEE Trans. Robotics and Automation*, vol. 12, no. 3, pp. 375–390, 1996.
- [2] G. Oriolo, A.D. Luca, and M. Vendittelli, “Wmr control via dynamic feedback linearization: Design, implementation and experimental validation,” *IEEE Trans. Control Systems Technology*, vol. 10, no. 6, pp. 835–852, 2002.
- [3] M.A. Minor, B.W. Albiston, and C.L. Schwensen, “Simplified motion control of a two-axle compliant framed wheeled mobile robot,” *IEEE Trans. Robotics*, vol. 22, no. 3, pp. 491–506, 2006.
- [4] S.M. Killough and F.G. Pin, “Design of an omnidirectional and holonomic wheeled platform prototype,” *IEEE Intl. Conf. Robotics and Automation*, vol. 1, pp. 84–90, 1992.
- [5] M. West and H. Asada, “Design of ball wheel mechanisms for omnidirectional vehicles with full mobility and invariant kinematics,” *Journal of Mechanical Design*, vol. 119, no. 2, pp. 153–161, 1997.
- [6] R. Holmberg and O. Khatib, “Development and control of a holonomic mobile robot for mobile manipulation tasks,” *Intl. Journal of Robotics Research*, vol. 19, no. 11, pp. 1066–1074, 2000.
- [7] P.F. Muir and C.P. Newman, “Kinematic modelling of wheeled mobile robots,” *Journal of Robotic Systems*, vol. 4, no. 2, pp. 281–340, 1987.
- [8] J.H. Chung, B-J Yi, W.K. Kim, and H. Lee, “The dynamic modeling and analysis for an omnidirectional mobile robot with three caster wheels,” *IEEE Intl. Conf. Robotics and Automation*, pp. 521–527, 2003.
- [9] L. Feng, Y. Koren, and J. Borenstein, “Cross-coupling motion controller for mobile robots,” *IEEE Control Systems Magazine*, vol. 13, no. 6, pp. 35–43, 1993.

- [10] J.Y. Wong, *Theory of Ground Vehicles*, John Wiley and Sons, Inc., 3rd edition, 2001.
- [11] M.G. Bekker, *Theory of Land Locomotion*, University of Michigan Press, 1956.
- [12] R. Balakrishna and A. Ghosal, “Modelling of slip for wheeled mobile robots,” *IEEE Trans. Robotics and Automation*, vol. 11, no. 1, pp. 126–130, 1995.
- [13] S. Shekhar, “Wheel rolling constraints and slip in mobile robots,” *IEEE Intl. Conf. Robotics and Automation*, pp. 2601–2607, 1997.
- [14] J. Svendenius and B. Wittenmark, “Review of wheel modelling and friction estimation,” *Department of Automatic control, Lund Institute of Technology*, 2003.
- [15] K. Iagnemma and S. Dubowsky, “Vehicle wheel-ground contact angle estimation: with application to mobile robot traction control,” *Intl. Symposium on Advances in Robot Kinematics*, pp. 137–146, 2000.
- [16] J. Borenstein, H.R. Everett, and L. Feng, “Where am i? systems and methods for mobile robot positioning,” *Technical Report, The University of Michigan, Ann Arbor, MI, USA*, 1996.
- [17] K. Yoshida and H. Hamano, “Motion dynamics and control of a planetary rover with slip-based traction control,” *SPIE 16th Intl. Symposium on Aerospace/Defense Sensing, Simulation and Controls*, vol. 4715, pp. 275–286, 2002.
- [18] X.X. Liu, L.B. Li, Y. Hori, T. Akiba, and R. Shirato, “Optimal traction control for ev utilizing fast torque response of electric motor,” *Industrial Electronics Society, 31st Annual Conference of IEEE*, pp. 2614–2619, 2005.
- [19] H. Cheng, G.F. Liu, Y.K. Yiu, Z.H. Xiong, and Z.X. Li, “Advantages and dynamics of parallel manipulators with redundant actuation,” *IEEE/RSJ Intl. Conf. Intelligent Robots and Systems*, pp. 171–176, 2001.
- [20] T.T. Park, J.H. Lee, B.J. Yi, W.K. Kim, B.J. You, and S.R. Oh, “Optimal design and actuator sizing of redundantly actuated omni-directional mobile robots,” *IEEE Intl. Conf. Robotics and Automation*, pp. 732–737, 2002.
- [21] J.C. Alexander and J.H. Maddocks, “On the kinematics of wheeled mobile robots,” *Intl. Journal of Robotics Research*, vol. 8, no. 5, pp. 15–27, 1989.
- [22] T.D. Murphey, “Control of multiple model systems,” PhD. Dissertation, 2002, California Institute of Technology, USA.

- [23] R. Holmberg, “Design and development of powered-caseter holonomic mobile robots,” PhD. Dissertation, 2000, Stanford University, USA.
- [24] D. Williams and O. Khatib, “The virtual linkage: A model for internal forces in multi-grasp manipulation,” *IEEE Intl. Conf. Robotics and Automation*, pp. 1025–1030, 1993.
- [25] G. Campion, G. Bastin, and B. D’Andrea-novel, “Structural properties and classification of kinematic and dynamic models of wheeled mobile robots,” *IEEE Trans. Robotics and Automation*, vol. 12, no. 1, pp. 47–62, 1996.
- [26] J. Barraquand and J-C Latombe, “Nonholonomic multibody mobile robots: Controllability and motion planning in the presence of obstacles,” *IEEE Intl. Conf. Robotics and Automation*, pp. 2328–2335, 1991.
- [27] J.P. Laumond, “Finding collision-free smooth trajectories for a non-holonomic mobile robot,” *Intl. Joint Conf. Artificial Intelligence*, pp. 1120–1123, 1987.
- [28] T. Skewis, J. Evans, V. Lumelsky, B. Krishnamurthy, and B. Barrows, “Motion planning for a hospital transport robot,” *IEEE Intl. Conf. Robotics and Automation*, pp. 58–63, 1991.
- [29] N. Sarkar, X.P. Yun, and V. Kumar, “Control of mechanical systems with rolling constraints: Application to dynamic control of mobile robots,” *Science Technical Report No. MS-CIS-92-44, University of Pennsylvania*, 1992.
- [30] A. Bloch and N.H. McClamroch, “Control of mechanical systems with nonholonomic constraints,” *IEEE Conf. Decision and Control*, pp. 201–205, 1989.
- [31] R.W. Brockett, R.S. Willmann, and H.J. Sussman, “Asymptotic stability and feedback stabilization,” *Differential Geometric Control Theory*, pp. 181–191, 1983.
- [32] R.L. Williams, B.E. Carter, P. Gallina, and G. Rosati, “Dynamic model with slip for wheeled omnidirectional robots,” *IEEE Trans. Robotics and Automation*, vol. 18, no. 3, pp. 285–293, 2002.
- [33] M. Wada and S. Mori, “Omnidirectional holonomic mobile robot using non-holonomic wheels,” *IEEE Intl. Conf. Robotics and Automation*, pp. 446 – 453, 1995.
- [34] M. Wada and S. Mori, “Holonomic and omnidirectional vehicle with conventional tires,” *IEEE Intl. Conf. Robotics and Automation*, pp. 3671–3676, 1996.

- [35] B-J Yi and W.K. Kim, “The kinematics for redundantly actuated omnidirectional mobile robots,” *Journal of Robotic Systems*, vol. 12, no. 6, pp. 255–267, 2002.
- [36] Y.P. Li, D.N. Oetomo, M.H. Ang Jr., and C.W. Lim, “Torque distribution and slip minimization in an omnidirectional mobile base,” *Intl. Conf. Advanced Robotics*, pp. 567–572, 2005.
- [37] Y. Zhao and L. BeMent, “Kinematics, dynamics and control of wheeled mobile robots,” *IEEE Intl. Conf. Robotics and Automation*, pp. 91–96, 1992.
- [38] B. d’Andrwa Novel, G. Bastin, and G. Campion, “Modelling and control of non-holonomic wheeled mobile robots,” *IEEE Intl. Conf. Robotics and Automation*, pp. 1130–1135, 1991.
- [39] P.F. Muir and C.P. Neuman, “Dynamic modeling of multibody robotic mechanisms: Incorporating closed-chains, friction, higher-pair joints, and unactuated and unsensed joints,” *IEEE Intl. Conf. Robotics and Automation*, pp. 1546–1551, 1988.
- [40] M. Huang, “Dynamic modelling and simulation of an agv (concic ii),” Master Thesis, 1991, Concordia University, Canada.
- [41] S. Kumar and J. Angeles, “Kinematics and dynamics of a three-wheeled 2-dof agv,” *IEEE Intl. Conf. Robotics and Automation*, pp. 1572–1577, 1989.
- [42] K. Thanjavur and R. Rajagopalan, “Ease of dynamic modelling of wheeled mobile robots (wmrs) using kane’s approach,” *IEEE Intl. Conf. Robotics and Automation*, pp. 2926–2931, 1997.
- [43] K-S Chang, R. Holmberg, and O. Khatib, “The augmented object model: Cooperative manipulation and parallel mechanism dynamics,” *IEEE Intl. Conf. Robotics and Automation*, pp. 470–475, 2000.
- [44] O. Khatib, “A unified approach for motion and force control of robot manipulators: The operational space formulation,” *IEEE Journal of Robotics and Automation*, vol. RA-3, no. 1, pp. 43–53, 1987.
- [45] Y.P. Li, T. Zielinska, M.H. Ang Jr., and W. Lin, “Wheel-ground interaction modelling and torque distribution for a redundant mobile robot,” *IEEE Intl. Conf. Robotics and Automation*, pp. 3362–3367, 2006.
- [46] B.J. Choi and S.V. Sreenivasan, “Control and kinematic design of multi-degree-of-freedom mobile robots with compliant linkage,” *IEEE Trans. Robotics and Automation*, vol. 11, no. 1, pp. 21–35, 1995.

- [47] B.J. Choi and S.V. Sreenivasan, “Gross motion characteristics of articulated mobile robots with pure rolling capability on smooth uneven surfaces,” *IEEE Trans. Robotics and Automation*, vol. 15, no. 2, pp. 340–343, 1999.
- [48] N. Chakraborty and A. Ghosal, “Dynamic modelling and simulation of a wheeled mobile robot for traversing uneven terrain without slip,” *Transactions of the ASME, Journal of Mechanical Design*, vol. 127, no. 5, pp. 901–909, 2005.
- [49] S. Shekhar, “Wheel rolling constraints and slip in mobile robots - simulation results,” *American Control Conference*, pp. 542–546, 1997.
- [50] R. Bauer, W. Leung, and T. Barfoot, “Experimental and simulation results of wheel-soil interaction for planetary rovers,” *IEEE/RSJ Intl. Conf. Intelligent Robots and Systems*, pp. 1427–1432, 2005.
- [51] G. Ishigami and K. Yoshida, “Steering characteristics of an exploration rover on loose soil based on all-wheel dynamics model,” *IEEE/RSJ Intl. Conf. Intelligent Robots and Systems*, pp. 2041–2046, 2005.
- [52] M. Thianwiboon and V. Sangveraphunsiri, “Traction control of a rocker-bogie field mobile robot,” *Intl. Journal of Science Technology*, vol. 10, no. 4, pp. 48–59, 2005.
- [53] Y.P. Li, T. Zielinska, M.H. Ang Jr., and W. Lin, “Vehicle dynamics of redundant mobile robots with powered caster wheels,” *CISM-IFTOMM Symposium on Robot Design, Dynamics, and Control*, pp. 221–228, 2006.
- [54] D.M. Helmick, Y. Cheng, D.S. Clouse, M. Bajracharya, L.H. Matthies, and S.I. Roumeliotis, “Slip compensation for a mars rover,” *IEEE/RSJ Intl. Conf. Intelligent Robots and Systems*, pp. 1419–1426, 2005.
- [55] D.M. Helmick, S.I. Roumeliotis, Y. Cheng, D.S. Clouse, M. Bajracharya, and L.H. Matthies, “Slip-compensated path following for planetary exploration rovers,” *Journal of Advanced Robotics*, vol. 20, no. 11, pp. 1257–1280, 2006.
- [56] Z.B. Song, Y.H. Zweiri, and L.D. Seneviratne, “Non-linear observer for slip estimation of skid-steering vehicles,” *IEEE Intl. Conf. Robotics and Automation*, pp. 1499 – 1504, 2006.
- [57] M. Seyr and S. Jakubek, “Proprioceptive navigation, slip estimation and slip control for autonomous wheeled mobile robots,” *IEEE Intl. Conf. Robotics and Automation*, pp. 109–114, 2006.

- [58] C.C. Ward and K. Iagnemma, “Model-based wheel slip detection for outdoor mobile robots,” *IEEE Intl. Conf. Robotics and Automation*, pp. 2724–2729, 2007.
- [59] G. Reina, L. Ojeda, A. Milella, and J. Borenstein, “Wheel slippage and sinkage detection for planetary rovers,” *IEEE Trans. Mechatronics*, vol. 11, no. 2, pp. 185–195, 2006.
- [60] L. Ojeda, D. Cruz, G. Reina, and J. Borenstein, “Current-based slippage detection and odometry correction for mobile robots and planetary rovers,” *IEEE Trans. Robotics*, vol. 22, no. 2, pp. 366–378, 2006.
- [61] A. Angelova, L. Matthies, D. Helmick, and P. Perona, “Slip prediction using visual information,” *Robotics: Science and Systems*, 2006.
- [62] K. Iagnemma and S. Dubowsky, “Traction control of wheeled robotic vehicles in rough terrain with application to planetary rovers,” *Intl. Journal of Robotics Research*, vol. 23, no. 10-11, pp. 1029–1040, 2004.
- [63] V.R. Kumar and K.J. Waldron, “Force distribution in closed kinematic chains,” *Journal of Robotics and Automation*, vol. 4, no. 6, pp. 657–664, 1988.
- [64] M.A. Nahon and J. Angeles, “Force optimization in redundantly-actuated closed kinematic chains,” *IEEE Intl. Conf. Robotics and Automation*, pp. 951–956, 1989.
- [65] J.F. O’Brien and J.T. Wen, “Redundant actuation for improving kinematic manipulability,” *IEEE Intl. Conf. Robotics and Automation*, pp. 1520–1525, 1999.
- [66] S.H. Lee, B-J Yi, S.H. Kim, and Y.K. Kwak, “Control of impact disturbance by redundantly actuated mechanism,” *IEEE Intl. Conf. Robotics and Automation*, pp. 3734–3741, 2001.
- [67] T. Yoshikawa, “Control algorithm for grasping and manipulation by multifingered robot hands using virtual truss model representation of internal force,” *IEEE Intl. Conf. Robotics and Automation*, pp. 369–376, 2000.
- [68] O. Brock and O. Khatib, “Elastic strips: A framework for motion generation in human environments,” *Intl. Journal of Robotics Research*, vol. 21, no. 12, pp. 1031–1052, 2002.
- [69] R. Jamisola, Jr. M.H. Ang, D. Oetomo, O. Khatib, T.M. Lim, and S.Y. Lim, “The operational space formulation implementation to canopy polishing using a mobile manipulator,” *IEEE Intl. Conf. Robotics and Automation*, pp. 400–405, 2002.

- [70] D. Oetomo, Jr. M.H. Ang, R. Jamisola, and O. Khatib, “Integration of torque controlled arm with velocity controlled base for mobile manipulation,” *CSM-IFToMM Symposium on Robotics*, pp. 189–200, 2002.
- [71] K.J. Astrom C. Canudas-De-Wit, H. Olsson and P. Lischinsky, “A new model for control of systems with friction,” *IEEE Trans. Automatic Control*, vol. 40, no. 3, pp. 419–425, 1995.
- [72] C. Canudas-De-Wit, P. Tsotras, E. Velenis, M. Basset, and G. Gissinger, “Dynamic friction models for road/tire longitudinal interaction,” *Intl. Journal of Vehicle System Dynamics*, vol. 39, no. 3, pp. 189–226, 2003.
- [73] U. Kiencke and A. Daiss, “Estimation of tyre friction for enhanced abs-systems,” *Intl. Symposium on Advanced Vehicle Control*, 1994.
- [74] S. Muller, M. Uchanski, and K. Hedrick, “Estimation of the maximum tire-road friction coefficient,” *ASME Journal of Dynamic Systems Measurement and Control*, vol. 125, no. 4, pp. 607–617, 2003.
- [75] L. Imsland, T.A. Johansen, T.I. Fossen, J.C. Kalkkuhl, and A. Suissa, “Vehicle velocity estimation using modular nonlinear observers,” *IEEE Conf. Decision Control*, pp. 6728–6733, 2003.
- [76] F.J. Jiang and Z.Q. Gao, “An adaptive nonlinear filter approach to vehicle velocity estimation for abs,” *IEEE Intl. Conf. Control Applications*, pp. 490–495, 2000.
- [77] C.R. Carlson and J.C. Gerdes, “Nonlinear estimation of longitudinal tire slip under several driving conditions,” *American Control Conference*, pp. 4975–4980, 2003.
- [78] A. Hac and E. Bedner, “Robustness of side slip estimation and control algorithms for vehicle chassis control,” *International Technical Conference on the Enhanced Safety of Vehicles Conference*, 2007.
- [79] Y. Fukada, “Slip-angle estimation for vehicle stability control,” *Vehicle System Dynamics*, vol. 32, no. 4-5, pp. 375–388, 1999.
- [80] D.R. Lindgren, T. Hague, P.J.P. Smith, and J.A. Marchant, “Relating torque and slip in an odometric model for an autonomous agricultural vehicle,” *Autonomous Robots*, vol. 13, no. 1, pp. 73–86, 2002.
- [81] C. Unsal and P. Kachroo, “Sliding mode measurement feedback control for antilock braking systems,” *IEEE Trans. Control System Technology*, vol. 7, no. 2, pp. 271–281, 1999.

- [82] M. Makatchev, S.Y.T. Lang, S.K. Tso, and J.J. McPhee, “Cross-coupling control for slippage minimization of a four-wheel-steering mobile robot,” *Intl. Symposium on Robotics*, pp. 42–47, 2000.
- [83] D.B. Reister and M.A. Unseren, “Position and constraint force control of a vehicle with two or more steerable drive wheels,” *IEEE Trans. Robots and Automation*, vol. 9, no. 6, pp. 723–731, 1993.
- [84] P. Lamon and R. Siegwart, “Wheel torque control in rough terrain - modeling and simulation,” *IEEE Intl. Conf. Robots and Automation*, 2005.
- [85] P. Lamon, A. Krebs, M. Lauria, R. Siegwart, and S. Shooter, “Wheel torque control for a rough terrain rover,” *IEEE Intl. Conf. Robots and Automation*, pp. 4682–4687, 2004.
- [86] T. Furuya, Y. Toyoda, and Y. Hori, “Implementation of advanced adhesion control for electric vehicle,” *Intl. Workshop on Advanced Motion Control*, vol. 2, pp. 430–435, 1996.
- [87] Y. Hori, Y. Toyoda, and Y. Tsuruoka, “Traction control of electric vehicle: Basic experimental results using the test ev “uot electric march”,” *IEEE Trans. Industry Applications*, vol. 34, no. 5, pp. 1131–1138, 1998.
- [88] S. Sakai, H. Sado, and Y. Hori, “Motion control in an electric vehicle with four independently driven in-wheel motors,” *IEEE/ASME Trans. Mechatronics*, vol. 4, no. 1, pp. 9–16, 1999.
- [89] H. Sado, S.I. Sakai, and Y. Hori, “Road condition estimation for traction control in electric vehicle,” *IEEE Intl. Symposium on Industrial Electronics*, pp. 973–978, 1999.
- [90] Y. Hori, “Future vehicle driven by electricity and control - research on four-wheel-motored “uot electric march ii”,” *IEEE Trans. Industrial Electronics*, vol. 51, no. 5, pp. 954–962, 2004.
- [91] J.J.E. Slotine and W.P. Li, *Applied Nonlinear Systems*, Prentice-Hall, 1991.
- [92] V.I. Utkin, *Sliding Mode in Control and Optimization*, Springer-Verlag, 1992.
- [93] K.R. Buckholtz, “Reference input wheel slip tracking using sliding mode control,” *SAE World Congr. No. 2002-01-0301*, 2002.
- [94] I. Haskara, C. Hatipoglu, and U. Ozguner, *Sliding Mode Compensation, Estimation and Optimization Methods in Automotive Control Problems*, Variable structure systems: towards the 21st century, pp. 155-174, 2002, Springer-Verlag, edited by X.H. Yu and J-X Xu.

- [95] H. Lee and M. Tomizuka, “Adaptive vehicle traction force control for intelligent vehicle highway systems (ivhss),” *IEEE Trans. Industrial Electronics*, vol. 50, no. 1, pp. 37–47, 2003.
- [96] A. Kawamura, H. Itoh, and K. Sakamoto, “Chattering reduction of disturbance observer based sliding mode control,” *IEEE Trans. Industry Applications*, vol. 30, no. 2, pp. 456–461, 1994.
- [97] V. Utkin and J.X. Shi, “Integral sliding mode in systems operating under uncertainty conditions,” *IEEE Conf. Decision and Control*, pp. 4591–4596, 1996.
- [98] J. Guldner V. Utkin and J.X. Shi, *Sliding Mode Control in Electromechanical Systems*, 1999.
- [99] E.J. Rossetter and J.C. Gerdes, “A study of lateral vehicle control under a ‘virtual’ force framework,” *Intl. Symposium on Advanced Vehicle Control*, 2002.
- [100] J.K. Park and C.Y. Kim, “Wheel slip control in traction control system for vehicle stability,” *Intl. Journal of Vehicle System dynamics*, vol. 31, no. 4, pp. 263–278, 1999.
- [101] K. Kin, O. Yano, and H. Urabe, “Enhancements in vehicle stability and steerability with slip control,” *JSAE Review*, vol. 24, no. 1, pp. 71–79, 2003.
- [102] K. Yi, K. Hedrick, and S.C. Lee, “Estimation of tire-road friction using observer based identifiers,” *Intl. Journal of Vehicle System Dynamics*, vol. 31, no. 4, pp. 233–261, 1999.
- [103] C. Canudas-De-Wit and R. Horowitz, “Observers for tire/road contact friction using only wheel angular velocity information,” *IEEE Conf. Decision and Control*, pp. 3932–3937, 1999.
- [104] C. Canudas-De-Wit, M.L. Petersen, and A. Shiriaev, “A new nonlinear observer for tire/road distributed contact friction,” *IEEE Conf. Decision and Control*, pp. 2246–2251, 2003.
- [105] B. Kwak and Y.J. Park, “Vehicle states observer using adaptive tire-road friction estimator,” *JSME Intl. Journal. Ser C. Mech Systems, Mach Elem Manuf*, vol. 44, no. 3, pp. 668–675, 2001.
- [106] F. Gustafsson, “Estimation and change detection of tire-road friction estimation using the wheel slip,” *IEEE Symposium on Compute Aided Control System Design*, pp. 99–104, 1996.
- [107] F. Gustafsson, “Monitoring tire-road friction estimation using the wheel slip,” *IEEE Conf. Control Systems*, pp. 42–49, 1998.

- [108] C. Lee, K. Hedrick, and K. Yi, “Real-time slip-based estimation of maximum tire-road friction coefficient,” *IEEE/ASME Trans. Mechatronics*, vol. 9, no. 2, pp. 454–458, 2004.
- [109] J.J. Craig, *Introduction to Robotics, Mechanics and Control*, Addison-Wesley, 2nd edition, 1989.
- [110] R.M. Murray, Z.X. Li, and S.S. Sastry, *A Mathematical Introduction to Robotic Manipulation*, CRC Press, 1994.
- [111] Y.K. Yiu and Z.X. Li, “Optimal forward kinematics map for a parallel manipulator with sensor redundancy,” *IEEE Intl. Symposium on Computational Intelligent in Robotics and Automation*, pp. 354–359, 2003.
- [112] F. Marquet, F. Pierrot, and O. Company, “A statistical approach for the computation of the forward kinematic model of redundantly actuated mechanisms,” *IEEE/RSJ Intl. Conf. Intelligent Robots and Systems*, pp. 3558–3563, 2003.
- [113] C. Gosselin and J. Angeles, “Singularity analysis of closed-loop kinematic chains,” *IEEE Trans. Robotics and Automation*, vol. 6, no. 3, pp. 281–290, 1990.
- [114] D.N. Oetomo, Y.P. Li, M.H. Ang Jr., and C.W. Lim, “Omnidirectional mobile robots with powered caster wheels: Design guidelines from kinematic isotropy analysis,” *IEEE/RSJ Intl. Conf. Intelligent Robots and Systems*, pp. 2708–2713, 2005.
- [115] D.N. Oetomo and Jr. M.H. Ang, “Singularity-free joint actuation for omnidirectional mobile platforms with powered caster wheels,” *JOURNAL OF MECHANICAL DESIGN*, vol. 130, no. 5, pp. 054501–1–054501–5, 2008.
- [116] P. Kachroo, “Nonlinear sliding mode control for vehicle control,” PhD. Dissertation, 1993, University of California at Berkeley, CA, USA.
- [117] Y.P. Li, M. H. Ang Jr., and W. Lin, “Slip modelling, detection and control for redundantly actuated wheeled mobile robots,” *IEEE/ASME Intl. Conf. Advanced Intelligent Mechatronics*, pp. 967–972, 2008.
- [118] F. Gustafsson, “Slip-based tire-road friction estimation,” *Automatica*, vol. 33, no. 6, pp. 1087–1099, 1996.
- [119] J.J.E. Slotine, J.K. Hedrick, and E.A. Misawa, “On sliding observers for nonlinear systems,” *ASME Journal of Dynamic Systems, Measurement, and Control*, vol. 109, pp. 245–252, 1987.

- [120] O. Khatib, “Motion/force redundancy of manipulators,” *Japan-U.S.A. Symposium on Flexible Automation*, pp. 337–342, 1990.
- [121] Frank L. Lewis, D. M. Dawson, and Chaouki T. Abdallah, *Robot Manipulator Control: Theory and Practice*, CRC Press, 2003.
- [122] G.C. Goodwin and K.S. Sin, *Adaptive Filtering: Prediction and Control*, Prentice-Hall, 1984.

APPENDIX A

PUBLICATIONS

A.1 Publications Arising from the PhD Work

- Yuan Ping Li, Marcelo H. Ang Jr. and Wei Lin, Slip Modelling, Detection and Control for Redundantly Actuated Wheeled Mobile Robots, In Proc. IEEE/ASME Intl. Conf. Advanced Intelligent Mechatronics, July, 2008.
- Yuan Ping Li, Teresa Zielinska, Marcelo H. Ang Jr. and Wei Lin, Vehicle Dynamics of Redundant Mobile Robots with Powered Caster Wheels, In Proc. CISM-IFToMM Symposium on Robot Design, Dynamics, and Control, June, 2006.
- Yuan Ping Li, Teresa Zielinska, Marcelo H. Ang Jr. and Wei Lin, Wheel-Ground Interaction Modelling and Torque Distribution for a Redundant Mobile Robot, In Proc. IEEE Intl. Conf. Robotics and Automation, May, 2006.
- Yuan Ping Li, Denny Oetomo, Marcelo H. Ang Jr. and Chee Wang Lim, Torque Distribution and Slip Minimization in an Omnidirectional Mobile Base, In Proc. Intl. Conf. Advanced Robotics, July, 2005.

- Denny Oetomo, Yuan Ping Li, Marcelo H. Ang Jr. and Chee Wang Lim, Omnidirectional Mobile Robots with Powered Caster Wheels: Design Guidelines from Kinematic Isotropy Analysis, In Proc. IEEE/RSJ Intl. Conf. Intelligent Robots and Systems, August, 2005.

A.2 Publications on Other Research Areas

- N.D. Vuong and M.H. Ang Jr. and Y.P. Li and S.Y. Lim, Improved Dynamic Identification of Robotic Manipulators in the Linear Region of Dynamic Friction, In Proc. Intl. IFAC Symposium on Robot Control, September, 2009.
- Tirthankar Bandyopadhyay, Yuan Ping Li, David Hsu and Marcelo H. Ang Jr., A Greedy Strategy for Tracking a Locally Predictable Target among Obstacles, In Proc. IEEE Intl. Conf. Robotics and Automation, May, 2006.
- Tirthankar Bandyopadhyay, Yuan Ping Li, Marcelo H. Ang Jr., Stealth Tracking of an Unpredictable Target among Obstacles, In Proc. The Sixth Intl. Workshop on the Algorithmic Foundations of Robotics, Springer, 2004.

APPENDIX B

AUGMENTED OBJECT MODEL FOR THE TESTED ROBOT

B.1 Kinetic Energy Matrix Λ

The operational space kinetic energy matrix Λ for the tested robot in this thesis. Following Figure 1.6 and 1.7, we model each PCW module of the robot as a 3-DOF serial manipulator. The difference between our modelling and that of Holmberg [6] is that we consider the chassis of the robot as the loading grasped by cooperative manipulators (wheels). This is expected to improve the modelling accuracy. In the following formulation, we assume the parameters for each wheel are exactly the same. It is noted that the unmeasurable twist joint angle is required for the dynamic model computation. This is obtained from the parallel kinematics of the mobile robot where the passive joint angles can be calculated from the measurement of the active joint angles. Slip will make this computation invalid, however, we ignore this special case.

$$\Lambda = \sum_{i=1}^4 \Lambda_i + \Lambda_\ell$$
$$\Lambda_i = \begin{bmatrix} \Lambda_i^{11} & \Lambda_i^{12} & \Lambda_i^{13} \\ -\Lambda_i^{12} & \Lambda_i^{22} & \Lambda_i^{23} \\ -\Lambda_i^{13} & -\Lambda_i^{23} & \Lambda_i^{33} \end{bmatrix}$$

$$\Lambda_\ell = \begin{bmatrix} m_\ell & 0 & 0 \\ 0 & m_\ell & 0 \\ 0 & 0 & 0.5m_\ell r^2 \end{bmatrix}$$

$$\begin{aligned} \Lambda_i^{11} = & \frac{1}{8b^2r^2}[(4I_{zz1} + 4I_{zz2} + h^2m_3)r^2 + 2b^2(I_{xx1} + I_{yy1} + r^2(2m_1 + 4m_2 + 4m_3)) \\ & + (2b^2(I_{xx1} + I_{yy1} + 2m_1r^2) - r^2(4I_{zz1} + 4I_{zz2} + h^2m_3))\cos(2(\beta_i - \phi_i)) \\ & - 4b^2(I_{xx1} - I_{yy1})\cos^2(\beta_i - \phi_i)\cos(2\sigma_i) - 8bhm_3r^2\sin(\beta_i)\sin(\beta_i - \phi_i)] \end{aligned}$$

$$\begin{aligned} \Lambda_i^{22} = & \frac{1}{8b^2r^2}[(4I_{zz1} + 4I_{zz2} + h^2m_3)r^2 + 2b^2(I_{xx1} + I_{yy1} + r^2(2m_1 + 4m_2 + 4m_3)) \\ & + (r^2(4I_{zz1} + 4I_{zz2} + h^2m_3) - 2b^2(I_{xx1} + I_{yy1} + 2m_1r^2))\cos(2(\beta_i - \phi_i)) \\ & + 4b^2(I_{yy1} - I_{xx1})\sin^2(\beta_i - \phi_i)\cos(2\sigma_i) - 8bhm_3r^2\cos(\beta_i)\cos(\beta_i - \phi_i)] \end{aligned}$$

$$\begin{aligned} \Lambda_i^{33} = & \frac{1}{8b^2r^2}[h^2r^2(4I_{zz1} + 4I_{zz2} + h^2m_3) + 2b^2(4r^2I_{zz3} + h^2(I_{xx1} + I_{yy1} + r^2(2m_1 \\ & + 4m_2 + m_3))) + h^2(-4bhm_3r^2\cos(\phi_i) + (r^2(4I_{zz1} + 4I_{zz2} + h^2m_3) \\ & - 2b^2(I_{xx1} + I_{yy1} + 2m_1r^2))\cos(2\phi_i) + 4b^2(I_{yy1} - I_{xx1})\cos(2\sigma_i)\sin^2(\phi_i))] \end{aligned}$$

$$\begin{aligned} \Lambda_i^{12} = & \frac{1}{8b^2r^2}[(2b^2(I_{xx1} + I_{yy1} + 2m_1r^2) - r^2(4I_{zz1} + 4I_{zz2} + h^2m_3) + 2b^2 \\ & (I_{yy1} - I_{xx1})\cos(2\sigma_i))\sin(2\beta_i - 2\phi_i) + 4bhm_3r^2\sin(2\beta_i - \phi_i)] \end{aligned}$$

$$\begin{aligned} \Lambda_i^{13} = & \frac{h}{8b^2r^2}[(2b^2(I_{xx1} + I_{yy1} + 2r^2(m_1 + m_2 + m_3)) - r^2(4I_{zz1} \\ & + 4I_{zz2} + h^2m_3))\sin(\beta_i) + (2b^2(I_{xx1} + I_{yy1} + 2m_1r^2) - r^2(4I_{zz1} \\ & + 4I_{zz2} + h^2m_3))\sin(\beta_i - 2\phi_i) + 2b(2b(I_{xx1} - I_{yy1})\cos(\beta_i - \phi_i) \\ & \cos(2\sigma_i)\sin(\phi_i) + hm_3r^2(2\sin(\beta_i - \phi_i) + \sin(\beta_i + \phi_i)))] \end{aligned}$$

$$\begin{aligned} \Lambda_i^{23} = & \frac{h}{8b^2r^2}[(r^2(4I_{zz1} + 4I_{zz2} + h^2m_3) + 2b^2(I_{xx1} + I_{yy1} + 2r^2(m_1 + m_2 \\ & + m_3))\cos(\beta_i) + (r^2(4I_{zz1} + 4I_{zz2} + h^2m_3) - 2b^2(I_{xx1} + I_{yy1} \\ & + 2m_1r^2))\cos(\beta_i - 2\phi_i) + 4b^2(I_{xx1} - I_{yy1})\cos(2\sigma_i)\sin(\beta_i - \phi_i) \\ & \sin(\phi_i) - 2bhm_3r^2(3\cos(\beta_i)\cos(\phi_i) + \sin(\beta_i)\sin(\phi_i))] \end{aligned}$$

B.2 Coriolis/Centrifugal Force Vector ϑ

$$\vartheta = J^{-T}b[\dot{q}\dot{q}] - \Lambda h[\dot{q}\dot{q}]$$

$$J^{-T} = \begin{bmatrix} \sin(\beta_i - \phi_i)/b & -\cos(\beta_i - \phi_i)/r & -\sin(\beta_i - \phi_i)/b \\ -\cos(\beta_i - \phi_i)/b & -\sin(\beta_i - \phi_i)/r & \cos(\beta_i - \phi_i)/b \\ -\cos(\phi_i)h/b & \sin(\phi_i)h/r & 1 + \cos(\phi_i)h/b \end{bmatrix}$$

$$b[\dot{q}\dot{q}] = \begin{bmatrix} hm_3\dot{\phi}_i(-0.5r\dot{\rho}_i\cos(\phi_i) - b(0.5\dot{\phi}_i + \dot{\sigma}_i)\sin(\phi_i)) \\ -0.5hm_3r\dot{\phi}_i(\dot{\phi}_i + \dot{\sigma}_i)\cos(\phi_i) \\ 0.5hm_3\dot{\sigma}_i(r\dot{\rho}_i\cos(\phi_i) + b\dot{\sigma}_i\sin(\phi_i)) \end{bmatrix}$$

$$h[\dot{q}\dot{q}] = \begin{bmatrix} -\dot{\phi}_i(r\dot{\rho}_i\sin(\beta_i - \phi_i) + b\dot{\sigma}_i\cos(\beta_i - \phi_i)) \\ \dot{\phi}_i(r\dot{\rho}_i + b\dot{\sigma}_i)\cos(\beta_i - \phi_i) \\ 0 \end{bmatrix}$$

APPENDIX C

BASICS OF SLIDING MODE

Sliding mode technique has been used in both state estimation and controller design in this thesis. It was used to design velocity observer to estimate the unmeasurable system states. It was also used to construct robust slip ratio controller.

We use a single input second order system to present the procedures of designing sliding mode observer/controller and derive the conditions that guarantee the accessibility/stability of the system.

A simple second order system with single input is:

$$\ddot{x} = f + u$$

where u is the control input, x is the state and f is a nonlinear function of x which is not exactly known but estimated as f_{eq} . The upper bound F of the uncertainty of f is defined as the smallest real number satisfying

$$|f_{eq} - f| \leq F$$

The aim of the controller is to drive the state x to a desired state x_d . Define the state error as:

$$e = x_d - x$$

Then,

$$\dot{e} = \dot{x}_d - \dot{x}$$

and,

$$\ddot{e} = \ddot{x}_d - \ddot{x}$$

The system equation becomes

$$\dot{e} = \dot{x}_d - f - u$$

A *sliding plane* is defined as:

$$s = \dot{e} + \lambda e$$

where λ is a positive constant which determines the convergence rate of the system when the sliding plane is hit. Consider

$$\dot{s} = \ddot{e} + \lambda \dot{e} = \ddot{x} - f - u + \lambda \dot{e}$$

When the system is staying on the sliding plane, it is controlled by the continuous control signal $u = u_{eq}$ which is called the *equivalent control*. Hence,

$$u_{eq} = \ddot{x} - f_{eq} + \lambda \dot{e}$$

To tackle the uncertainty of f , a discontinuous control signal u_{dis} is added to the control input.

$$u = u_{eq} + u_{dis}$$

$$u_{dis} = k \operatorname{sgn}(s)$$

where sgn is the sign function. k is a positive constant that describes the amplitude of the discontinuous control signal. It should be large enough to overcome the uncertainty of f . To ensure the system stability, the existence and the reachability of the

sliding plane, the following *sliding condition* should be satisfied:

$$s\dot{s} < -\eta |s|$$

where η is a positive constant that governs the reaching time, i.e. the time taken to hit the sliding plane if the initial state is not on the plane.

$$s\dot{s} = s(f_{eq} - f) - k|s| < -\eta|s|$$

A sufficient condition for k is

$$k > F + \eta$$

The above derivation is a complete design of a sliding mode controller.

APPENDIX D

VIRTUAL PROTOTYPING

Simulation is the first step to design, identify and control robots and it's a powerful technique to improve quality and productivity of research work. Using software environment, one can visually design and model systems by means of simulating separate parts of these systems and investigating its behavior under conditions that are close to real ones.

The simulation platform used in this thesis is known as Virtual Prototyping. Virtual Prototyping is ordinary tool nowadays to simulate mechanical systems.

Fig. D.1 shows the important role of Virtual Prototyping in system development. Between the conceptual design and the physical prototyping, Virtual Prototyping synchronizes mechanical design and control design.

Virtual Prototyping is formed by integrating three simulation platforms to be a powerful and realistic simulation environment.

- 3D graphical modelling platform.

3D modelling packages such as ProEngineer, UniGraphics, Solidworks and Solid-Edge, are used to construct the 3D CAD model of mechanism.

Fig. D.2 shows the modelling of the tested mobile robot using SOLIDWORKS and its COSMOS/MOTION module.

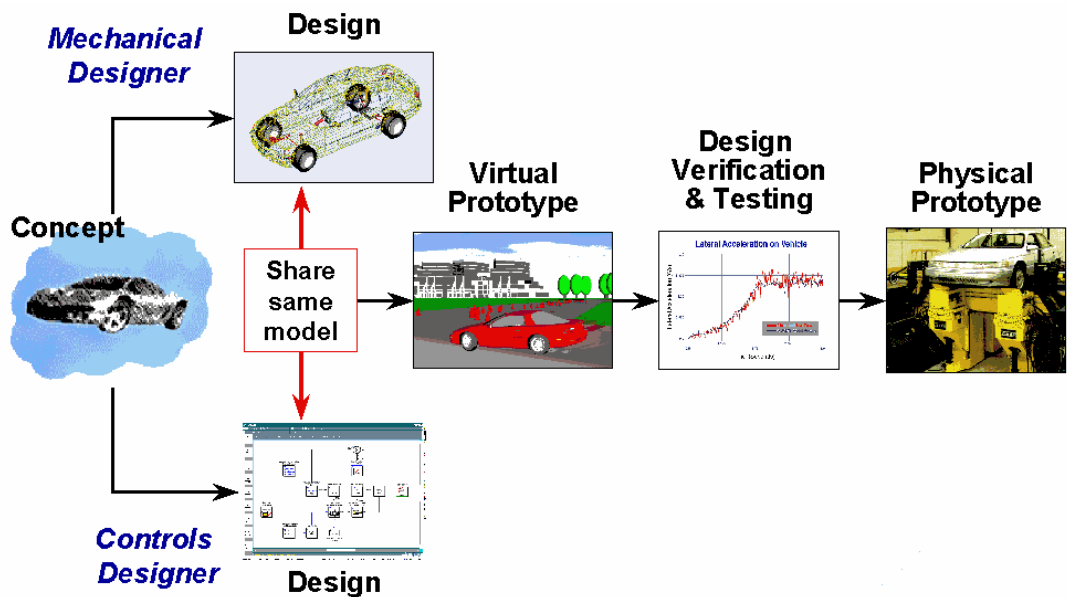


Figure D.1: Virtual Prototyping is an important step between conceptual design stage and physical prototyping stage. Image source: mscsoftware.com.

- Mechanical system simulation platform.

MSC.ADAMS is the world's most widely used mechanical system simulation software. It is a motion simulation solution for analyzing complex behavior of mechanical systems.

For simple mechanical systems, the modelling can directly be done in MSC.ADAMS.

For complex systems, MSC.ADAMS provides the interface for importing 3D models from widely known CAD systems such as CATIA, PRO-ENGINEER, UNIGRAPHICS, SOLIDWORKS and SOLIDEDGE. Fig. D.3 shows the system model imported into MSC.ADAMS from SOLIDWORKS.

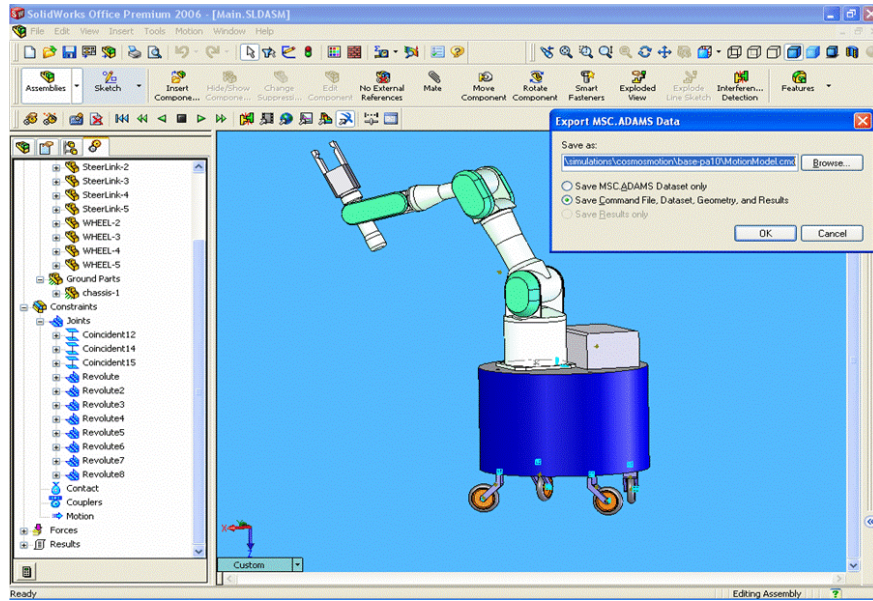


Figure D.2: Usually the first step of virtual prototyping is to construct the 3D mechanical structure using CAD packages such as Solidworks, UniGraphics or ProEngineer. This image shows the 3D Solidworks CAD model of the tested mobile manipulator. The next step is to import the CAD model to the MSC.ADAMS package for realistic dynamic simulation.

For modelling and simulation of complex mechanical dynamical systems, MSC.ADAMS is a very useful software package. Unfortunately, it has some disadvantages with respect to the design of controllers for these systems. For these purposes, MSC.ADAMS provides interface for it to work with sophisticated controller design software such as MATLAB/SIMULINK. System inputs and outputs are first defined in the MSC.ADAMS model as shown in Fig. D.3, and then the model is exported to a format that can be read by the control application.

- Control system simulation platform.

Matlab/SIMULINK is the de-facto software environment for both numerical and graphical simulation. One of the powerfulness of MATLAB/SIMULINK is its

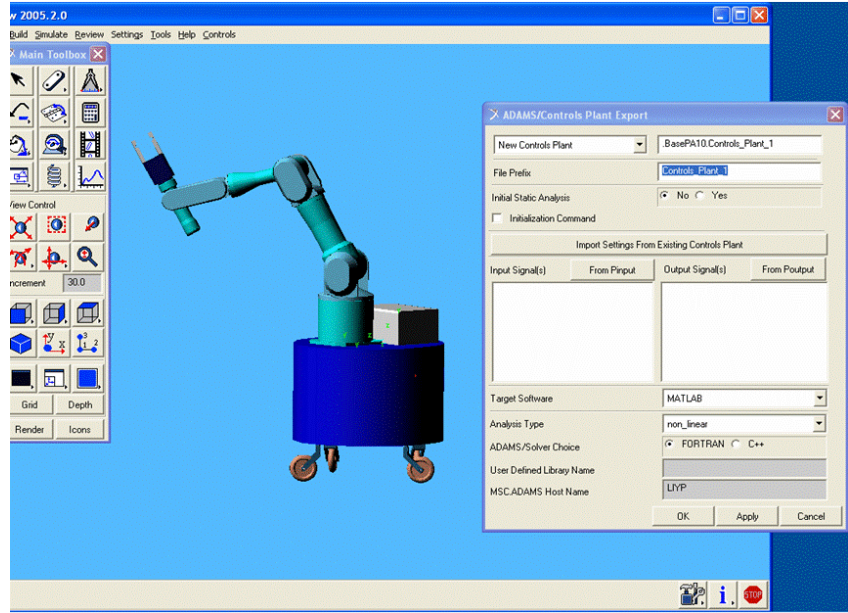


Figure D.3: Co-simulation between MSC.ADAMS (multi-body dynamics simulation package) and Matlab/Simulink (control design package) is done after the 3D CAD model of the system is imported into the MSC.ADAMS. The interface between MSC.ADAMS and Matlab/Simulink is the system inputs and outputs defined in MSC.ADAMS.

convenience of constructing controllers because it has a lot of build-in control strategies and analysis tools, both linear and nonlinear.

There are two possibilities to co-simulate the controller and the system using MSC.ADAMS and Matlab/SIMULINK. First of all there is an option in MSC.ADAMS to linearize and export systems as a set of linear state space matrices. These are very convenient for controller-design and system analysis using Matlab/SIMULINK. There is also an ADAMS-plugin called ADAMS/Controls that uses state variables to interact with Matlab/SIMULINK, intended to simplify controller-design (using Matlab/SIMULINK only for the controller and

MSC.ADAMS for accurate simulation of the mechanical system). We adopted the second way of co-simulation in this thesis.

Fig. D.5 shows a controller diagram constructed in Simulink. The MSC.ADAMS model appears as a subsystem in Simulink that has as many inputs and outputs as defined in MSC.ADAMS. Now a controller can be build in Simulink. The inputs for the controller are the outputs from the MSC.ADAMS subsystem and the outputs from the controller are the inputs for the MSC.ADAMS subsystem as shown in Fig. D.4. The communication between the control design package Matlab/Simulink and multi-body dynamics simulation package MSC.ADAMS is through either PIPE or TCP/IP protocol.

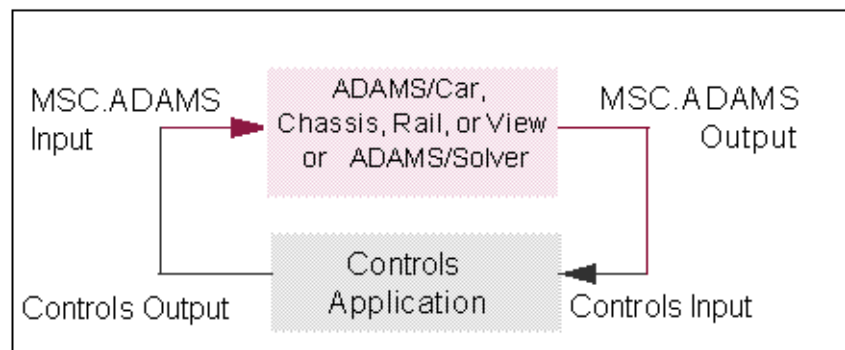


Figure D.4: The interface between MSC.ADAMS and Matlab/Simulink is based on the system input/output concept. A virtual prototype is built with the close loop simulation that combines the virtual controller and the multi-body dynamic physics engine. Image source: mscsoftware.com.

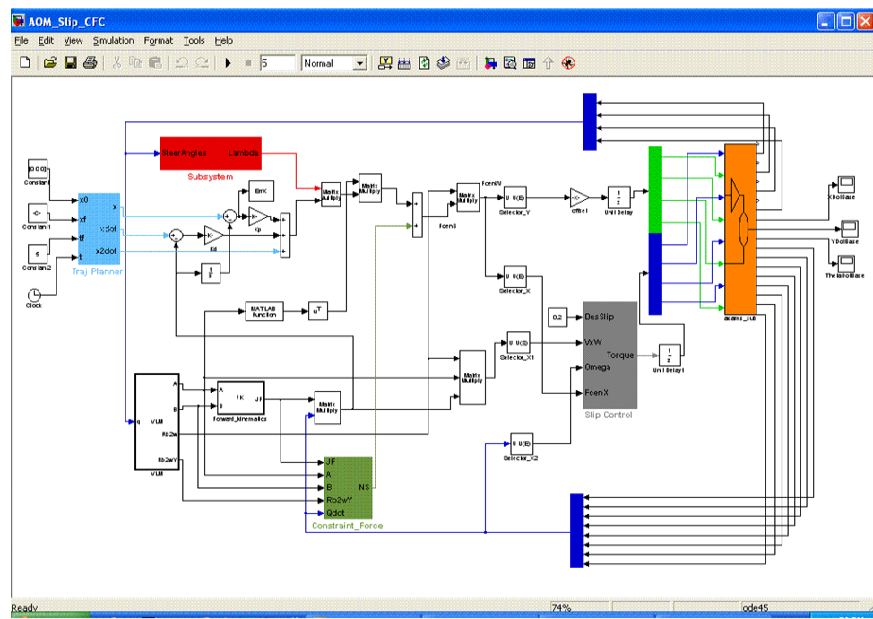


Figure D.5: After the virtual prototype is built, users can focus on the virtual controller design. This image shows a trajectory tracking controller designed for the tested wheeled mobile robot with Simulink.